

PASSIVE PENDULUM BALANCER FOR ROTOR SYSTEMS

Except where reference is made to the work of others, the work described in this dissertation my own or was done in collaboration with my advisory committee.
This dissertation does not include proprietary or classified information.

Roland Horváth

Certificate of approval:

Subhash C. Sinha
Professor
Mechanical Engineering

George T. Flowers, Chair
Professor
Mechanical Engineering

John E. Cochran, Jr.
Professor
Aerospace Engineering

Dan B. Marghitu
Professor
Mechanical Engineering

Stephen L. McFarland
Acting Dean
Graduate School

PASSIVE PENDULUM BALANCER FOR ROTOR SYSTEMS

Roland Horváth

A Dissertation

Submitted to

the Graduate Faculty of

Auburn University

in Partial Fulfillment of the

Requirements for the

Degree of

Doctor of Philosophy

Auburn, Alabama

May 11, 2006

PASSIVE PENDULUM BALANCER FOR ROTOR SYSTEMS

Roland Horváth

Permission is granted to Auburn University to make copies of this dissertation at its discretion, upon request of individuals or institutions and at their expense.
The author reserves all publication rights.

Signature of Author

Date of Graduation

VITA

Roland Horváth, son of János Horváth and Erzsébet Fazekas, was born on August 16, 1972, in Kaposvár, Hungary. He entered the Budapest University of Technology and Economics (former Technical University of Budapest), September 1994, where he received Master of Science degree in Mechanical Engineering. He joined the doctoral program in Mechanical Engineering at Auburn University, Auburn, Alabama, in the fall of 2000.

DISSERTATION ABSTRACT

PASSIVE PENDULUM BALANCER FOR ROTOR SYSTEMS

Roland Horváth

Doctor of Philosophy, May 11, 2006
(M.E., the Budapest University of Technology and Economics, 2000)

152 Typed Pages

Directed by George T. Flowers

Automatic, passive self-balancing systems are important tools for reducing the effects of synchronous vibration in a variety of rotating machinery. Such systems are ideally capable of precise balancing, subject to certain dynamic restrictions. There are a number of designs that are used, but the most common type is the ball balancer system that employs balls that move inside a cylindrical race or channel. However, such systems may be subject to a variety of effects that arise due to rolling resistance. An alternative approach uses pendulums rather than balls to provide the balancing. In the present work, a passive pendulum balancer system is investigated from several aspects. A mathematical model has been developed to discover the stability characteristic of the pendulum balancer. Because of the obvious potential for practical application pendulum balancers this system was investigated from engineering point of view. These investigations tried to cover all the possible differences that could arise when the mathematical model would be materialized as a real passive balancing device. The application of non identical

pendulums was studied in detail and its advantages and disadvantages are discussed. The influences of rolling resistance and shaft misalignment on the functional capability of pendulum self-balancing systems are specifically examined.

The study of a passive pendulum balancer with non-isotropic suspension is also presented. The existence of two natural frequencies results in two distinct areas of stability. These stable areas are determined by Floquet analysis and verified by numerical simulations and experimental measurements.

ACKNOWLEDGMENTS

The author would like to express his appreciation and thanks to his advisor Professor George T. Flowers, Department of Mechanical Engineering for his guidance and support toward the completion of this dissertation. The author also wishes to acknowledge the following committee members: Dr. Subhash C. Sinha, Professor, Dr. Dan Marghitu, Associate Professor, Department of Mechanical Engineering; and Dr. John Cochran, Jr., Department Head and Professor of Department of Aerospace Engineering.

The author is thankful for the invaluable initial guidance to his former professor Dr. Gábor Stépán, DSc, Department of Applied Mechanics Budapest University of Technology and Economics. As well, the author would like to thank his friend, Dr. Tamás Insperger, Associate Professor, Department of Applied Mechanics Budapest University of Technology and Economics, for his great advice and ideas.

Finally, the author would like to thank János Torma and Béla Pallos, his former teachers for supporting and believing in him.

Journal used: Journal of Sound and Vibration

Computer software used: Microsoft Office Word 2003

TABLE OF CONTENTS

LIST OF TABLES	xii
LIST OF FIGURES	xiii
1 INTRODUCTION	1
1.1 Background	1
1.2 Motivation for research	4
1.3 Organization of Dissertation	5
2 BASIC TWO DEGREES OF FREEDOM (DOF) MATHEMATICAL MODEL	6
3 PASSIVE PENDULUM BALANCER WITH ISOTROPIC SUSPENSION	12
3.1 Balancing boundaries (relative balancing areas) of a two-pendulum balancer with non-identical pendulums	14
Visualization of balancing capability: “CG circles”	17
Singular Points and Stability Characteristics	20
Stability Analysis	29
3.2 EXPERIMENTAL INVESTIGATION	41
3.2.1 Pendulum Balancer Experimental Facility	41
3.2.2 Experimental validation for non-identical pendulums	45
Subcritical operation	45

Supercritical operation	47
3.2.3 Numerical and Experimental validation	50
Special case: Identical pendulums	52
Numerical and Experimental validation	54
3.3 Influence of Pendulum Shaft Misalignment	58
3.3.1 Experimental investigation of pendulum shaft misalignment	62
Pendulum Balancer Experimental Facility	62
Implementation of shaft misalignment	62
Description of experimental procedure.....	63
3.3.2 Experimental comparison of the sensitivity and consistency of ball and pendulum balancers	67
Ball Balancer Experimental Facility	67
Ball Balancer Experimental Results	68
Pendulum Balancer Experimental Results.....	74
4 PASSIVE PENDULUM BALANCER WITH NON-ISOTROPIC SUSPENSION	78
4.1 Analytical investigation	78
4.1.1 Stability of homogeneous linear system with time periodic coefficients .	84
4.1.2 Floquet analysis: piecewise approximation	86
4.1.3 Floquet analysis with numerical integration: single pass scheme	88
4.1.4 The result of Floquet analysis.....	90
Floquet characteristic multipliers for the Type I singular point	93

4.1.5	Stability changes for different damping coefficients	96
4.2	Experimental facility with non-isotropic suspension.....	99
4.2.1	Description of experimental facility	99
4.2.2	Description of experimental procedure.....	105
4.3	Numerical and experimental investigation	106
4.4	Summary of validation.....	112
5	CONCLUSIONS AND FUTURE WORK.....	113
	BIBLIOGRAPHY.....	115
	APPENDIX A PARAMETERS OF EXPERIMENTAL FACILITY	119
	APPENDIX B MATLAB SOURCE CODES	121
5.1	MatLab source code: Model40.m	122
5.2	MatLab source code: ODE01.m	131
5.3	MatLab source code: wRunUp.m	132

LIST OF TABLES

Table 3.1	Stability table of Type I singular point	32
Table 3.2	Stability table of Type II singular point.....	34
Table 3.3	Stability table of Type III singular point	35
Table 3.4	Stable configuration for two operational and three constructional cases	36

LIST OF FIGURES

Figure 2.1 Two DOF model with radial mass imbalance: M_p	6
Figure 2.2 Magnitude and phase shift of the frequency response.....	9
Figure 2.3 Configurations of the frequency response and the three forces of the pendulum as a function of phase shift.....	11
Figure 3.1 4 DOF model of rotor with two-non-identical pendulum balancer in a rotating coordinate system.....	13
Figure 3.2 Balancing boundaries and relative balancing areas of two-pendulum set.....	16
Figure 3.3 Balancing boundaries of two-pendulum set for a series of mass imbalance S_p	17
Figure 3.4 CG circles relative to a certain radial mass imbalance S_p	18
Figure 3.5 Illustrations of the three types of singular point.....	26
Figure 3.6 Singular point loss as a function of relative damping and operational speed for properly oversized pendulums	38
Figure 3.7 Singular point loss as a function of relative damping and operational speed for improperly oversized pendulums.....	39
Figure 3.8 The side view of pendulum balancer experimental facility.....	43
Figure 3.9 Top view of pendulum balancer experimental facility.....	44
Figure 3.10 Side view of pendulum assembly	44
Figure 3.11 Analytical and experimental results for the amplitude of vibration (subcritical operation).....	46

Figure 3.12 Analytical and experimental results for the position of pendulums (subcritical operation)	47
Figure 3.13 Analytical and experimental results for the amplitude of vibration (supercritical operation)	49
Figure 3.14 Analytical and experimental results for the position of pendulums (supercritical operation)	49
Figure 3.15 Results of numerical simulation and experimental measurement of two-non-identical pendulum	51
Figure 3.16 Analytical and experimental results for the amplitude of vibration (supercritical operation)	53
Figure 3.17 Analytical and experimental results for the position of pendulums (supercritical operation)	54
Figure 3.18 Results of numerical simulation and experimental measurement of two-identical pendulum	55
Figure 3.19 Possible design solutions for pendulum balancing systems	57
Figure 3.20 Mathematical model of rotor system with non-centered pendulums	58
Figure 3.21 Simulation results showing the non-dimensionalized rotor vibration level for the system with pendulum shaft misalignment	60
Figure 3.22 Simulation results showing the absolute and relative positions of the pendulums for the system with pendulum shaft misalignment	61
Figure 3.23 Experimental results showing the non-dimensionalized rotor vibration level for the system with pendulum shaft misalignment	64
Figure 3.24 Experimental results showing the absolute and relative positions of the pendulums for the system with pendulum shaft misalignment	65
Figure 3.25 Side view of ball balancer experimental facility	69
Figure 3.26 Top view of ball balancer experimental facility	70

Figure 3.27 The final positions of balancing balls and vibration level for different startups	71
Figure 3.28 Deformation of contact surfaces and force distribution of the balancing ball and channel	73
Figure 3.29 The final positions of balancing pendulums and the level of vibration for different startups	75
Figure 3.30 The final positions of balancing pendulums and the level of vibration on the zoomed plot for different startups.....	76
Figure 3.31 Force distribution of pendulum and ball balancer	77
Figure 4.1 Coarse Floquet stability map of Type I singular point.....	91
Figure 4.2 Fine Floquet stability map of Type I singular point with the points used for numerical and experimental validation.....	92
Figure 4.3 The unit cylinder and the biggest Floquet characteristic multiplier as a function of relative running speed.	94
Figure 4.4 Three different views of unit cylinder and the Floquet characteristic multipliers of Type I singular point	95
Figure 4.5 Floquet stability map of Type I singular point for different relative damping coefficients of rotor suspension	97
Figure 4.6 Floquet stability map of Type I singular point for different damping coefficients of pendulums.....	98
Figure 4.7 Side view of pendulum balancer experimental facility with non-isotropic suspension.....	102
Figure 4.8 Top view of rotor assembly	103
Figure 4.9 Side view of rotor assembly	104
Figure 4.10 Numerical and experimental validation of point A	107
Figure 4.11 Numerical and experimental validation of point B	108

Figure 4.12 Numerical and experimental validation of point C	109
Figure 4.13 Numerical and experimental validation of point D	110
Figure 4.14 Numerical and experimental validation of point E.....	111

NOMENCLATURE

t	=	Time [s]
T	=	Time period [s]
ϕ	=	Phase angle [deg]
Ψ	=	Angular displacement of disk [deg]
$\omega(t)$	=	Angular velocity of the disk [rad/s]
ω_n	=	Natural angular velocity [rad/s]
f_{ni}	=	i^{th} Natural frequency [Hz]
$\Theta_{1,2}$	=	Linear degrees of freedom [m]
$\Theta_{3,4}$	=	Angular degrees of freedom [deg]
$Y_{1,2E}$	=	Linear coordinates of singular points, (linearized system) [m]
$Y_{3,4E}$	=	Angular coordinates of singular points (linearized system) [deg]
M_D	=	Mass of disk [kg]
M_P	=	Mass imbalance [kg]
M_{BA}	=	Mass of pendulum A [kg]
M_{BB}	=	Mass of pendulum B [kg]
M_S	=	Mass of the entire rotor system [kg]
I_D	=	Mass moment of inertia of disk [kgm^2]
P_3	=	Radial perturbation variable [m]
R_D	=	Radius of disk [m]

- R_{BA} = Length of pendulum A [m]
 R_{BB} = Length of pendulum B [m]
 e = Linear distance of CG of imbalanced rotor [m]
 $k_{1,2}$ = Linear spring stiffness [N/m]
 $c_{1,2}$ = Linear damping coefficients [Ns/m]
 $c_{3,4}$ = Angular damping coefficients [Nms/rad]
 ζ = Relative damping coefficient [-]
 ρ_C = Non-dimensionalized shaft misalignment [-]
 R_C = Shift of suspension of pendulums [m]
 e = Linear distance of CG of imbalanced rotor [m]
 α = Non-dimensionalized amplitude of vibration [-]
 A_{PR} = Amplitude of vibration with released pendulums [m]
 A_{PL} = Amplitude of vibration with locked pendulums [m]
 N = Amplification factor [-]
 A = Amplitude of vibration [m]
 A_{Stat} = Static amplitude of vibration [m]
 $[I]$ = Identity matrix
 $[M]$ = Inertia matrix
 $[D]$ = Damping matrix
 $[G]$ = Gyroscopic matrix
 $[K]$ = Elastic matrix
 $[N]$ = Non-conservative force matrix
 $[A]$ = Coefficient matrix

$[\Phi]$	=	Fundamental matrix
$[C]$	=	Floquet Principal Matrix
λ	=	Characteristic multiplier
Ω	=	Relative running speed [-]
K	=	Relative spring stiffness [-]
$S_{A,B}$	=	First order moment of inertia of pendulums [kgm]
S_P	=	First order moment of inertia of mass imbalance [kgm]
T	=	Sum of all kinetic energies [J]
V	=	Sum of all potential energies [J]
D	=	Sum of dissipation energies [J]
$Q_{1,2}$	=	Generalized forces [N]
$Q_{3,4}$	=	Generalized torques [Nm]
F_{CF}	=	Centrifugal force [N]
F_C	=	Constraining force [N]
F_F	=	Friction force [N]
F_R	=	Force of rolling resistance [N]
F_B	=	Balancing force [N]

1 INTRODUCTION

1.1 Background

Rotating machinery is commonly used in civil, military and industrial applications including vehicle wheels, machining tools, industrial rotating machinery aircraft gas turbine engines and helicopter blades. One of the primary sources of vibration is mass imbalance, which occurs when the principal axis of inertia of the rotor is not coincident with its rotational axis.

There are two common balancing methods which are used to align the principal inertia axis and rotational axis. One method is off-line balancing in which the rotating machine is stopped for the adjustment of mass distribution. The second method is on-line balancing in which the mass distribution rearrangement happens continuously during rotation. Such automatic balancing can be either active or passive. Active balancing systems use sensors to measure the unbalance level and actuators to shift the mass distribution. Passive balancing systems perform a similar task but without sensors, control laws and external power supplies.

The simplicity, reliability and relatively low cost of passive balancing systems make them a very attractive solution and thus, have been the subject of significant past research.

The first documented appearance of an auto balancing device was by A. Fesca who patented improved centrifugal machine equipped with three ring balancer in 1872 [1] The second documented automatic balancer is also a ring balancer patented by G. W. Ledyard in 1896. Ledyard used a series of rings around the outer diameter of his centrifugal machine [2]. In the same year a new type of rotor balancing system was registered by

United States Patent Office. M. Leblanc patented his automatic balancer for rotating bodies. In his design, the balancer consists of a simple cylindrical chamber filled with a heavy liquid [3]. Thearle [4] in 1932 published a detailed experimental study. Probably this design was the first to use self-aligning balls to achieve passive balancing. The first documentation of pendulum type balancer is also a patented invention by K. Clark 1946 [5]. Clark used four non-centrally attached pendulums to reduce the level of centrifugal machines. Thearle [6] investigated in detail the Leblanc balancer and summarized the requirements of ideal balancers. In the same journal, Thearle [7] compared several different types of automatic dynamic balancers, such as a ring, pendulum and ball balancers. This is the first appearance of an automatic pendulum-balancer in the literature. In his paper Thearle concluded that by placing the pivot of pendulums at the center of rotation the pendulum balancer become equivalent to the ring balancer, his analysis was heuristic and did not include a rigorous and detailed analytical study. In addition, he concluded that ball balancers were a superior system.

Since the 1950's, the majority of researchers have concentrated their efforts on investigations of ball-balancing systems. Sharp [8] provided a stability analysis of the balanced condition for a two-ball balancer on a planar rotor, and he presented the results of a parametric study of that system. Conclusions were drawn regarding the satisfactory operation of such a balancer. Bövic and Högfors [10] in 1986 by using the method of multiple scales showed that an automatic ball-balancer reduces vibration for planar and non-planar 6 DOF rotor systems. Their research is a detailed analytical study but it was not verified by any experimental measurements.

Wettergren [11] investigated a ball-balancing system with one and two balls in a cylindrical groove. He also examined the effect of oil viscosity and found a relationship between the viscosity and the stability properties of the balancing system. However, his research was analytical in nature and not verified experimentally. Huang and his colleagues [12] in 2002 presented a combined analytical and experimental study of the loss of balancing capability for a ball-type balancing system due to runway eccentricity and rolling resistance. Other investigators [13] have considered the effects of dry friction on ball balancer systems. This is a specific concern if such units are operated in an unlubricated condition, which is desirable for some applications (such as optical drives) where lubricants can cause contamination and damage. It was demonstrated that, “even for very low friction coefficients” the balancing behavior can deteriorate considerably. K. Green and his colleagues demonstrated a nonlinear bifurcation analysis of an automatic ball balancer [14]. Applying only analytical methods they discovered large regions in the parameter space where the ball balancer shows instability. They also investigated the effect of perturbations and transient dynamics.

The only substantial study in the current literature on pendulum-based passive balancing systems was conducted by Kubo and his colleagues, who presented their research on an automatic balancer using pendulums [9]. This paper was concerned with theoretical and experimental investigations on the dynamic behavior and stability of an automatic balancer using centrifugal pendulums. Although they noted the most important requirement that has to be satisfied for proper balancing such as the pivot of the pendulums have to be placed to the center of rotor, the experimental facility was equipped with non-centrally attached pendulums. Additionally this paper has a

fundamental flaw. In their study they model the suspension of disk as single DOF. This is not an adequate model for a rotating disk especially when a centrifugal force has a balancing effect.

1.2 Motivation for research

Providing reliable, on line balancing for wide range of applications is a great challenge. The complexity of active on line balancing reduces its reliability. This complexity does not suit zero tolerance applications and it requires tremendous research hours to develop a somewhat reliable and robust active balancing system, which is expensive production cost and this way rejects any application on mass production level.

Application of automatic balancers on a mass production level causes a focus of efforts on implementation of the simplest passive balancing system: the ball balancer. The extreme simplicity of ball balancer systems has generated a huge amount of research effort but the widespread utilization of ball balancer systems has not taken place. The effect of rolling resistance greatly reduces number of potential applications of automatic ball balancers.

The desire to design and build a simple, reliable passive balancing device has not been fulfilled. This research purposefully targeted this technological deficiency. The discovery of such a system would initiate numerous potential applications:

- Providing artificial gravity in space
- Centrifuges for Gravitational biology research
- Helicopter blade balancing
- Centrifugal casting
- Handheld power tools

1.3 Organization of Dissertation

This research effort is a study of a passive pendulum balancer. The research work was performed in the Vibration Analysis Laboratory of the Department of Mechanical Engineering at Auburn University. Specifically, the work includes:

- Development of mathematical model
- Development of numerical procedures
- Development and testing of experimental facilities

2 BASIC TWO DEGREES OF FREEDOM (DOF) MATHEMATICAL MODEL

In order to provide an appropriate background for the current work, this discussion begins by considering the behavior of a 2 DOF thin disk model rotating in a horizontal plane with a radial mass imbalance represented by a point mass M_P that is shifted from the center of disk by P_3 in the \bar{I}' direction, as shown in Figure 2.1.

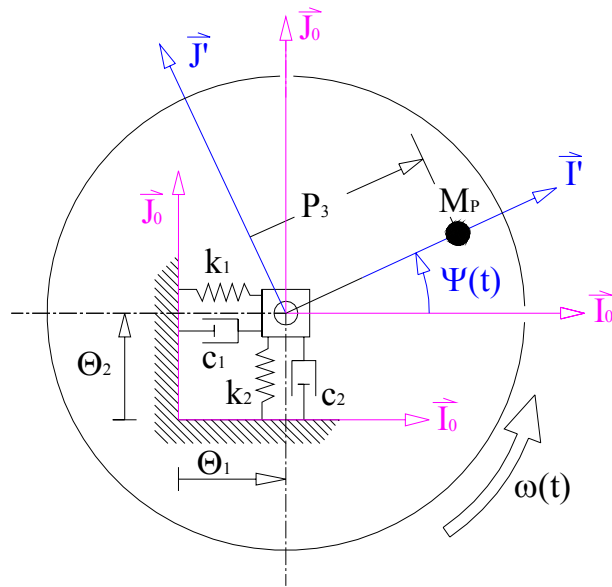


Figure 2.1 Two DOF model with radial mass imbalance: M_P

The disk model has two degrees of freedom, Θ_1 and Θ_2 , which are mutually orthogonal linear displacements in the same horizontal plane. The model is symmetric, having the same spring stiffness $k_{1,2}$ and damping coefficient $c_{1,2}$ in both directions, which yields coincident natural angular velocity ω_n .

The differential equations of motion are:

$$\ddot{\Theta}_1 M + \dot{\Theta}_1 c + \Theta_1 k = P_3 M_p \omega^2 \cos(\omega t) \quad (2-1)$$

$$\ddot{\Theta}_2 M + \dot{\Theta}_2 c + \Theta_2 k = P_3 M_p \omega^2 \sin(\omega t) \quad (2-2)$$

$$M = M_D + M_P \quad (2-3)$$

$$c = c_1 = c_2 \quad (2-4)$$

$$k = k_1 = k_2 \quad (2-5)$$

The solution of radially unbalanced system is:

$$\Theta_1(t) = \frac{\omega^2 e}{\sqrt{\left(\frac{k}{M} - \omega^2\right)^2 + \left(\frac{c\omega}{M}\right)^2}} \cos(\omega t - \phi) \quad (2-6)$$

$$\Theta_2(t) = \frac{\omega^2 e}{\sqrt{\left(\frac{k}{M} - \omega^2\right)^2 + \left(\frac{c\omega}{M}\right)^2}} \sin(\omega t - \phi) \quad (2-7)$$

$$\text{Where: } e = \frac{P_3 M_p}{M_D + M_P} \quad (2-8)$$

The phase angle of frequency response is:

$$\phi(\omega) = \tan^{-1} \left[\frac{\omega c}{M \left(\frac{k}{M} - \omega^2 \right)} \right] \quad (2-9)$$

The magnitude of frequency response is:

$$N(\omega) = \frac{M\omega^2}{\sqrt{\omega^2 c^2 + k^2 - 2k\omega^2 M + \omega^4 M^2}} \quad (2-10)$$

$$N(\omega) = \frac{|A|}{A_{Stat}} \quad (2-11)$$

$$|A| = \sqrt{\Theta_1^2 + \Theta_2^2} \quad (2-12)$$

$$A_{Stat} = \frac{M_P}{M} P_3 \quad (2-13)$$

The rotating position vector, directed from the center of rotation to the center of disk, has a lag angle (phase angle ϕ) relative to the forcing vector. The forms of the phase angle and magnitude relations are shown in Equations (2-9) and (2-10), respectively, with plots for several different relative damping coefficients shown in Figure 2.2. As is well known, the response amplitude and phase are sensitive to damping level.

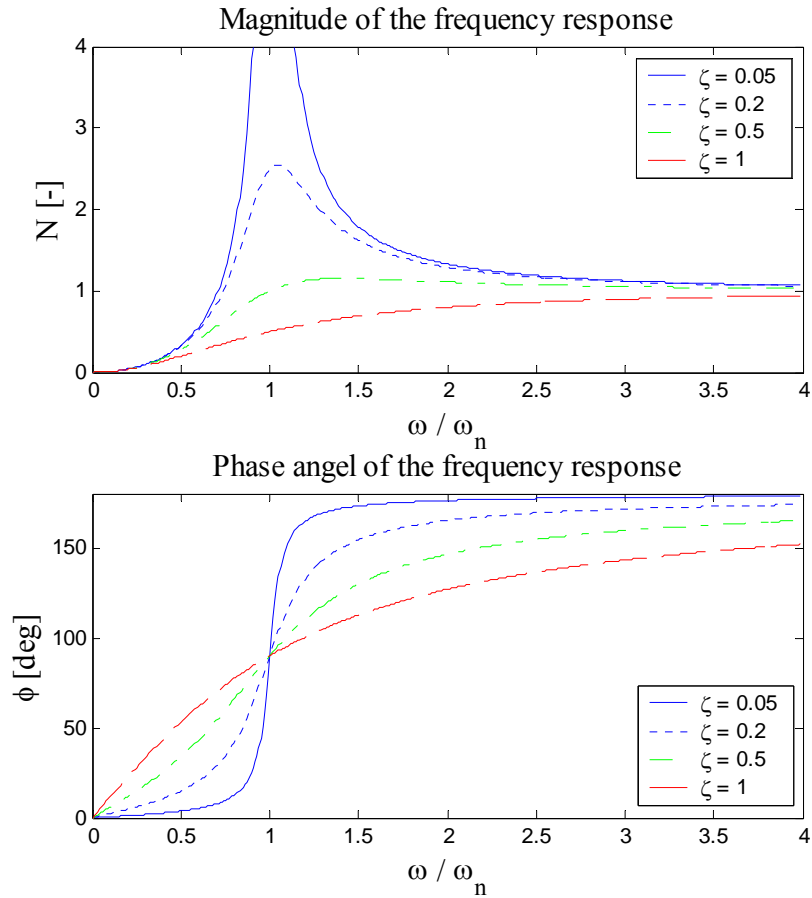


Figure 2.2 Magnitude and phase shift of the frequency response

A series of thought experiments using this 2 DOF model provides substantial insight into self-balancing using pendulum balancers. Figure 2.3 is a series of snapshots of the basic system for three operating speeds. The center of the centrifugal force field is the origin of the first two DOF, Θ_1 and Θ_2 . An imaginary (almost massless) pendulum is also shown as a part of this discussion to illustrate the force distribution along the path where a real pendulum would move.

For each case, the combined effects of centrifugal force and the constraining force acting on the system will cause the position of the imaginary pendulum to change until these two forces become parallel.

For subcritical operating speeds, the steady-state phase delay of the displacement related to the exciting force is less than 90° . In this case, the stable pendulum position will be between 0° and 90° as measured from the horizontal axis (as shown in Figure 2.3.a) which exacerbates the mass imbalance of the system.

For the resonance case, the phase delay is 90° , and the equilibrium position of the pendulum is 90° behind the position of the imbalance mass, as shown in Figure 2.3.b. Again, the effect of the pendulum is to shift the CG further from the origin though not quite as far as in the subcritical case.

Figure 2.3.c shows the system operating at a supercritical running speed. The phase delay is between 90° and 180° . The resultant effect of the centrifugal and the constraining force acting on the pendulum will drive it toward a position on the opposite side of the disk from the mass imbalance, partially compensating the unbalancing effect.

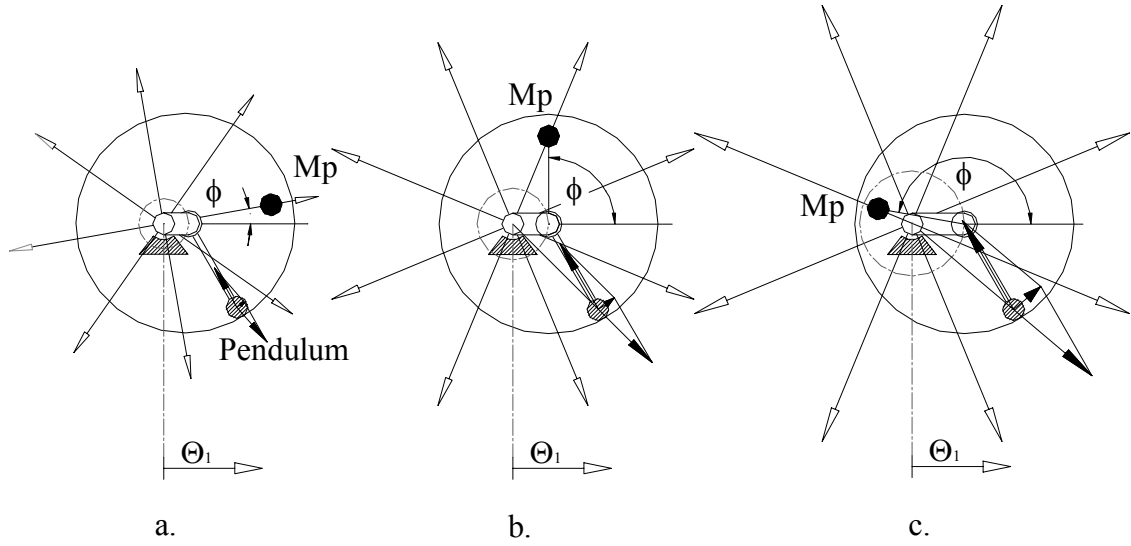


Figure 2.3 Configurations of the frequency response and the three forces of the pendulum as a function of phase shift

3 PASSIVE PENDULUM BALANCER WITH ISOTROPIC SUSPENSION

In this chapter, the passive pendulum balancer is investigated with isotropic suspension equipped with a pendulum balancing system consisting of two non-identical pendulums. From a practical point-of-view, basic differences in the pendulums (mass or length) may be incidental due to manufacturing variations or accidental damage. On the other hand, differences may be an intentionally designed into the system if they are determined to be advantageous to the operation and/or performance of the balancing system.

In the following paragraphs, a model of rotor with a two balancing system with non-identical pendulums is developed and analyzed. The basic elements of the mechanical model are shown in Figure 3.1. The first two degrees of freedom (Θ_1 , Θ_2) are linear displacements that describe the position of the rotor center. The third and the fourth are angular displacements that describe the positions of pendulum A and pendulum B, respectively.

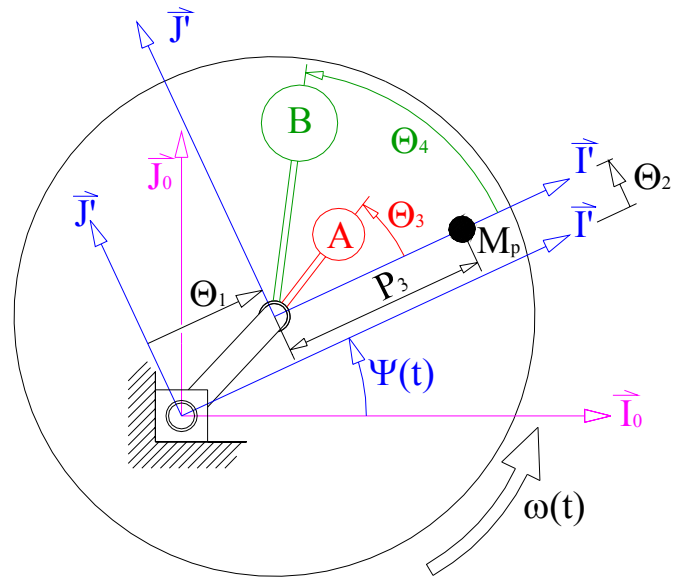


Figure 3.1 4 DOF model of rotor with two-non-identical pendulum balancer in a rotating coordinate system

3.1 Balancing boundaries (relative balancing areas) of a two-pendulum balancer with non-identical pendulums

First, consider the balancing capability of a pendulum balancing system with non-identical pendulums. Because the pendulums are not identical, the ability of the system to counter a given imbalance level depends very strongly on the relationship between the parameters of the individual pendulums and the initial imbalance level. A useful parametric description for pendulums is the first mass moment of inertia with unit: [kg-m]. It should be noted that two non-identical pendulums may have the same first moment of inertia. For each of the two pendulums, A and B, and for the mass imbalance, the following relations define the first mass moments of inertia.

$$S_A = M_{BA} R_{BA} \quad (3-1)$$

$$S_B = M_{BB} R_{BB} \quad (3-2)$$

$$S_P = M_P P_3 \quad (3-3)$$

The balancing boundaries of the pendulum system for a variety of S_A and S_B combinations and for a specified mass imbalance, S_P , are shown in Figure 3.2. The shaded area ABCD with the dark line border shows the parametric values which can compensate for the given level of imbalance. If the parametric values are in this shaded area (as described by Equation (3-4)) then the pendulums are able to counterbalance the mass imbalance. For values outside this area, the pendulums are unable to completely compensate for the mass imbalance because they are either undersized or improperly oversized.

$$S_A + S_B \geq S_P \quad \text{and} \quad |S_A - S_B| \leq S_P \quad (3-4)$$

For parametric combinations either above line AD or below line BC in Figure 3.2, the pendulums are improperly oversized relative to the mass imbalance, S_P . The magnitude of the difference between the first mass moments of the pendulums is greater than the mass imbalance, as described by Equation (3-5). If this is the case, there are no pendulum locations where the net unbalancing forces resulting from the two pendulums and the rotor mass imbalance can completely cancel and the rotor will remain unbalanced. The final level of net imbalance may be higher or lower than the initial level without a balancing system depending upon the relative differences between the two pendulums.

$$|S_A - S_B| > S_P \quad (3-5)$$

If the parametric combination is located in the OAB triangle (Equation (3-6)) then the pendulums can only partially counterbalance the mass imbalance. In this case, the pendulum set is undersized relative to the mass imbalance.

$$S_A + S_B < S_P \quad (3-6)$$

A series of similar relative balancing areas for a variety of mass imbalances are illustrated in Figure 3.3. If the two pendulums have the same first mass moment ($S_A = S_B$), then the parametric configuration will be located on a line that starts from the origin with

a 45° slope, as shown in figure 6 with a dashed line. For this case, the pendulums are either undersized or properly oversized relative to any mass imbalance S_p .

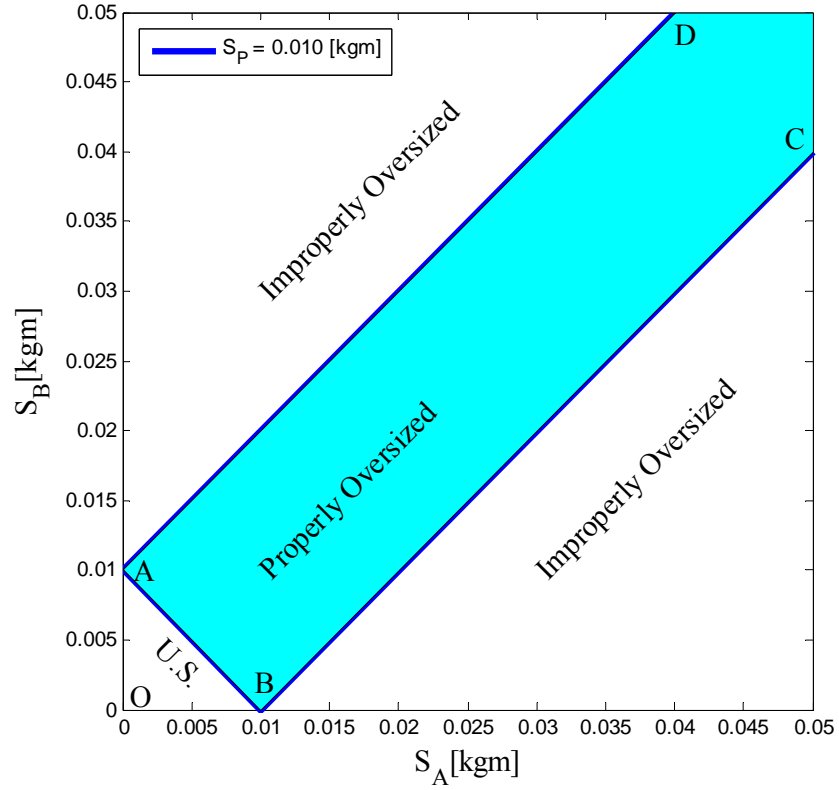


Figure 3.2 Balancing boundaries and relative balancing areas of two-pendulum set

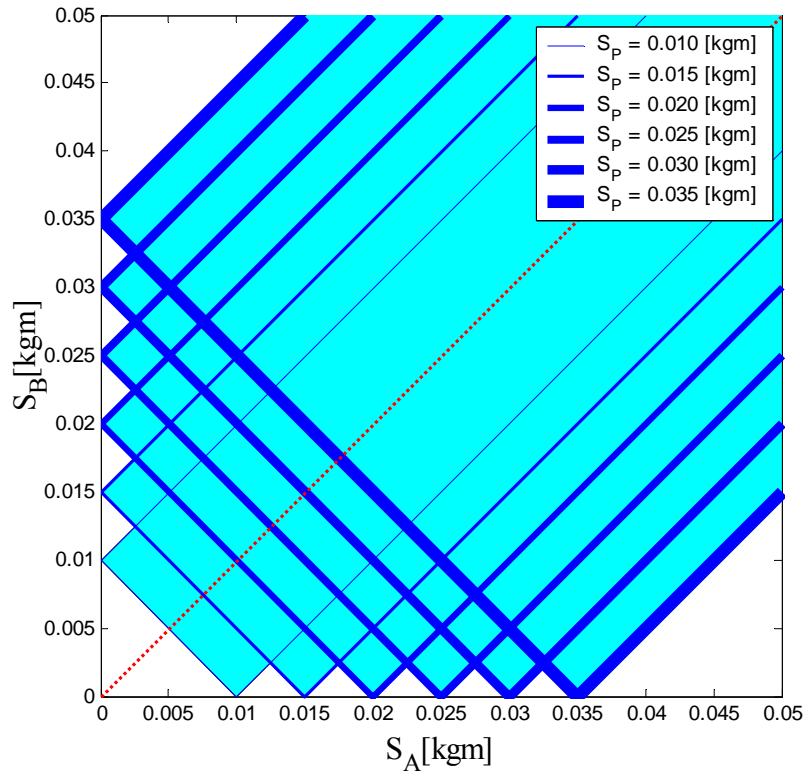


Figure 3.3 Balancing boundaries of two-pendulum set for a series of mass imbalance S_p

Visualization of balancing capability: “CG circles”

The balancing capability of a pendulum balancing system can also be characterized by the resulting steady-state location of the center of gravity of the entire rotor system (rotor, pendulums and mass imbalance). Figure 3.4 shows a relative balancing boundary plot which uses a series of circular symbols with a darkened area, which are referred to herein as CG circles where the pendulums are able to relocate the CG of the entire system. If these dark CG circles include the center of the rotor, then balancing can be archived for proper operational conditions.

Again, for the case of same first mass moment, the CG circles are located on the 45° dashed line. Leaving this line the CG circles have an internal “blind spot”. Having this

blind spot not necessarily means the pendulums cannot do the balancing. If the chosen pendulum combination stays inside the ABCD area the pendulums would balance regardless of the existence of blind spot. Under the BC or above the AD line the blind spot is over the center of the rotor this means balancing cannot be achieved because the pendulums bother each other they are insufficiently oversized. In order to achieve balancing the point of chosen pendulums combination has to stay in the ABCD area. This condition is specified by Equations (3-4).

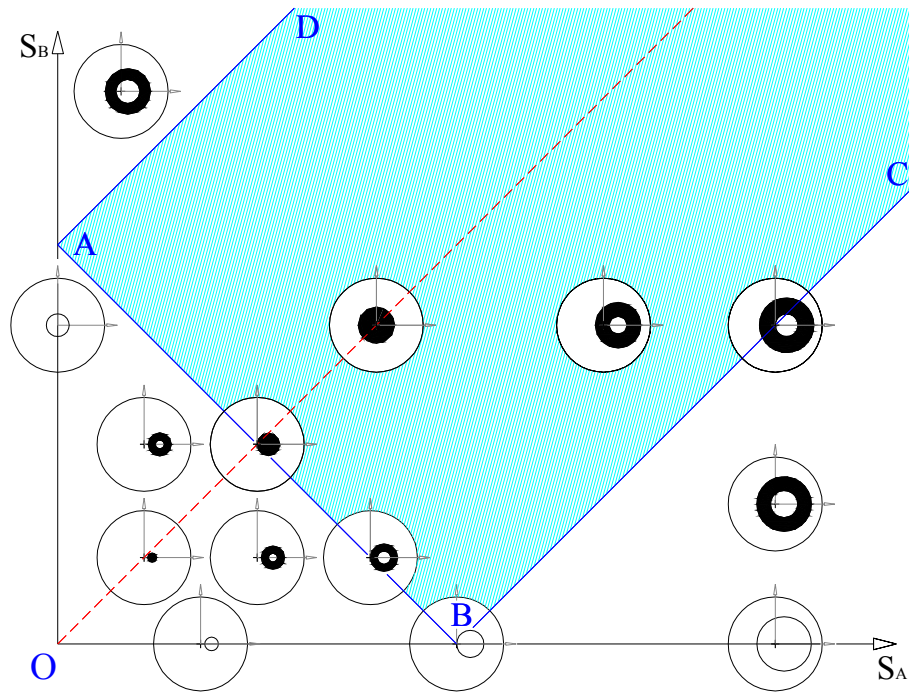


Figure 3.4 CG circles relative to a certain radial mass imbalance S_p

In general, all of the relative-balancing-area plots shown above (Figure 3.2 - Figure 3.4) contain three distinct areas:

Rectangular region ABCD

If the parametric combination is located in this area, the pendulum system is capable of counterbalancing the entire mass imbalance. The system is properly oversized relative to the mass imbalance.

Triangular region OAB

If the parametric combination is located in this area, the pendulum system is not capable of counterbalancing the entire mass imbalance. They are undersized relative to the mass imbalance.

Regions above the AD line and below the BC line

If the parametric configuration of the pendulum system is located in either of these regions, the pendulums are not capable of counterbalancing the entire mass imbalance. They are improperly oversized relative to the mass imbalance and may partially reduce the level of vibration if:

$$|S_A - S_B| < S_P \quad (3-7)$$

Otherwise, such an improperly oversized system will exacerbate the synchronous vibration resulting in a higher amplitude of vibration than if the balancer was not present.

Singular Points and Stability Characteristics

The above discussion has examined the fundamental capability of a balancing system with two non-identical pendulums. The actual dynamic behavior of such a system depends on its equilibrium points and their associated stability characteristics. So, the next step in this investigation considers the occurrence of singular points and the stability of motion in the vicinity of such points. The governing equations of motion for a symmetric rotor suspension ($c = c_1 = c_2$ and $k = k_1 = k_2$) in a disk-fixed coordinate system can be represented as:

$$\frac{d}{dt} \left(\frac{\partial T}{\partial \dot{\Theta}_i} \right) - \frac{\partial T}{\partial \Theta_i} + \frac{\partial V}{\partial \Theta_i} + \frac{\partial D}{\partial \dot{\Theta}_i} = Q_i \quad i = 1, 2, 3, 4 \quad (3-8)$$

Where:

- T = Sum of all kinetic energies
- V = Sum of all potential energies
- D = Rayleigh dissipation function
- Θ_i = Generalized coordinates
- Q_i = Generalized forces

$$\begin{aligned}
T = & \frac{1}{2} \omega^2 \left(S_A (R_{BA} + 2\Theta_1 \cos(\Theta_3) + 2\Theta_2 \sin(\Theta_3)) + \right. \\
& + S_B (R_{BB} + 2\Theta_1 \cos(\Theta_4) + 2\Theta_2 \sin(\Theta_4)) + \\
& + S_P (P_3 + 2\Theta_1) + (M_D + M_{BA} + M_{BB} + M_P) (\Theta_1^2 + \Theta_2^2) + \left. \frac{1}{2} M_D R_D^2 \right) + \\
& + \omega \left(M_{BA} \dot{\Theta}_2 \Theta_1 + S_A \Theta_2 \sin(\Theta_3) \dot{\Theta}_3 + M_P \dot{\Theta}_2 \Theta_1 + \right. \\
& + S_B \Theta_1 \cos(\Theta_4) \dot{\Theta}_4 + S_A R_{BA} \dot{\Theta}_3 + M_{BB} \dot{\Theta}_2 \Theta_1 + M_D \dot{\Theta}_2 \Theta_1 + \\
& + S_P \dot{\Theta}_2 + S_A \dot{\Theta}_3 \Theta_1 \cos(\Theta_3) - S_B \dot{\Theta}_1 \sin(\Theta_4) + \\
& + S_B \Theta_2 \sin(\Theta_4) \dot{\Theta}_4 - M_{BA} \dot{\Theta}_1 \Theta_2 + S_A \dot{\Theta}_2 \cos(\Theta_3) + \\
& + S_B \dot{\Theta}_2 \cos(\Theta_4) - \dot{\Theta}_1 M_D \Theta_2 + S_B R_{BB} \dot{\Theta}_4 - M_{BB} \dot{\Theta}_1 \Theta_2 - \\
& - S_A \dot{\Theta}_1 \sin(\Theta_3) - \dot{\Theta}_1 M_P \Theta_2 \left. \right) + \\
& + \frac{1}{2} (M_D + M_{BA} + M_{BB} + M_P) \dot{\Theta}_2^2 + \frac{1}{2} (M_D + M_{BA} + M_{BB} + M_P) \dot{\Theta}_1^2 + \\
& + \frac{1}{2} S_A R_{BA} \dot{\Theta}_3^2 + \frac{1}{2} S_B R_{BB} \dot{\Theta}_4^2 + S_A \dot{\Theta}_2 \dot{\Theta}_3 \cos(\Theta_3) + S_B \dot{\Theta}_2 \dot{\Theta}_4 \cos(\Theta_4) + \\
& - S_B \dot{\Theta}_1 \dot{\Theta}_4 \sin(\Theta_4) - S_A \dot{\Theta}_1 \dot{\Theta}_3 \sin(\Theta_3)
\end{aligned} \tag{3-9}$$

$$V = \frac{1}{2} k (\Theta_1^2 + \Theta_2^2) \tag{3-10}$$

$$D = \frac{1}{2} c (\dot{\Theta}_1^2 + \dot{\Theta}_2^2) - c \omega (\dot{\Theta}_1 \Theta_2 - \dot{\Theta}_2 \Theta_1) + \frac{1}{2} c \omega^2 (\Theta_1^2 + \Theta_2^2) + \frac{1}{2} (c_3 \dot{\Theta}_3^2 + c_4 \dot{\Theta}_4^2) \tag{3-11}$$

$$Q_i = 0 \tag{3-12}$$

The resulting equations of motion are:

$$\begin{aligned}
& -S_A \left(2\omega \cos(\Theta_3) \dot{\Theta}_3 + \sin(\Theta_3) \ddot{\Theta}_3 + \omega^2 \cos(\Theta_3) + \cos(\Theta_3) \dot{\Theta}_3^2 \right) - \\
& -S_B \left(2\omega \cos(\Theta_4) \dot{\Theta}_4 + \cos(\Theta_4) \dot{\Theta}_4^2 + \sin(\Theta_4) \ddot{\Theta}_4 + \omega^2 \cos(\Theta_4) \right) - \\
& -M_P \left(\omega^2 \Theta_1 - \ddot{\Theta}_1 + 2\omega \dot{\Theta}_2 + \omega^2 P_3 \right) + (M_D + M_{BA} + M_{BB}) \ddot{\Theta}_1 + \\
& + c \left(\dot{\Theta}_1 - \omega \Theta_2 \right) + k \Theta_1 - (M_D + M_{BA} + M_{BB}) \left(2\omega \dot{\Theta}_2 + \omega^2 \Theta_1 \right) = 0
\end{aligned} \tag{3-13}$$

$$\begin{aligned}
& -S_A \left(2\omega \sin(\Theta_3) \dot{\Theta}_3 - \cos(\Theta_3) \ddot{\Theta}_3 + \omega^2 \sin(\Theta_3) + \sin(\Theta_3) \dot{\Theta}_3^2 \right) - \\
& -S_B \left(2\omega \sin(\Theta_4) \dot{\Theta}_4 + \sin(\Theta_4) \dot{\Theta}_4^2 - \cos(\Theta_4) \ddot{\Theta}_4 + \omega^2 \sin(\Theta_4) \right) - \\
& -M_P \left(\omega^2 \Theta_2 - \ddot{\Theta}_2 - 2\omega \dot{\Theta}_1 \right) + (M_D + M_{BA} + M_{BB}) \ddot{\Theta}_2 + \\
& + c \left(\dot{\Theta}_2 + \omega \Theta_1 \right) + k \Theta_2 + (M_D + M_{BA} + M_{BB}) \left(2\omega \dot{\Theta}_1 - \omega^2 \Theta_2 \right) = 0
\end{aligned} \tag{3-14}$$

$$\begin{aligned}
& S_A \left(-\sin(\Theta_3) \ddot{\Theta}_1 + R_{BA} \ddot{\Theta}_3 + \cos(\Theta_3) \ddot{\Theta}_2 + 2 \sin(\Theta_3) \omega \dot{\Theta}_2 + \right. \\
& \left. + 2 \cos(\Theta_3) \omega \dot{\Theta}_1 - \omega^2 \cos(\Theta_3) \Theta_2 + \omega^2 \sin(\Theta_3) \Theta_1 \right) + c_3 \dot{\Theta}_3 = 0
\end{aligned} \tag{3-15}$$

$$\begin{aligned}
& S_B \left(-\sin(\Theta_4) \ddot{\Theta}_1 + R_{BB} \ddot{\Theta}_4 + \cos(\Theta_4) \ddot{\Theta}_2 + 2 \sin(\Theta_4) \omega \dot{\Theta}_2 + \right. \\
& \left. + 2 \cos(\Theta_4) \omega \dot{\Theta}_1 - \omega^2 \cos(\Theta_4) \Theta_2 + \omega^2 \sin(\Theta_4) \Theta_1 \right) + c_4 \dot{\Theta}_4 = 0
\end{aligned} \tag{3-16}$$

The singular points are found by setting the time derivative terms in Equations (3-13) - (3-16) to zero. This results in the following set of algebraic equations.

$$-\omega^2 (Y_{1E} M_S + S_A \cos(Y_{3E}) + S_B \cos(Y_{4E})) - \omega c Y_{2E} + k Y_{1E} = 0 \quad (3-17)$$

$$-\omega^2 (Y_{2E} M_S + S_A \sin(Y_{3E}) + S_B \sin(Y_{4E})) + \omega c Y_{1E} + k Y_{2E} = 0 \quad (3-18)$$

$$S_A (Y_{1E} \sin(Y_{3E}) - Y_{2E} \cos(Y_{3E})) \omega^2 = 0 \quad (3-19)$$

$$S_B (Y_{1E} \sin(Y_{4E}) - Y_{2E} \cos(Y_{4E})) \omega^2 = 0 \quad (3-20)$$

These equations are nonlinear and are not, in general, easy to solve in a closed form. However, the possible solutions are of three distinct types. The different types of singular points and the associated stability characteristics are detailed below.

Type I:

The Type I singular points represent a configuration where the rotor base motions (Y_{1E} and Y_{2E}) are zero, as illustrated in Figure 3.5.a. The pendulums settle into the positions where they counter the mass imbalance, M_p . The resulting closed form solutions for Y_{3E} and Y_{4E} , in terms of a four quadrant inverse tangent function, are shown in Equations (3-21) and (3-22). Of course, this configuration only occurs when the pendulums are physically capable of balancing the system, which means the parametric configuration is in the ABCD region. When the parametric configuration is outside of that region, the terms under the square roots in Equations (3-21) and (3-22) takes on a negative value and there is no real solution.

From the perspective of balancing effectiveness, this singular point is the most important of the three types. If this singular point is stable, the center of rotor is not vibrating because the relative locations of the pendulums and mass imbalance result in a balanced system.

$$Y_{3E} = \arctan_4 \left(-\frac{\sqrt{-AB}}{2S_p S_A}, -\frac{S_A^2 - S_B^2 + S_p^2}{2S_p S_A} \right) \quad (3-21)$$

$$Y_{4E} = \arctan_4 \left(\frac{\sqrt{-AB}}{S_p S_B}, \frac{S_A^2 - S_B^2 - S_p^2}{S_p S_B} \right) \quad (3-22)$$

$$\text{Where: } A = (S_A + S_B - S_p)(S_A + S_B + S_p)$$

$$B = (S_A - S_B - S_p)(S_A - S_B + S_p)$$

Type II:

The Type II singular points (as shown in (3-24) and illustrated in Figure 3.5.b) represent a configuration where $Y_{4E} = Y_{3E} + 180^\circ$. If this type of singular point is stable, the rotor exhibits a steady state synchronous whirl, because Y_{1E} and Y_{2E} are not zero in the rotor fixed coordinate system. Please note that, although closed form symbolic solutions were developed for both the Type II and the Type III singular points, they are not shown here because of the large size of those expressions.

Type III:

The Type III singular points (as shown in Equation (3-25) and illustrated in Figure 3.5.c). In the algebraic equation system $Y_{4E} = Y_{3E}$. The Type III singular point also includes a steady state synchronous whirling of the rotor, but for this case the pendulums are overlapping one other.

$$\text{Type I: } [Y_{1E} = 0 \quad Y_{2E} = 0 \quad Y_{3E} \quad Y_{4E}] \quad (3-23)$$

$$\text{Type II: } [Y_{1E} \neq 0 \quad Y_{2E} \neq 0 \quad Y_{3E} \quad Y_{4E} = Y_{3E} + 180^\circ] \quad (3-24)$$

$$\text{Type III: } [Y_{1E} \neq 0 \quad Y_{2E} \neq 0 \quad Y_{3E} \quad Y_{4E} \equiv Y_{3E}] \quad (3-25)$$

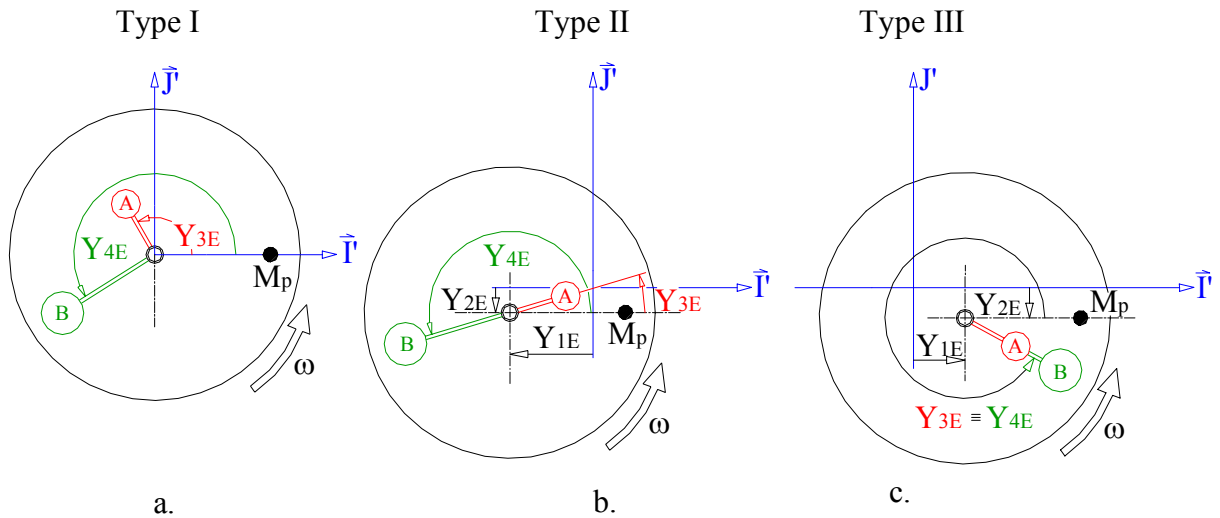


Figure 3.5 Illustrations of the three types of singular point

In order to assess the stability characteristics of each type of singular point, the differential equations of motions were linearized in the neighborhood of the singular points.

The resulting equations in vector-matrix form are:

$$[M]\ddot{\bar{Y}} + [D + G]\dot{\bar{Y}} + [K + N]\bar{Y} = 0 \quad (3-26)$$

The inertia matrix is:

$$[M] = \begin{bmatrix} M_S & 0 & -S_A \sin(Y_{3E}) & -S_B \sin(Y_{4E}) \\ 0 & M_S & S_A \cos(Y_{3E}) & S_B \cos(Y_{4E}) \\ -S_A \sin(Y_{3E}) & S_A \cos(Y_{3E}) & S_A R_{BA} & 0 \\ -S_B \sin(Y_{3E}) & S_B \cos(Y_{4E}) & 0 & S_B R_{BB} \end{bmatrix} \quad (3-27)$$

$$\text{Where : } M_S = M_D + M_{BA} + M_{BB} + M_P$$

The damping and the gyroscopic matrix is:

$$[D + G] = \begin{bmatrix} c & -2M_S \omega & -2\omega S_A \cos(Y_{3E}) & -2\omega S_B \cos(Y_{4E}) \\ 2M_S \omega & c & -2\omega S_A \sin(Y_{3E}) & -2\omega S_B \sin(Y_{4E}) \\ 2\omega S_A \cos(Y_{3E}) & -2\omega S_A \sin(Y_{3E}) & c_3 & 0 \\ 2\omega S_B \cos(Y_{4E}) & -2\omega S_B \sin(Y_{4E}) & 0 & c_4 \end{bmatrix} \quad (3-28)$$

The elastic and the non-conservative force matrix is:

$$[K + N] = \begin{bmatrix} -M_S \omega^2 + k & -\omega c & \omega^2 S_A \sin(Y_{3E}) & \omega^2 S_B \sin(Y_{4E}) \\ \omega c & -M_S \omega^2 + k & -\omega^2 S_A \cos(Y_{3E}) & -\omega^2 S_B \cos(Y_{4E}) \\ \omega^2 S_A \sin(Y_{3E}) & -\omega^2 S_A \cos(Y_{4E}) & S_A KN_{33} & 0 \\ \omega^2 S_B \sin(Y_{4E}) & -\omega^2 S_B \cos(Y_{4E}) & 0 & S_B KN_{44} \end{bmatrix} \quad (3-29)$$

$$\text{Where: } KN_{33} = Y_{2E} \sin(Y_{3E}) + Y_{1E} \cos(Y_{3E})$$

$$KN_{44} = Y_{2E} \sin(Y_{4E}) + Y_{1E} \cos(Y_{4E})$$

The Cauchy transformation of equation (3-26) results in a system of first order linear differential equation system represented by 8x8 coefficient matrix [A]. Where:

$$\bar{X} = \begin{bmatrix} \bar{Y} \\ \dot{\bar{Y}} \end{bmatrix} \quad (3-30)$$

$$\dot{\bar{X}} = [A] \bar{X} \quad (3-31)$$

$$[A] = \begin{bmatrix} [0] & [I] \\ -[M]^{-1}[K + N] & -[M]^{-1}[D + G] \end{bmatrix} \quad (3-32)$$

Stability Analysis

For the purposes of this stability investigation, all three types of singular points were examined separately for subcritical and supercritical operation. Because of the symmetric rotor suspension ($k = k_1 = k_2$), the undamped first and the second natural frequencies are the same, as indicated by the following expression:

$$\omega_n = \sqrt{\frac{k}{M_D + M_{BA} + M_{BB} + M_P}} \quad (3-33)$$

The sub and supercritical stability investigation also had to be further divided for the three relative balancing areas. This means for one certain singular point there is 2x3 cases to investigate.

Each case was also further examined separately for each of the three relative balancing areas. So, six cases are considered for each type of singular point. The specific cases that were investigated - subcritical or supercritical operation and each of the three relative balancing areas are shown in a series of Tables (1-3) in the following pages. The specific parametric combinations were chosen to encompass all three relative balancing areas, with the specific location of each test case marked by a dot. The real part of the calculated eigenvalues as a function of pendulum damping, c_{34} , is also shown on the right side of each table.

Stability investigation of Type I singular point

From a balancing perspective, this is the most important singular point. If it is stable for a given operating condition, the synchronous vibration caused by mass imbalance will be eliminated. The stability characteristics of this singular point are only investigated inside the ABCD relative balancing area. The Type I singular point does not exist outside of that region. The analysis results are shown in Table 3.1. They demonstrate that the Type I singular point is stable for supercritical operation and unstable for subcritical operation.

In addition, it is important to note that the stable position of the pendulums could be mirrored about axis X. This operation has no effect on the location of the common CG of the pendulums. Basically, Type I singular point consists of two sets that produce identical balancing results.

Stability investigation of Type II singular point

For the Type II singular points, the steady-state locations of the pendulums are directly opposite to one another. Solving the associated equations resulted in two sets of explicit symbolic solutions.

Table 3.2 summarizes the stability analysis results for each of the six cases that were considered (as described above). This singular point is only stable for supercritical operation and when the parametric configuration is improperly oversized relative to the mass imbalance. For the other five cases, this singular point is unstable.

Stability investigation of Type III singular point

For the Type III singular points, the steady-state locations of the pendulums are directly on top of each other. Table 3.3 summarizes the stability analysis results for each of the six cases that were considered, in a fashion similar to that done for the other two types of singular points. This singular point is stable for subcritical operation regardless of the parametric configuration with regard to the relative balancing areas. In addition, it is also stable for supercritical operation when the parametric configuration is undersized relative to the mass imbalance. For the other two cases, this singular point is unstable.

		Type I
Subcritical operation		<p>UNSTABLE</p>
		Singular point does not exist
Supercritical operation		<p>STABLE</p>
		Singular point does not exist

Table 3.1 Stability table of Type I singular point

Further investigation has demonstrated, that for certain cases, the stable singular point is a function of the damping coefficient of the rotor suspension. Table 3.4 summarizes the stable singular points for all of the six cases and their dependence on rotor suspension damping.

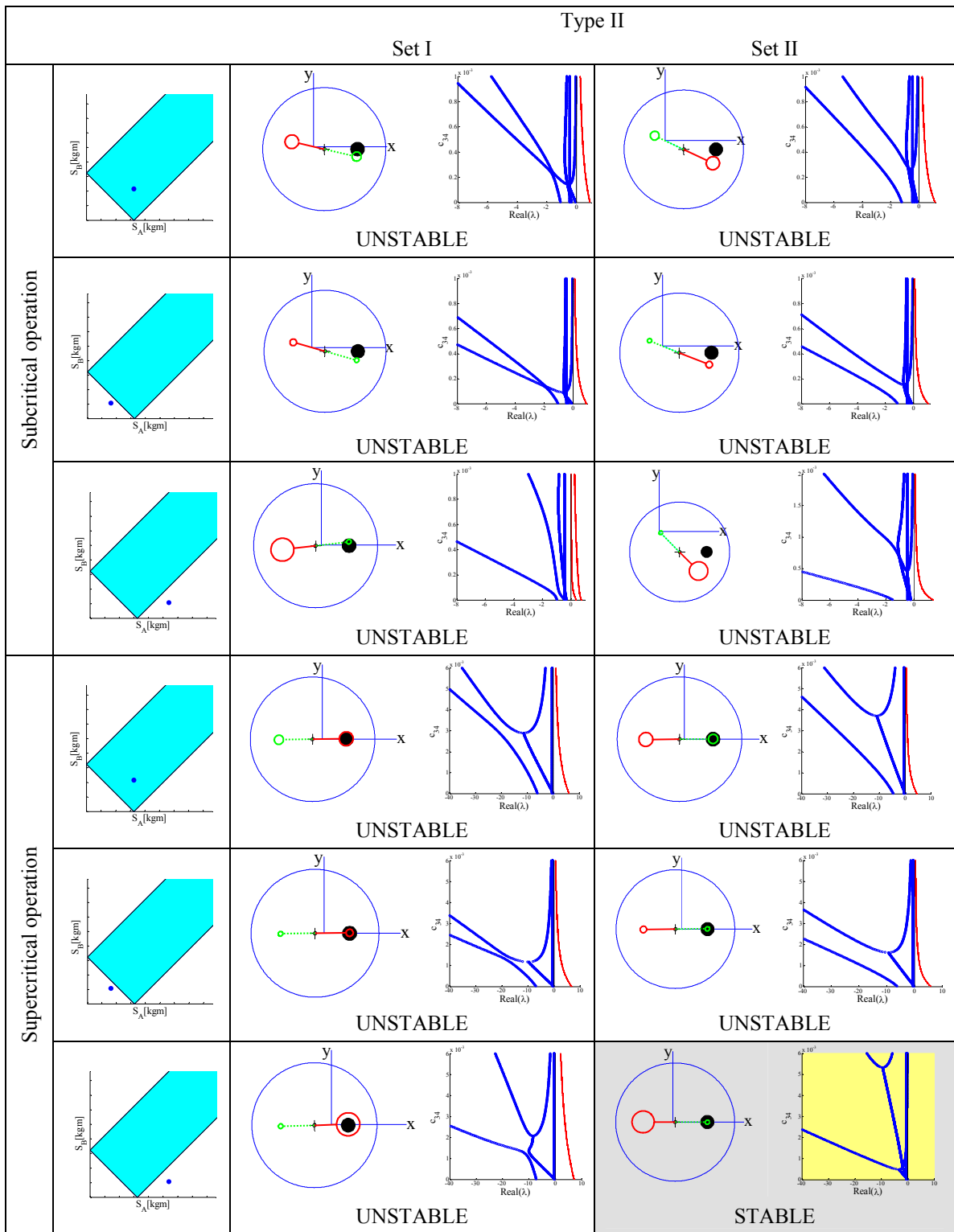


Table 3.2 Stability table of Type II singular point

		Type III			
		Set I		Set II	
Subcritical operation					
		UNSTABLE		STABLE	
	UNSTABLE		STABLE		
	UNSTABLE		STABLE		
Supercritical operation					
		UNSTABLE		UNSTABLE	
	UNSTABLE		STABLE		
	UNSTABLE		UNSTABLE		

Table 3.3 Stability table of Type III singular point

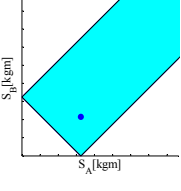
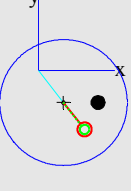
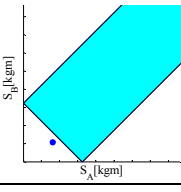
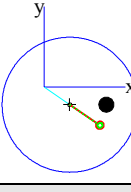
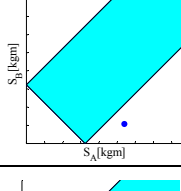
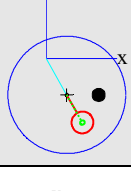
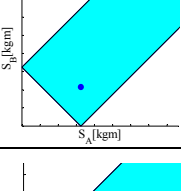
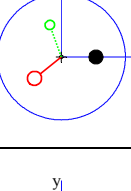
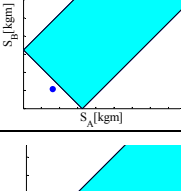
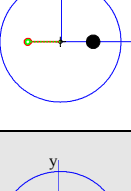
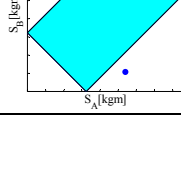
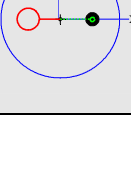
Subcritical operation		Type III: (function of rotor damping)	
		Type III:	
		Type III: (function of rotor damping)	
Supercritical operation		Type I:	
		Type III:	
		Type II: (function of rotor damping)	

Table 3.4 Stable configuration for two operational and three constructional cases

A close examination of the characteristics of the various singular points shows that for a certain level of rotor suspension damping there is a rotor speed domain where certain singular points become complex. Such a result has no physical meaning and the singular points do not exist for those cases.

Figure 3.6 shows a highlighted area in which the singular point is lost for properly oversized pendulums. For supercritical operation, the stable singular point is Type I and it is independent of damping. This configuration is represented by the horizontal upper boundary line of this area. For subcritical operation, the stable singular point is Type III and it is a function of damping. The Type III singular point does not exist when the system is operating slightly below the critical speed and the damping is relatively high.

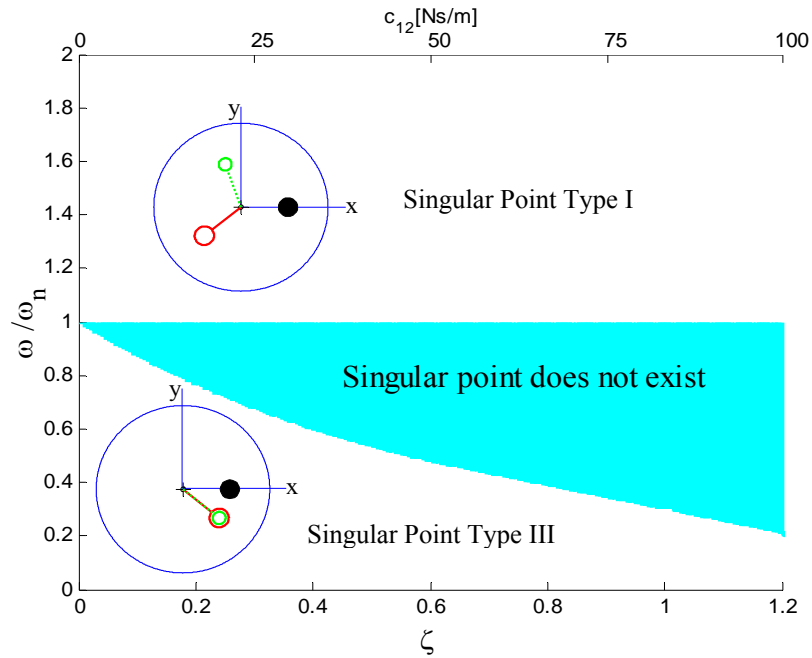


Figure 3.6 Singular point loss as a function of relative damping and operational speed for **properly oversized** pendulums

Figure 3.7 shows the dark area where the singular point is lost for improperly oversized pendulums. For supercritical operation, the stable singular point is Type II and for subcritical operation the stable singular point is type III. Both are a function of damping. The damping dependence results in a singular point loss near the critical speed for cases with a relatively high rotor damping.

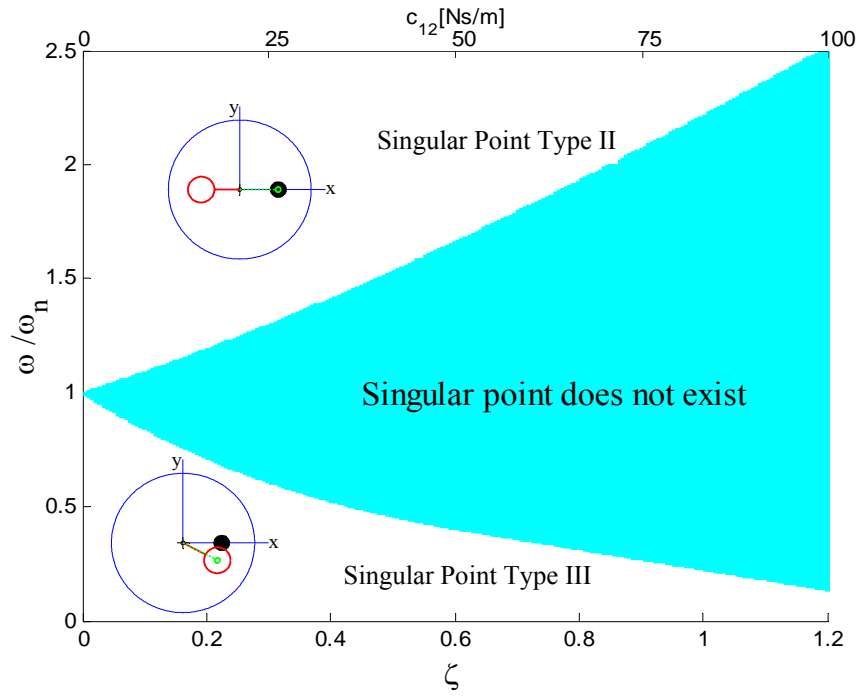


Figure 3.7 Singular point loss as a function of relative damping and operational speed for **improperly oversized pendulums**

Table 4 shows that the stable singular points for relatively undersized pendulum combinations have no damping dependence. This means there is no singular point loss for any operational speed or rotor damping.

In summary, for each of the six cases, there is only one stable singular point. For subcritical operation, only the Type II singular point is stable regardless of location within the relative balancing areas. When the pendulums are oversized, either properly or improperly, relative to the mass imbalance the singular point is a function of damping when the system is operating subcritically. When the pendulums are undersized and the rotor system is operating subcritically, there is no damping dependence.

For supercritical operation, if the pendulums are undersized relative to the mass imbalance the stable singular point is damping independent. When the pendulums are oversized, the stable singular point is Type III and is independent of damping. Improperly oversized pendulums for supercritical operation have a stable Type II singular point which is damping dependent.

3.2 EXPERIMENTAL INVESTIGATION

3.2.1 Pendulum Balancer Experimental Facility

In order to gain detailed insight into the dynamic characteristics and performance of a pendulum balancing system, an experimental facility was designed, fabricated and used for a series of tests. The design of this test rig is such that the weights of the pendulums can be changed while maintaining the same lengths.

Figure 3.8 shows a side view of the entire experimental system. The disk rotation is in the horizontal plane. It is supported by a base plate (5) which is mounted on the shaft of a DC motor (11). The DC motor is supported by a column attached to the ground with a flexible joint. This vertical column is supported from in the horizontal (x and y) directions by springs attached at their opposite ends to fixed supports. This arrangement allows the disk to move in nearly horizontal plane with minimal friction.

Figure 3.9 shows a top-view and Figure 3.10 a side view of the pendulum assembly. In these figures, the shaft of the pendulums (1) and the pendulums themselves (2) and (3) can be seen. Each pendulum is attached to an aluminum disk and supported at the center by two small ball bearings. The pendulums can be locked at the 0 and 180° positions by plastic pins (6) to the frame of the pendulum assembly (4) when the system is stopped. The motion of the pendulums is regulated by a damping system, which consists of two magnet magazine rims (9) which can accommodate up to 12 small rear earth magnets (10). One of the damping magazines is placed beneath the bottom pendulum and the other is placed above the top pendulum. Between the pendulums there is a steel magnetic field guide (12). The pendulums, the damping rims and the magnetic field guide comprise a sandwich structure. This arrangement generates eddy currents inside the aluminum disk

of each pendulum, producing a velocity proportional damping force that can be controlled by the number and the polarity of the magnets (10). The pendulum assembly (4) is fixed to the base plate (5) by two bolts from underneath. The gross imbalance of the system center of mass is set by adjusting the brass weights (7, 8), M_p , and its radial position, P_3 . Weights (7) are basically identical brass nuts on threaded radial rods. When these weights (7) are twisted to the base (showed on Figure 3.9) and the auxiliary mass imbalance (8) is removed from the system the rotor is balanced because the main brass weights (7) are counterbalancing each other. By changing the location of one of these brass weights the desired mass imbalance can be added to the rotor system.

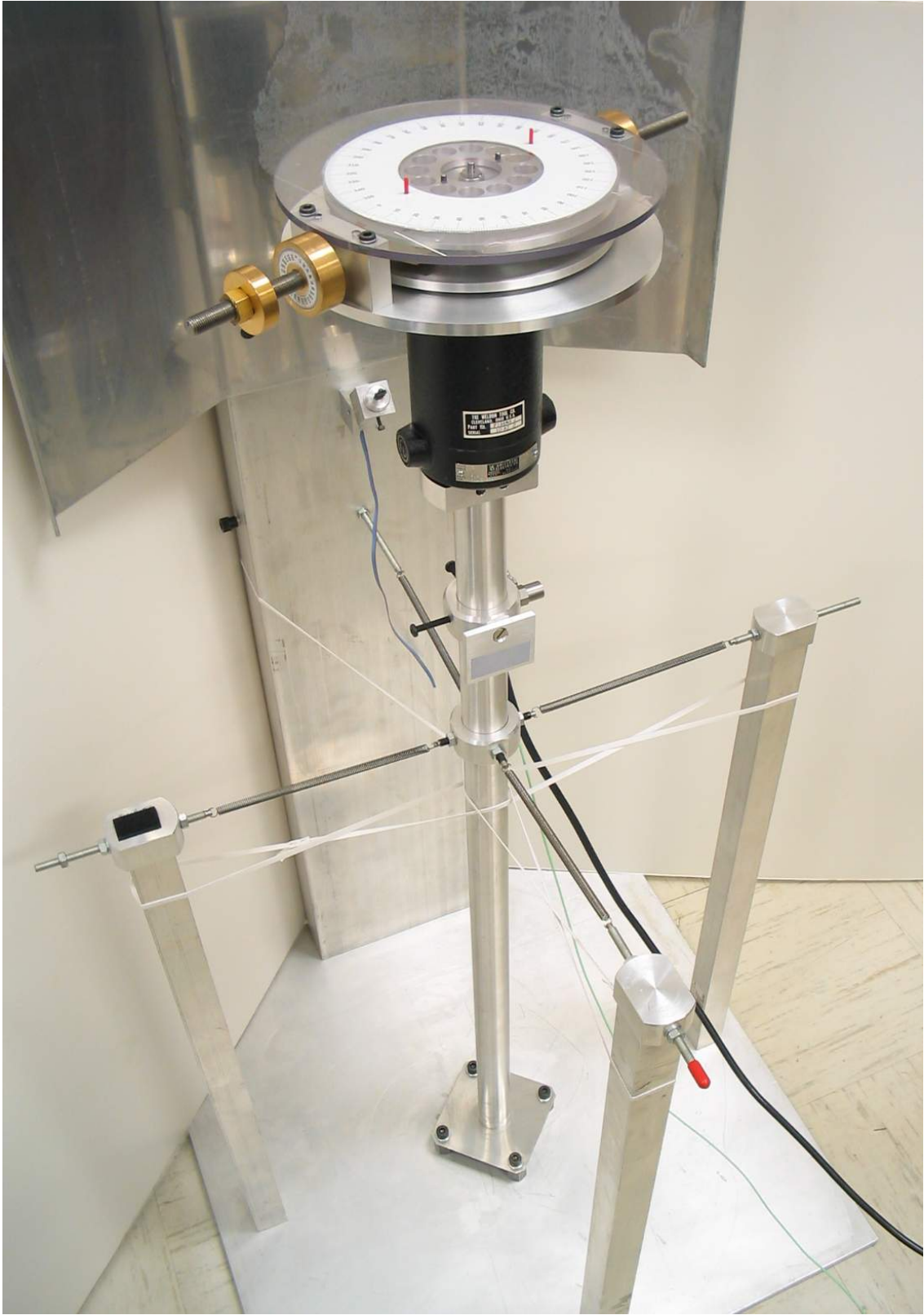


Figure 3.8 The side view of pendulum balancer experimental facility

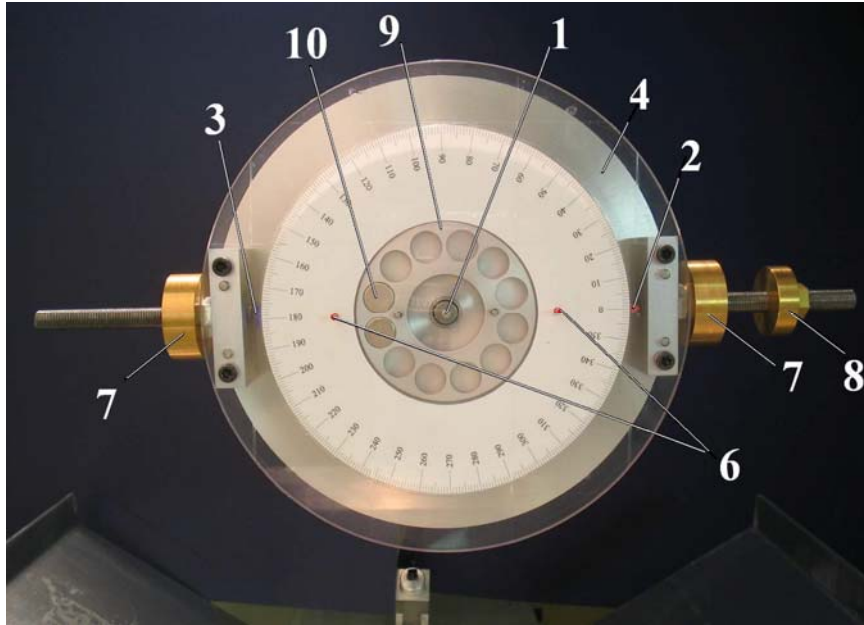


Figure 3.9 Top view of pendulum balancer experimental facility

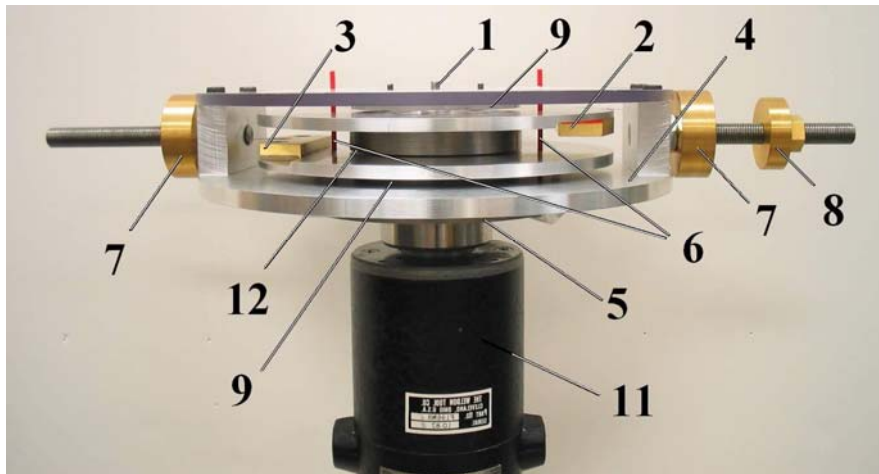


Figure 3.10 Side view of pendulum assembly

Using this pendulum balancing facility, a series of experiments were conducted to validate the analytical results obtained in the previous section. The details and results of these experiments are presented in the following sections.

3.2.2 Experimental validation for non-identical pendulums

For the first series of experimental measurements, the facility was equipped with two non-identical pendulums. The parameters of the pendulums were not changed. But, the magnitude of the rotor imbalance was adjusted by changing the radial position of the brass weight. In this way, the three relative balancing areas were investigated for both subcritical and supercritical operation.

Subcritical operation

As shown in Table 4, for subcritical operation only the Type III singular point is stable regardless of balancing area. For this configuration, the center of rotor will have a steady-state whirling motion even for zero mass imbalance. The analysis results are shown with a continuous line on Figure 3.11, along with the results from the experimental measurements. The horizontal axis is the first moment of the mass imbalance, S_p , and the vertical axis is the vibration amplitude.

In similar fashion, Figure 3.12 also shows the analytical and experimental results but the vertical axis represents the steady-state position of the pendulums. The “circle” symbols represent pendulum “A” which has the higher first mass moment, S_A , compared to pendulum “B” which is represented by the “x” symbols. The experiments show that the pendulums stayed together regardless of the location of the system within the relative

balancing areas, which tended to verify quite well the previously described analysis results for subcritical operation.

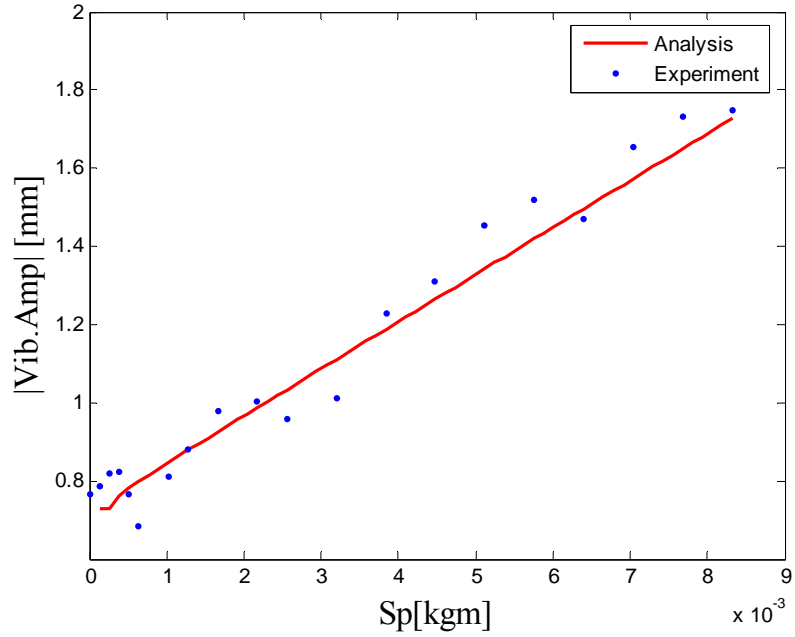


Figure 3.11 Analytical and experimental results for the amplitude of vibration (subcritical operation)

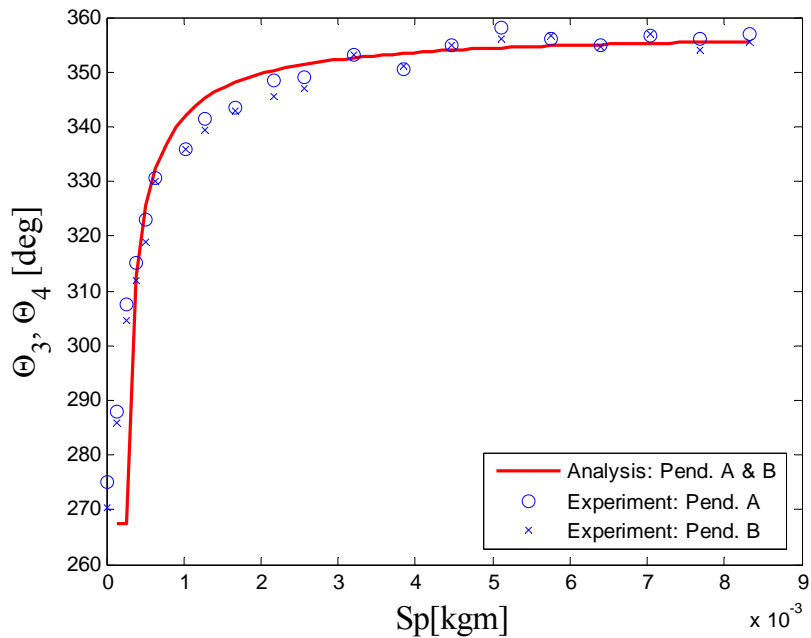


Figure 3.12 Analytical and experimental results for the position of pendulums
(subcritical operation)

Supercritical operation

In contrast to the situation just described for subcritical operation, it is important to distinguish the three relative balancing areas for supercritical operation. As summarized in Table 3.4, for supercritical operation each relative balancing area has a different type of stable singular point. Figure 3.13 and Figure 3.14 show the three relative balancing areas and the transition regions using five small relative balancing area plots. For both the analytical results and for the experimental results described, the pendulum parametric combination is held constant and the mass imbalance was varied. This is why the point of pendulum combination shown is at the same location on all of the relative balancing plots, while the ABCD open area changes.

The first configuration that will be considered is for low mass imbalance, which results in the pendulums being improperly oversized relative to the mass imbalance. This

situation is represented by the leftmost section of Figure 3.13 and Figure 3.14. The pendulums do not have the same first mass moment, and cannot properly counterbalance each other. This results in a stable Type II singular point, with the rotor engaging in a steady-state whirling motion. As the mass imbalance is increased, the rotor vibration amplitude decreases until the configuration transitions to a properly oversized condition in which the steady-state rotor vibration ceases.

The middle section of Figure 3.13 and Figure 3.14 shows the results for pendulum combinations that are properly oversized. The relative balancing area plot shows the point of pendulum combination on the $S_A S_B$ plane is inside the ABCD rectangular area. For this configuration, the Type I singular point is stable.

As the mass imbalance is increased further, the pendulums do not have sufficient balancing capability to properly compensate and the pendulum combination is undersized relative to the mass imbalance. The pendulums come together opposite to the mass imbalance, resulting in a stable Type III singular point. The pendulum system is able to counterbalance only part of the mass imbalance. In this case, if the mass imbalance is increased further, the rotor vibration amplitude increases also.

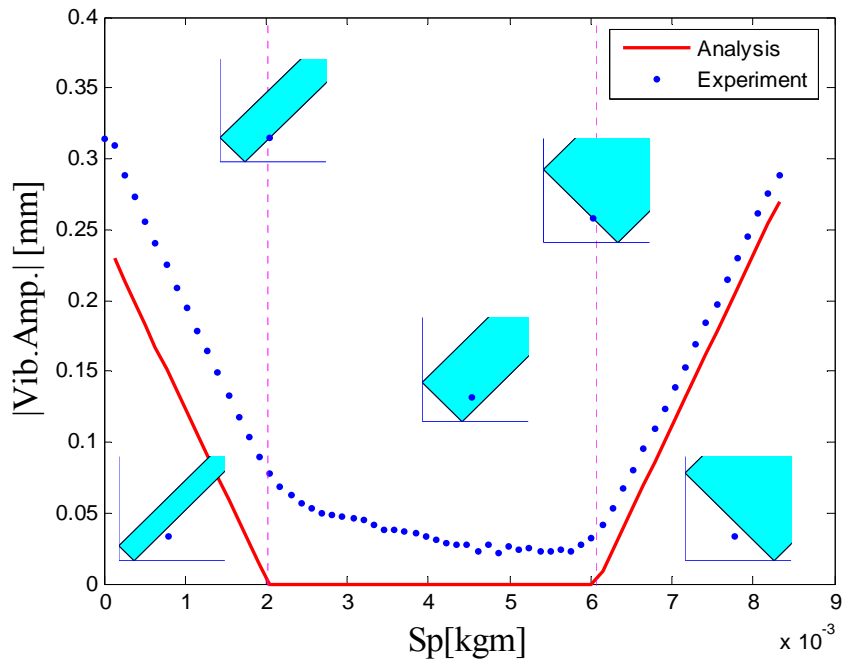


Figure 3.13 Analytical and experimental results for the amplitude of vibration
(supercritical operation)

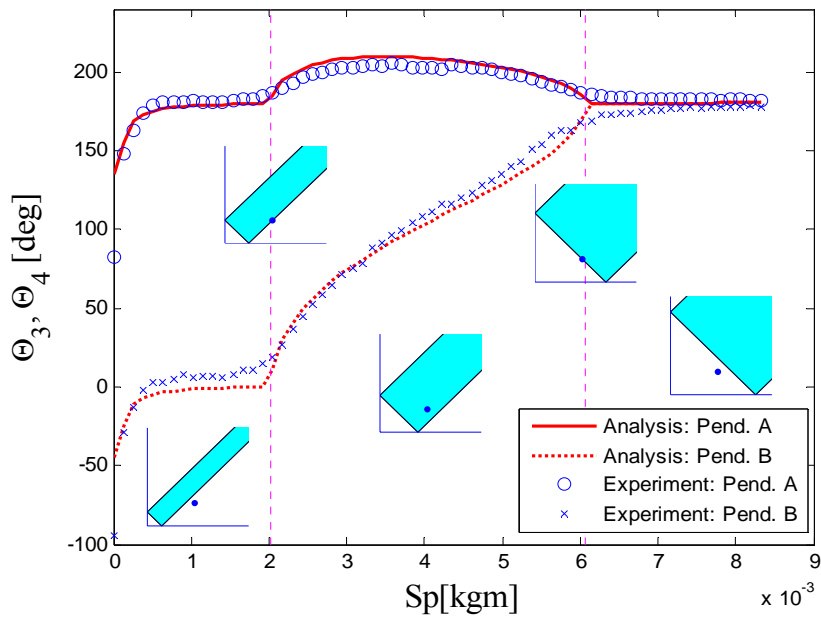


Figure 3.14 Analytical and experimental results for the position of pendulums
(supercritical operation)

3.2.3 Numerical and Experimental validation

In this chapter the result of numerical simulation and experimental measurements are discussed and compared. After several repeated measurement the system parameters were identified. These parameters were used as input parameters of simulations.

Both in the numerical simulation and the experimental measurement the after the startup a proper amount of time was spent to let the transients die out. During this time the pendulums were locked at their base position 0° and 180° . From a balancing point of view, this initial position of pendulum would be neutral if the pendulums had the same first order moment of inertial. This part of research investigated non identical pendulums with different first order moment of inertia. In the numerical simulation and in the experiment initially the pendulum, with higher first moment of inertia was locked at 0° location. This initial configuration added extra imbalance to the system and resulted higher amplitude of vibration. The results of numerical simulation and the experimental measurement the logged coordinates $\Theta_{1..4}$ showed in time from prior pendulum release 3 seconds.

The comparison of numerical simulation and experiment had resulted in quite similar system response for pendulum release proving the success of the model development and system parameter identification.

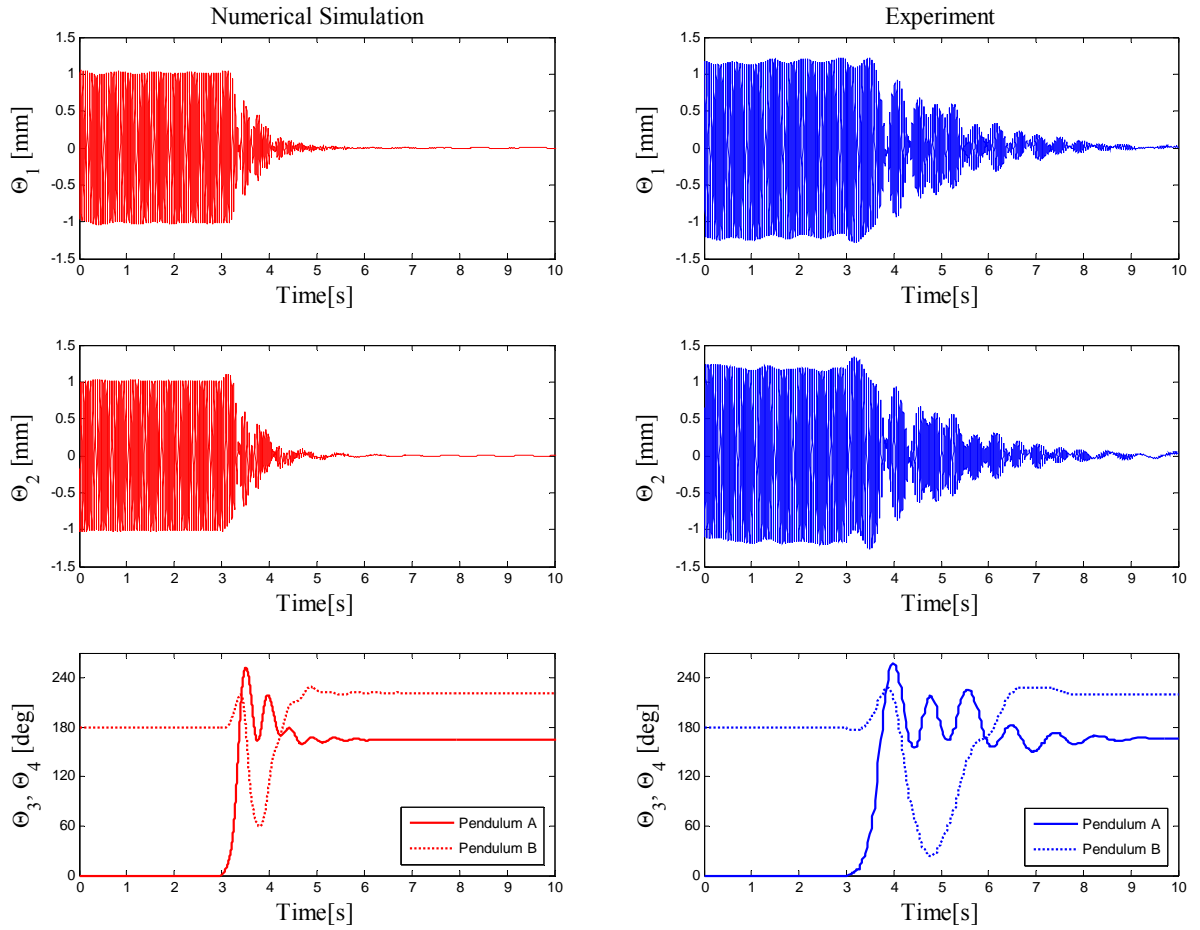


Figure 3.15 Results of numerical simulation and experimental measurement of two-non-identical pendulum

Special case: Identical pendulums

Now, consider the special case in which the pendulums are identical. For such a configuration, the pendulums can counterbalance each other even if there is no mass imbalance in the rotor system. So, the improperly oversized condition cannot exist and there are only two relative balancing areas – (1) properly oversized, and (2) undersized relative to the mass imbalance. Figure 3.16 and Figure 3.17 show these two domains separated by a vertical dash line. On the leftmost side, the pendulums are properly oversized. For this configuration, the Type I singular point is stable and the center of the rotor is not vibrating. On the rightmost side, the rotor mass imbalance is beyond the balancing capability of the two pendulums and the system is undersized. The Type III singular point is stable and the center of the rotor moves on a steady-state circular path. The pendulums overlap each other in an angular location opposite to that of the mass imbalance and partially counterbalance the system. For the case of identical pendulums, the “wishbone” shaped section of the curve in Figure 3.17 is symmetric, as compared to the non-symmetric appearance of the similar region for the non-identical pendulum system, as shown in Figure 3.14.

An interesting phenomenon can be observed in the responses illustrated by Figure 3.16 and Figure 3.17. The first pendulum, indicated by an “x”, generally settles in the location described by the upper curve and the pendulum, indicated by an “o”, generally settles in the location represented by the lower curve of Figure 3.17 as the mass imbalance is increased. However, the two pendulums occasionally switch positions, with the “x” pendulum associated with the lower curve and the “o” pendulum associated with the upper curve. Inspection of Figure 3.16 shows this switching behavior results in an

abrupt change in the magnitude of the rotor vibration. This is in spite of the fact that the pendulums are theoretically identical and should be interchangeable. However, in practice the pendulums are not identical and have some small differences due to the fabrication process. These differences produce the observed sensitivity to the switching behavior described above, which is itself a result of initial conditions for the experimental system, which are random for every startup of the pendulums. From a balancing point of view, these switched positions are not equivalent because the residual mass imbalance is different for the two cases. However, as the mass imbalance of the system is increased to a sufficiently high value (around $S_p = 0.005[\text{kg}\cdot\text{m}]$ for the experimental system) this sensitivity to initial conditions disappears and the settled positions of the pendulums are consistent and appear independent of the initial conditions.

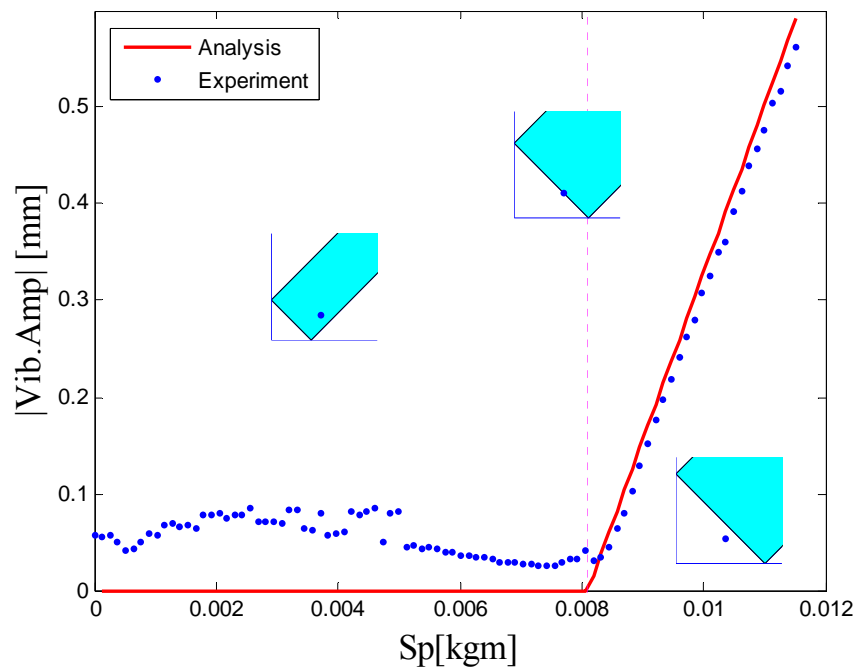


Figure 3.16 Analytical and experimental results for the amplitude of vibration
(supercritical operation)

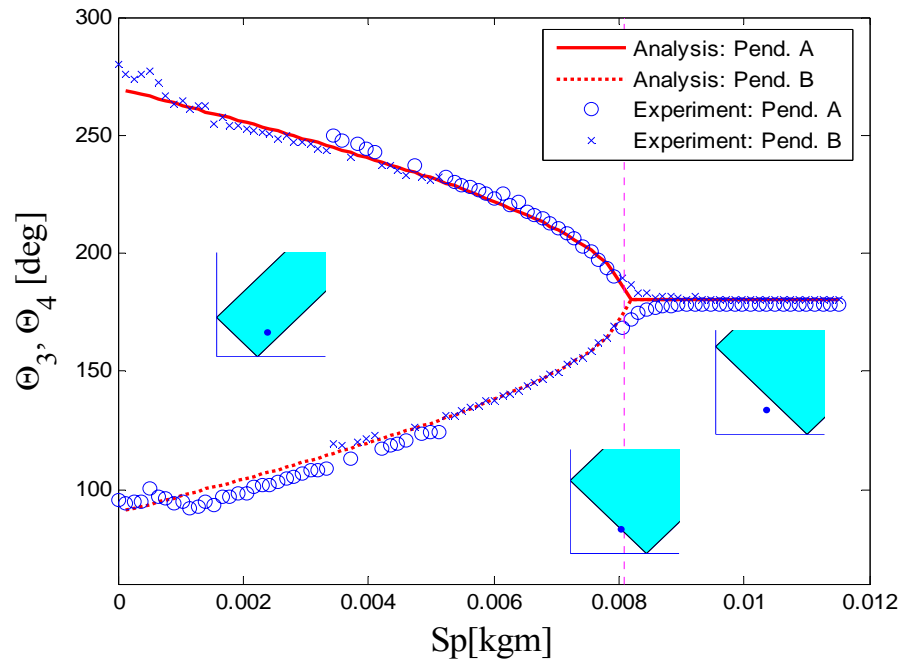


Figure 3.17 Analytical and experimental results for the position of pendulums (supercritical operation)

Numerical and Experimental validation

In this chapter, the result of numerical simulation and experimental measurements are discussed and compared in similar fashion as it was showed for non-identical pendulums. Because of the application of identical pendulums, the initially locked pendulums had no effect on the level of mass imbalance. They simple counterbalanced each other. The results of numerical simulation and experimental measurement are summarized in Figure 3.18.

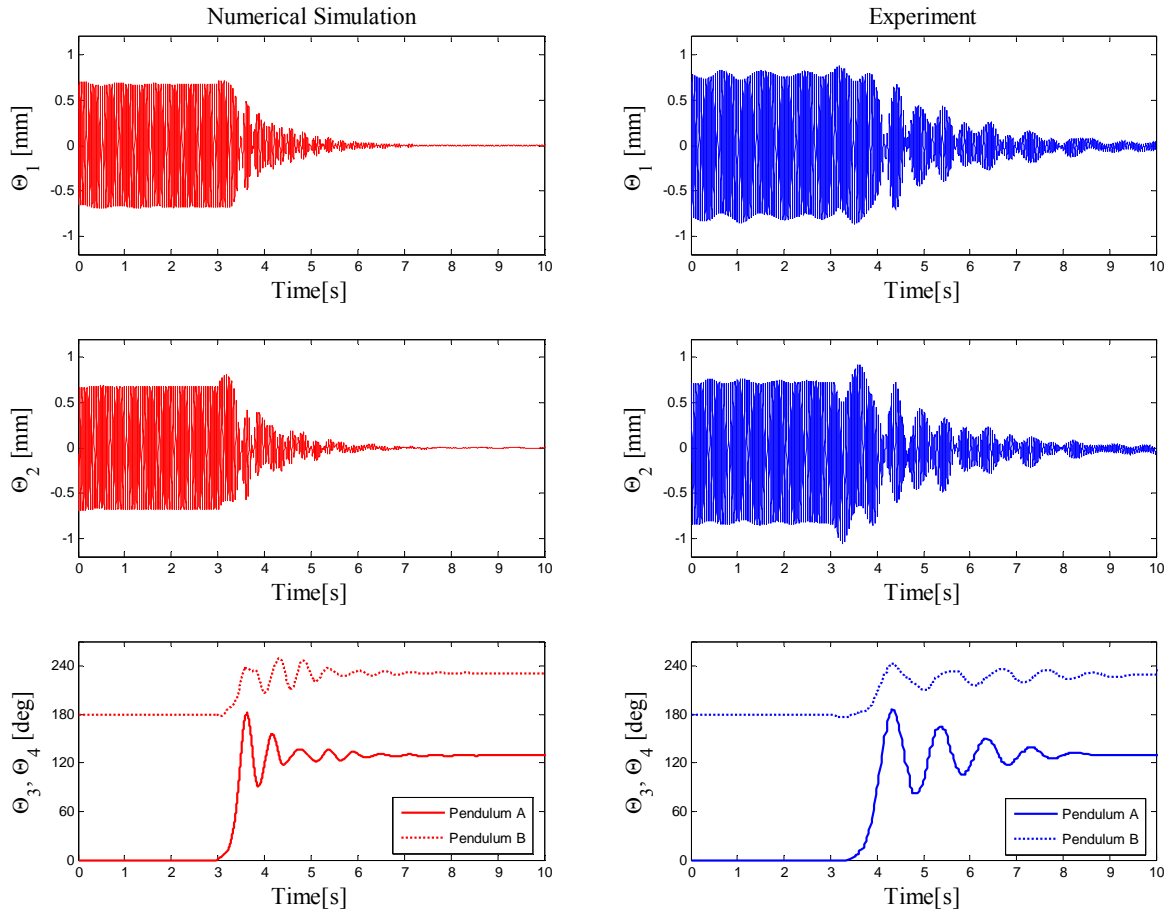
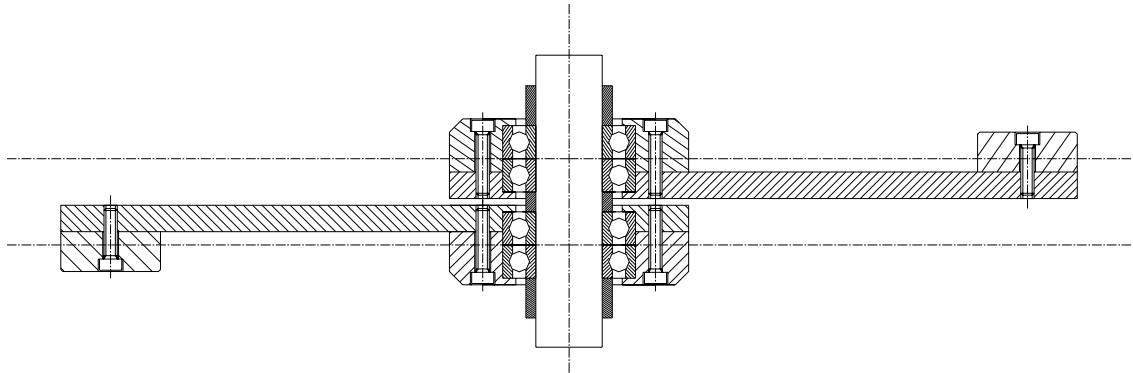


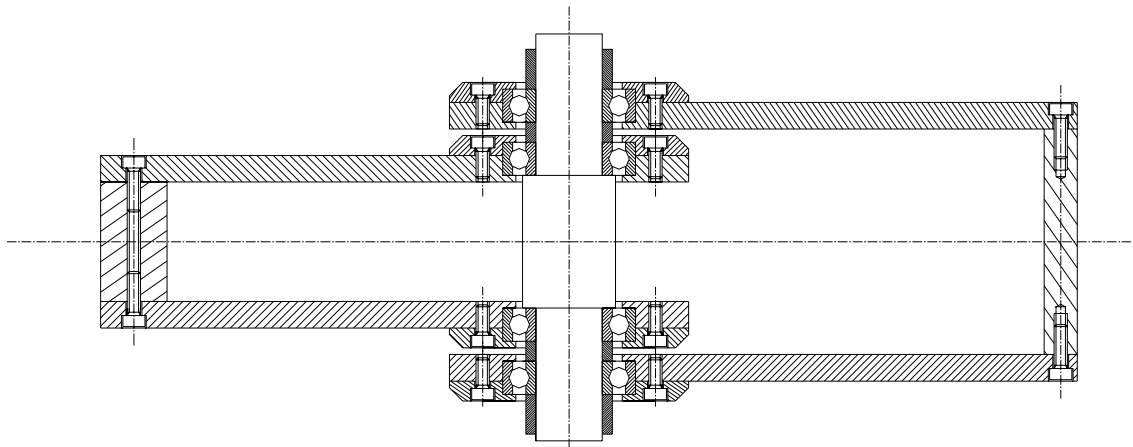
Figure 3.18 Results of numerical simulation and experimental measurement of two-
identical pendulum

It is important to notice the learned property of identical pendulums is also valid for pendulum combinations where the pendulums are not physically identical but they have a same first order moment of inertia. The value of this discovery is important from engineering point of view.

Two pendulums can be manufactured to be quite identical, but the CG of these two pendulums never will move on the same plane as it is shown by Figure 3.19.a. These pendulums will produce a dynamic imbalance on the rotor as they are rotating around the shaft. Figure 3.19.b. shows another (better) possible design solution based upon the above results. In this case, each of the pendulums has a different length but they have the same first order moment of inertia around the axis of the shaft. In this design, the CG of each individual pendulum moves in the same plane and will not dynamically imbalance the system. This also provides a better force distribution on the bearing system. The experimental setup had similar design to the engineering design showed by Figure 3.19.a.



a.



b.

Figure 3.19 Possible design solutions for pendulum balancing systems

3.3 Influence of Pendulum Shaft Misalignment

It was demonstrated analytically above that a pendulum self-balancing system is ideally capable of exact radial balancing. However, imperfections in the fabrication and assembly of such a system will compromise some of the modeling assumptions that provided this result. One major imperfection is shaft misalignment, which can easily occur due to improper design, fabrication and assembly. In the following sections, the effect of misalignment between the center of rotation of the pendulums and rotor shaft is examined in detail.

Figure 3.20 illustrates the basic configuration for a system with non-centered pendulums. The position of the center of the shaft is described in a disk-fixed rotating coordinate system. The shaft of the pendulums is shifted from the center of the rotor by an amount, R_C , in the Θ_1 direction.

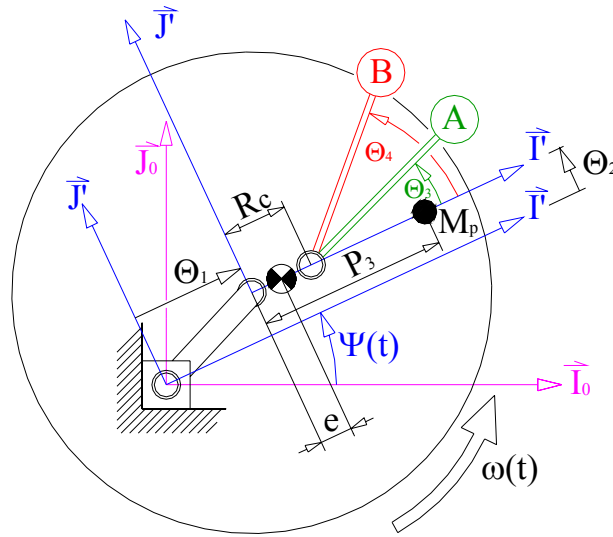


Figure 3.20 Mathematical model of rotor system with non-centered pendulums

Using this model, a series of simulation studies were performed for a variety of R_C . In order to better generalize the results, the non-dimensional parameter, ρ_C and α are used.

$$\rho_C = \frac{R_C}{e}, \quad \text{Where:} \quad e = \frac{P_3 M_P}{M_D + M_P} \quad (3-34)$$

$$\alpha = \frac{|A_{PR}|}{|A_{PL}|} \quad (3-35)$$

R_C is the offset of the pendulum center of rotation and e is the imbalance eccentricity of imbalanced rotor system.

Where A_{PR} is the amplitude of the steady state vibration with the pendulums free to rotate and A_{PL} is the amplitude of vibration with the pendulums locked at the 0° and 180° positions, respectively.

Figure 3.21 and Figure 3.22 summarize the results of these simulations. The angular velocity of the rotor system is higher than the first critical speed of the system, which is a basic requirement for this type of passive balancing system to work properly. In the numerical simulations, the operational speed was set at almost 20 times higher than the first critical speed and the damping ratio for the rotor suspension was small, which resulted in the frequency transfer function having a magnitude close to one.

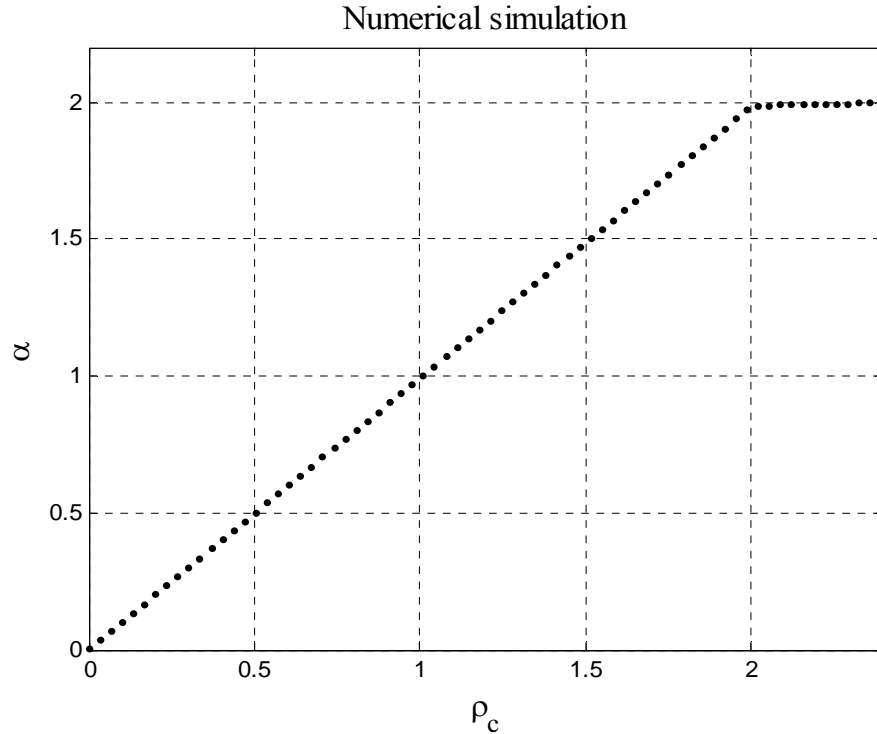


Figure 3.21 Simulation results showing the non-dimensionalized rotor vibration level for the system with pendulum shaft misalignment

The upper part of Figure 3.22 shows the angular positions of the pendulums (Θ_3 and Θ_4) as a function of ρ_C . The lower part of this figure shows the closest relative angular distance between the two pendulums. Examination of this figure shows that when ρ_C is zero, the pendulums are close to the 180° position and almost overlapping one other, which indicates that the radial imbalance of the system is only slightly less than the balancing limit of the pendulums. At $\rho_C = 1.0$, the two pendulums are the farthest apart at 180° . For higher values of ρ_C , they move closer together and for $\rho_C = 2.0$, the pendulums converge to overlapping angular positions and stay in that configuration for further increases of ρ_C . At this ρ_C value, there is a break-point in the vibration level of the center

of the rotor (as shown in Figure 3.21). The rate of increase for the vibration amplitude changes abruptly and almost settles into a plateau.

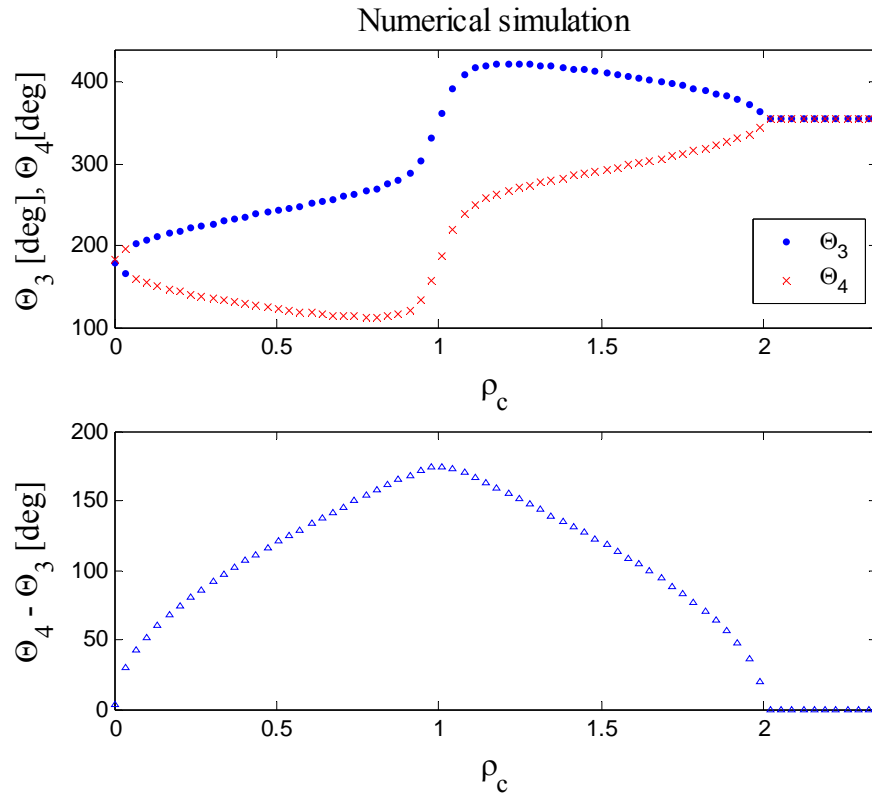


Figure 3.22 Simulation results showing the absolute and relative positions of the pendulums for the system with pendulum shaft misalignment

3.3.1 Experimental investigation of pendulum shaft misalignment

Pendulum Balancer Experimental Facility

To gain detailed insight into the dynamic characteristics and performance of a pendulum balancing system with misalignment shaft the same experimental facility was used that was described in chapter 3.2.1. The design of this test rig is such that the pendulum rotation center could be offset in the Θ_1 direction from the center of the rotor by an amount R_C .

Implementation of shaft misalignment

The pendulum assembly (4) is fixed to the base plate (5) by two bolts from underneath. When these bolts are loosened, the pendulum assembly can be shifted in the Θ_1 direction by an amount, R_C , while still maintaining the shaft of the pendulums parallel to the shaft to the DC motor (11). However, shifting the pendulum assembly and the structural parts surrounding the pendulums, itself also produces an additional mass imbalance, which is undesirable for the purposes of the present study. This imbalance can be offset by adjusting the brass weights (7) in the radial direction. The gross imbalance of the system center of mass is set by adjusting the brass weight (8), M_P , and its radial position, P_3 .

Description of experimental procedure

Using the pendulum balancing facility described previously, a series of experiments was conducted to validate the simulation results obtained in the previous section and to gain further insight into the influence of specific imperfections and non-idealities on the dynamic performance of such passive balancing system. The steps in the testing process are described below:

1. Pendulums are locked at 0° and 180° respectively with plastic pins
2. The pendulum assembly is shifted by an amount R_C relative to the base plate
3. The rotor was spun-up to the test operating speed and balanced.
4. A specific gross mass imbalance was set and the pendulums were released
5. The rotor was spun-up to the test operating speed and three sets of data were measured and recorded:
 - The magnitude of vibration [mm], measured by a laser displacement system
 - The final angular position of each pendulum Θ_3 and Θ_4 [deg]

Figure 3.23 and Figure 3.24 summarize the results for a typical set of experiments, which are quite similar to the predicted behavior from the simulation results (Figure 3.21 and Figure 3.22). Inspection of these figures shows that increasing the shift of the pendulums, ρ_C , produces a proportional increase in rotor vibration level until the pendulums are overlapping one other. At $\rho_C = 2.0$, there is again a break-point, after which further shifting of the pendulum axis has only a slight effect on the rotor vibration, in a fashion similar to that observed in the numerical simulations.

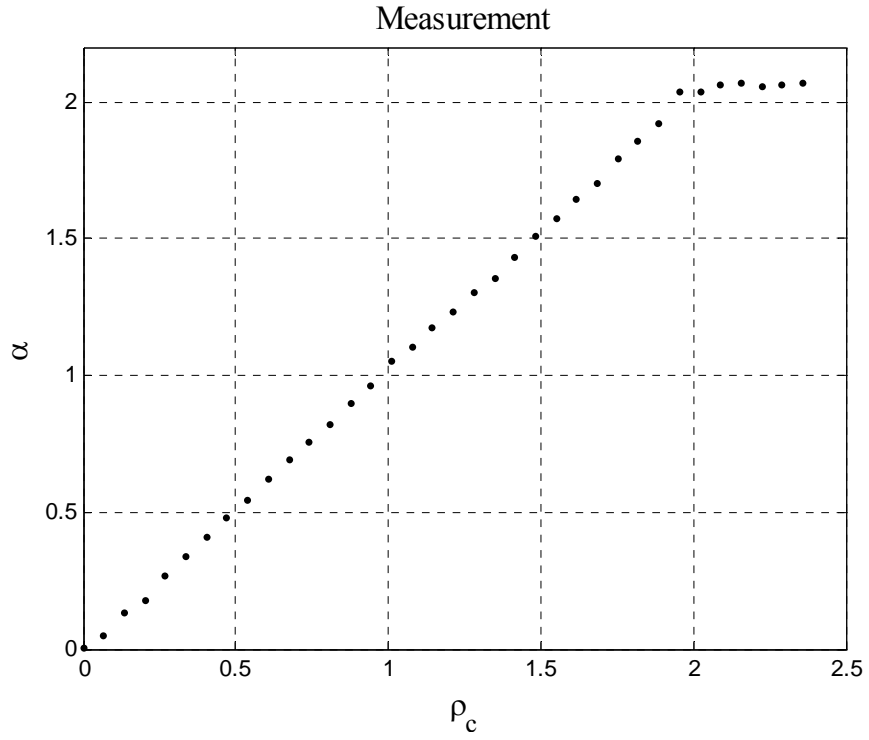


Figure 3.23 Experimental results showing the non-dimensionalized rotor vibration level for the system with pendulum shaft misalignment

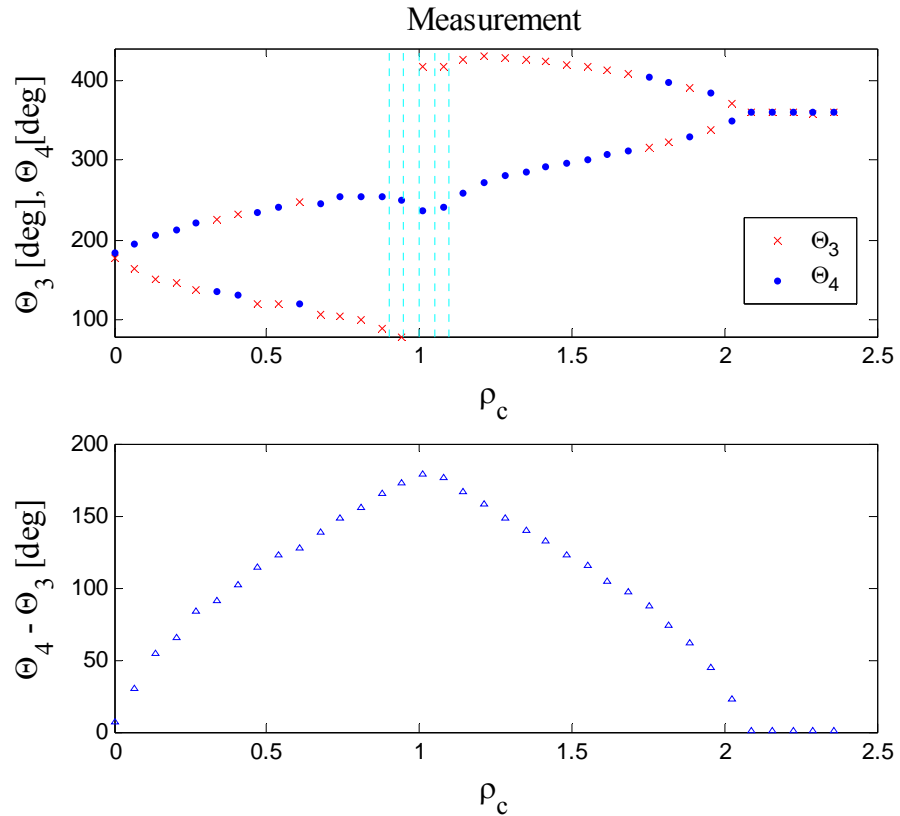


Figure 3.24 Experimental results showing the absolute and relative positions of the pendulums for the system with pendulum shaft misalignment

Top part of Figure 3.24 shows the absolute position of the pendulums and the bottom part of this figure shows the relative position to each other. Again, obvious similarity can be found between these experimental results and the numerical simulation results shown in Figure 3.24. In particular, the lower graphs (showing the relative position of pendulums) are almost identical. The upper graphs are also similar. However, for values of ρ_c near 1.0, the experimental and simulation results differed for the absolute position of the pendulums. This area is marked by dashed lines on the upper part of Figure 3.24. Since the relative angular velocity (ω/ω_n) is nearly 20 and the damping ratio

is quite low, the transfer function is close to 1. Thus, the center of rotation is very close to the CG of the imbalanced rotor system, which is also the location of the pendulum when ρ_C is near 1.0. This means the center of pendulums is near the source of the centrifugal force field. So at this location, the relative position of the pendulums will be 180° but the absolute position of the pendulum configuration is indeterminate from the perspective of balancing the system. When the suspension point of the pendulums is moved slightly from the CG of the unbalanced rotor, the relative distance of the pendulums slightly decreases and this neutral state will change. Thus, small effects that are not included in the simulation model but that are present in the experimental facility, such as rolling resistance and friction, will tend to produce a different absolute position of the pendulums from that predicted by the simulations. This explains the differences between the numerical simulations and the experimental measurements in the region where ρ_C is near 1.0.

3.3.2 Experimental comparison of the sensitivity and consistency of ball and pendulum balancers

This investigation begins by considering the effects of rolling resistance. Previous investigators have noted that rolling-resistance and dry friction are significant problems that tend to degrade the consistent performance of ball balancer systems [12], [13]. However, previous work has not considered the influence of such effects on pendulum balancers. A basic question is: *Are pendulum balancers less susceptible to such effects (rolling resistance and dry friction) than ball balancer systems?* Accordingly, in the following sections, a comparison is made between the performance of these two types of systems with the goal of providing some insight into this question. Two comparable test rigs are developed, one with a ball-balancer system and the other with a pendulum balancer system, and experimental results from each are compared. The observed results are discussed and some insights into the expected relative performance of such systems are presented.

Ball Balancer Experimental Facility

Photographs of the ball balancer test facility are shown in Figure 3.25 (side view) and Figure 3.26 (top view). The same central suspension was used as for the pendulum balancer described earlier. This suspension allows the center of the disk to move in a nearly horizontal plane without significant friction.

Distinct from the pendulum balancer system, the moving elements are two steel balls (2, 3) guided by a cylindrical channel (4) (also a secondary channel (5) can be seen for later investigations) machined in an aluminum disk (1). The channels are covered by a

plexi-glass cover (7) for safety reasons and to support the dial plate. The rotating disk and the plexi-glass cover together are well balanced. The imbalance is generated by component (6) which is a brass block whose position in the radial direction can be adjusted.

Ball Balancer Experimental Results

Using this facility, a series of experiments was performed to evaluate the performance and consistency of this system. The experimental test procedure consisted of the following steps.

First, the balance state of the rotor was set using the following procedure. The steel balls were locked at $\pm 30^\circ$ (as shown in Figure 3.26) and the system was balanced by adjusting the radial position of the brass block (6). Accordingly, the magnitude of the imbalance and the desired settling position of the balancing balls (when released) are precisely known.

Next, the balancing balls were released and repeated startups were performed without changing any of the other physical properties of the system. For each startup, the system was started from rest and was driven until the rotor disk had reached 1500 rpm. The amplitude of the steady-state vibration and the position of the balancing balls were then recorded.



Figure 3.25 Side view of ball balancer experimental facility

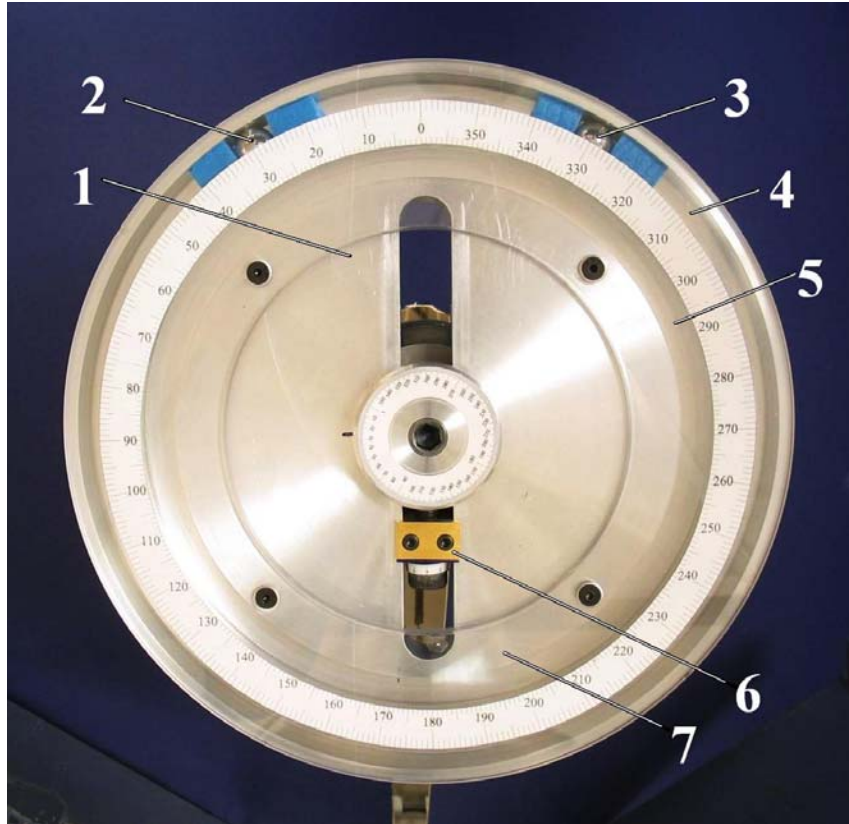


Figure 3.26 Top view of ball balancer experimental facility

Figure 3.27 serves to graphically summarize the results of these experiments. The horizontal axis shows the positions of the balancing balls. Each pair is shown by a different symbol and is connected by a dashed horizontal line. The vertical axis shows the measured amplitude of the center of disk in the Θ_1 direction. The smallest measured vibration level was recorded when the balancing balls were locked at $\pm 30^\circ$. The highest vibration level was recorded when the rotating disk was not equipped with the balancing balls. This level of vibration (0.80475 [mm]) would be the amplitude of the steady state motion of the rotating system without any passive balancing mechanism. For all of the other test cases, the balancing balls tended to reduce the overall vibration but they settled

to different locations each time with a relatively large scattering. The above experiment was repeated with a variety of different sizes and numbers of balls, with similar results.

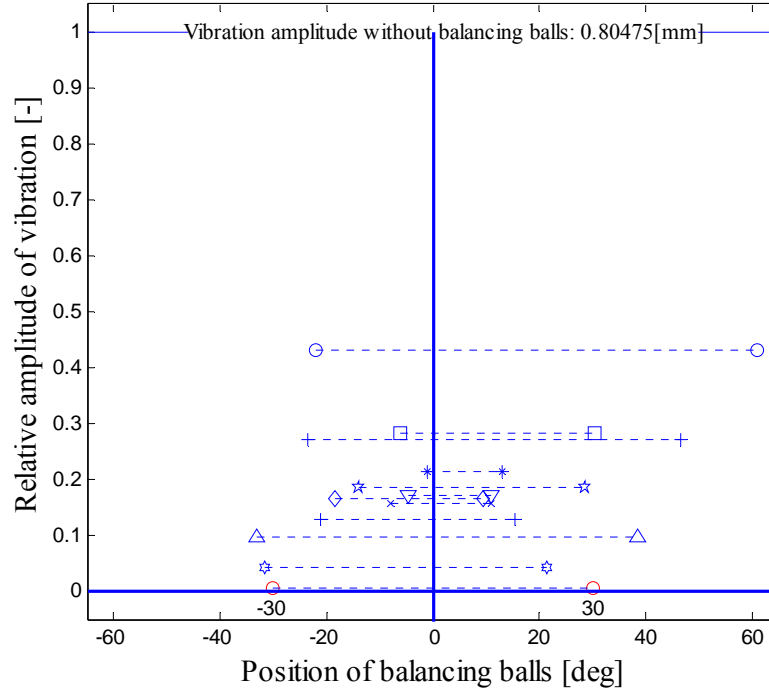


Figure 3.27 The final positions of balancing balls and vibration level for different startups

These results clearly indicated that there are some physical effects that prevent the balancing balls from settling into the proper positions and achieving more consistent results. This effect can be traced to the deformation of the contact point of the ball and channel surface due to the high normal forces generated by the centripetal acceleration and the resulting dry friction. For the specific experimental setup used for the present tests, the mass of each 15[mm] diameter chrome steel ball was 13.8[gram] moving in 114[mm] radius and the material of the channel was alloy 6061 aluminum. This material

and geometrical combination resulted in an approximately 16 [μm] deformations at the ball contact points when the disk was rotating at 1500 rpm.

Figure 3.28 illustrates a graphical explanation of rolling resistance. The deformation of both channel and ball forms a pocket at contact point A and the idealized point-to-point contact becomes a surface as a result of high centrifugal force F_{CF} . This elastically formed pocket changes the direction of constraining force, F_{CS} , that was directed toward the center of rotation in the idealized model. So, the constraining force has a component that tends to oppose the balancing force, F_B . In the ball balancing system that was investigated, the centrifugal force, F_C , is much greater than the gravitational force, mg . Because of this high force ratio, the ball contact motion will primarily be rolling at point A and slipping at point B. Relative motion at the contacting surfaces at point B will result in a friction force, F_F , which also tends to oppose the balancing force, F_B . The action of these combined forces tends to stop the motion of the balancing balls before they reach the complete balancing position, resulting in a nonzero balance state for this system. This remaining mass imbalance produces synchronous vibration, which is thus the indirect result of rolling resistance.

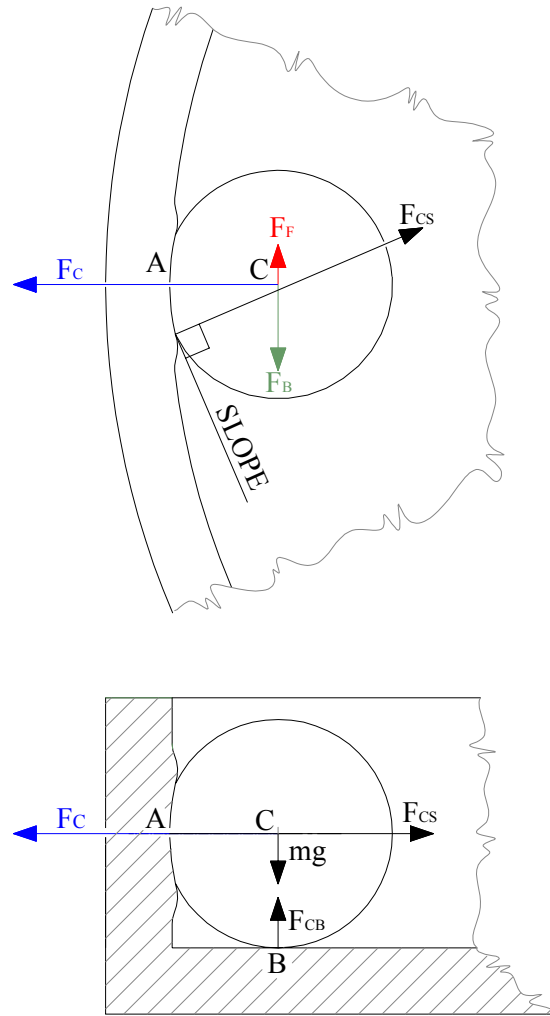


Figure 3.28 Deformation of contact surfaces and force distribution of the balancing ball and channel

Pendulum Balancer Experimental Results

A similar series of experiments were performed for the pendulum balancing system. The rotor was repeatedly started without changing any parameters of the system. The rotor vibration level and the position of the pendulums were captured when the system reached the final speed and exhibited steady-state behavior. The results of these experiments are summarized in Figure 3.29 and Figure 3.30, in a fashion similar to that which was used for the foregoing ball balancer experiments.

In Figure 3.29, the amplitude of the steady-state periodic motion is also shown to illustrate the relationship of the different counterbalancing levels. When the pendulums are locked at the 0° and 180° positions respectively, the overall vibration level of the system is 1.75[mm]. Figure 3.30 shows a closer (zoomed) view of the settled pendulum positions for better insight. A comparison of the results for the ball balancer system and the pendulum balancer system shows that the pendulum balancing system has a much greater consistency.

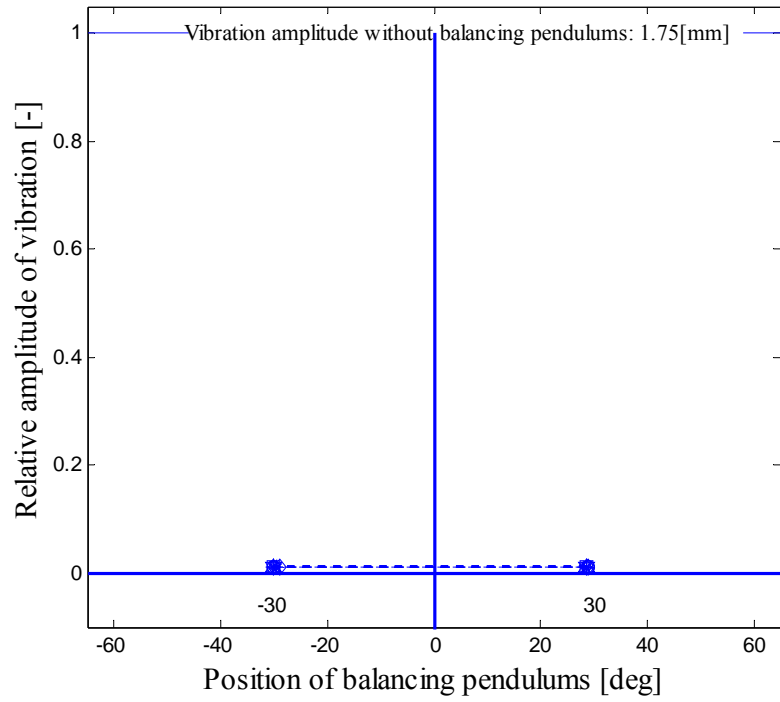


Figure 3.29 The final positions of balancing pendulums and the level of vibration for different startups

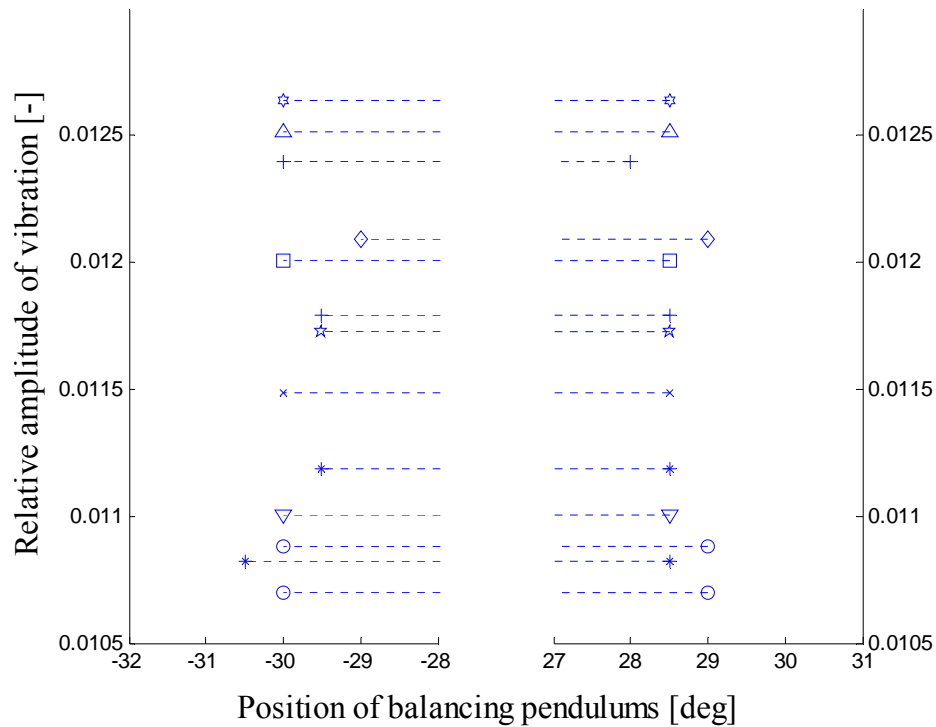


Figure 3.30 The final positions of balancing pendulums and the level of vibration on the zoomed plot for different startups

Figure 3.31 illustrates the force distribution of a pendulum balancer system and of a ball balancer system. F_{RR} is the rolling resistance generated by the deformation of the contact surface, friction and other less significant forces. F_{CF} is the centrifugal force. F_C is the constraint force which guides the moving masses, pendulums or balls, in a circular path. F_B is the balancing force. Inspection of these diagrams show that the pendulum balancing system has a better overall force distribution in the sense that (in general) a larger percentage of the forces are directed toward achieving relocation of the balancing mass. This serves to dramatically improve the overall sensitivity of the pendulum balancer system with respect to a similar ball balancer system. Thus, pendulum balancer

systems tend to be inherently less susceptible to inconsistencies and errors as a result of rolling resistance.

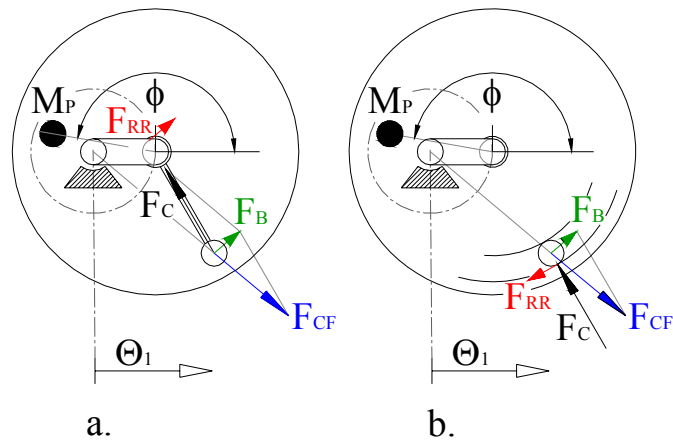


Figure 3.31 Force distribution of pendulum and ball balancer

4 PASSIVE PENDULUM BALANCER WITH NON-ISOTROPIC SUSPENSION

4.1 Analytical investigation

The previous studies have targeted isotropic suspension of rotor system where the spring stiffness and the damping were identical. Identical suspension results two identical natural frequencies. It was demonstrated that the Type I singular point of an isotropic pendulum system showed stability when the system was operating supercritically.

This part of the research has investigated a rotor system equipped with a pendulum balancer and supported from Θ_1 and Θ_2 directions by non-identical springs and dampers. The application of two different supports results in two distinct natural frequencies. The analytical investigation starts with the development of the equations of motion.

$$\frac{d}{dt} \left(\frac{\partial T}{\partial \dot{\Theta}_i} \right) - \frac{\partial T}{\partial \Theta_i} + \frac{\partial V}{\partial \Theta_i} + \frac{\partial D}{\partial \dot{\Theta}_i} = Q_i \quad i = 1, 2, 3, 4 \quad (4-1)$$

Where:

- T = Sum of all kinetic energies
- V = Sum of all potential energies
- D = Rayleigh dissipation function
- Θ_i = Generalized coordinates
- Q_i = Generalized forces

$$\begin{aligned}
T = & \frac{1}{2} \omega^2 \left(S_A (R_{BA} + 2\Theta_1 \cos(\Theta_3) + 2\Theta_2 \sin(\Theta_3)) + \right. \\
& + S_B (R_{BB} + 2\Theta_1 \cos(\Theta_4) + 2\Theta_2 \sin(\Theta_4)) + \\
& + S_P (P_3 + 2\Theta_1) + (M_D + M_{BA} + M_{BB} + M_P) (\Theta_1^2 + \Theta_2^2) + \left. \frac{1}{2} M_D R_D^2 \right) + \\
& + \omega \left(M_{BA} \dot{\Theta}_2 \Theta_1 + S_A \Theta_2 \sin(\Theta_3) \dot{\Theta}_3 + M_P \dot{\Theta}_2 \Theta_1 + \right. \\
& + S_B \Theta_1 \cos(\Theta_4) \dot{\Theta}_4 + S_A R_{BA} \dot{\Theta}_3 + M_{BB} \dot{\Theta}_2 \Theta_1 + M_D \dot{\Theta}_2 \Theta_1 + \\
& + S_P \dot{\Theta}_2 + S_A \dot{\Theta}_3 \Theta_1 \cos(\Theta_3) - S_B \dot{\Theta}_1 \sin(\Theta_4) + \\
& + S_B \Theta_2 \sin(\Theta_4) \dot{\Theta}_4 - M_{BA} \dot{\Theta}_1 \Theta_2 + S_A \dot{\Theta}_2 \cos(\Theta_3) + \\
& + S_B \dot{\Theta}_2 \cos(\Theta_4) - \dot{\Theta}_1 M_D \Theta_2 + S_B R_{BB} \dot{\Theta}_4 - M_{BB} \dot{\Theta}_1 \Theta_2 - \\
& - S_A \dot{\Theta}_1 \sin(\Theta_3) - \dot{\Theta}_1 M_P \Theta_2 \left. \right) + \\
& + \frac{1}{2} (M_D + M_{BA} + M_{BB} + M_P) \dot{\Theta}_2^2 + \frac{1}{2} (M_D + M_{BA} + M_{BB} + M_P) \dot{\Theta}_1^2 + \\
& + \frac{1}{2} S_A R_{BA} \dot{\Theta}_3^2 + \frac{1}{2} S_B R_{BB} \dot{\Theta}_4^2 + S_A \dot{\Theta}_2 \dot{\Theta}_3 \cos(\Theta_3) + S_B \dot{\Theta}_2 \dot{\Theta}_4 \cos(\Theta_4) + \\
& - S_B \dot{\Theta}_1 \dot{\Theta}_4 \sin(\Theta_4) - S_A \dot{\Theta}_1 \dot{\Theta}_3 \sin(\Theta_3)
\end{aligned} \tag{4-2}$$

$$V = \frac{1}{2} k_1 (\cos(\omega t) \Theta_1 - \sin(\omega t) \Theta_2)^2 + \frac{1}{2} k_2 (\sin(\omega t) \Theta_1 + \cos(\omega t) \Theta_2)^2 \tag{4-3}$$

$$\begin{aligned}
D = & \frac{1}{2} \dot{\Theta}_1^2 (c_1 \cos(\omega t)^2 + c_2 \sin(\omega t)^2) + \\
& + \dot{\Theta}_1 \left(c_1 (-\cos(\omega t) \omega \Theta_2 - \sin(\omega t) (\dot{\Theta}_2 + \Theta_1 \omega)) \cos(\omega t) + \right. \\
& \quad \left. + c_2 (-\sin(\omega t) \omega \Theta_2 + \cos(\omega t) (\dot{\Theta}_2 + \Theta_1 \omega)) \sin(\omega t) \right) + \\
& + \frac{1}{2} c_1 (-\cos(\omega t) \omega \Theta_2 - \sin(\omega t) (\dot{\Theta}_2 + \Theta_1 \omega))^2 + \frac{1}{2} c_3 \dot{\Theta}_3^2 + \\
& + \frac{1}{2} c_2 (-\sin(\omega t) \omega \Theta_2 + \cos(\omega t) (\dot{\Theta}_2 + \Theta_1 \omega))^2 + \frac{1}{2} c_4 \dot{\Theta}_4^2
\end{aligned} \tag{4-4}$$

$$Q_i = 0 \tag{4-5}$$

The most general form of the equations of motion are:

$$\begin{aligned}
& -S_A \left(2\omega \cos(\Theta_3) \dot{\Theta}_3 + \sin(\Theta_3) \ddot{\Theta}_3 + \omega^2 \cos(\Theta_3) + \cos(\Theta_3) \dot{\Theta}_3^2 \right) - \\
& -S_B \left(2\omega \cos(\Theta_4) \dot{\Theta}_4 + \cos(\Theta_4) \dot{\Theta}_4^2 + \sin(\Theta_4) \ddot{\Theta}_4 + \omega^2 \cos(\Theta_4) \right) - \\
& -M_P \left(\omega^2 \Theta_1 - \ddot{\Theta}_1 + 2\omega \dot{\Theta}_2 + \omega^2 P_3 \right) + (M_D + M_{BA} + M_{BB}) \ddot{\Theta}_1 + \\
& + c_1 \cos(\omega t) \left(-\cos(\omega t) \omega \Theta_2 - \sin(\omega t) (\dot{\Theta}_2 + \omega \Theta_1) \right) + \\
& + c_2 \sin(\omega t) \left(-\sin(\omega t) \omega \Theta_2 + \cos(\omega t) (\dot{\Theta}_2 + \omega \Theta_1) \right) + \\
& + k_1 \cos(\omega t) \left(\cos(\omega t) \Theta_1 - \sin(\omega t) \Theta_2 \right) + \\
& + k_2 \sin(\omega t) \left(\sin(\omega t) \Theta_1 + \cos(\omega t) \Theta_2 \right) - \\
& - (M_D + M_{BA} + M_{BB}) (2\omega \dot{\Theta}_2 + \omega^2 \Theta_1) = 0
\end{aligned} \tag{4-6}$$

$$\begin{aligned}
& -S_A \left(2\omega \sin(\Theta_3) \dot{\Theta}_3 + \cos(\Theta_3) \ddot{\Theta}_3 + \omega^2 \sin(\Theta_3) + \sin(\Theta_3) \dot{\Theta}_3^2 \right) - \\
& -S_B \left(2\omega \sin(\Theta_4) \dot{\Theta}_4 + \sin(\Theta_4) \dot{\Theta}_4^2 - \cos(\Theta_4) \ddot{\Theta}_4 + \omega^2 \sin(\Theta_4) \right) - \\
& -M_P \left(\omega^2 \Theta_2 - \ddot{\Theta}_2 + 2\omega \dot{\Theta}_1 \right) + (M_D + M_{BA} + M_{BB}) \ddot{\Theta}_2 + \\
& + c_1 \sin(\omega t) \left(-\sin(\omega t) \omega \Theta_2 - \cos(\omega t) (\dot{\Theta}_2 + \omega \Theta_1) \right) + \\
& + c_2 \cos(\omega t) \left(-\cos(\omega t) \omega \Theta_2 + \cos(\omega t) (\dot{\Theta}_2 + \omega \Theta_1) \right) + \\
& + k_1 \sin(\omega t) \left(\sin(\omega t) \Theta_1 - \cos(\omega t) \Theta_2 \right) + \\
& + k_2 \cos(\omega t) \left(\cos(\omega t) \Theta_1 + \cos(\omega t) \Theta_2 \right) + \\
& + (M_D + M_{BA} + M_{BB}) (2\omega \dot{\Theta}_1 - \omega^2 \Theta_2) = 0
\end{aligned} \tag{4-7}$$

$$\begin{aligned}
& S_A \left(-\sin(\Theta_3) \ddot{\Theta}_1 + R_{BA} \ddot{\Theta}_3 + \cos(\Theta_3) \ddot{\Theta}_2 + \right. \\
& \left. 2 \sin(\Theta_3) \omega \dot{\Theta}_2 + 2 \cos(\Theta_3) \omega \dot{\Theta}_1 - \right. \\
& \left. - \omega^2 \cos(\Theta_3) \Theta_2 + \omega^2 \sin(\Theta_3) \Theta_1 \right) + c_3 \dot{\Theta}_3 = 0
\end{aligned} \tag{4-8}$$

$$\begin{aligned}
& S_B \left(-\sin(\Theta_4) \ddot{\Theta}_1 + R_{BB} \ddot{\Theta}_4 + \cos(\Theta_4) \ddot{\Theta}_2 + \right. \\
& \left. + 2 \sin(\Theta_4) \omega \dot{\Theta}_2 + 2 \cos(\Theta_4) \omega \dot{\Theta}_1 - \right. \\
& \left. - \omega^2 \cos(\Theta_4) \Theta_2 + \omega^2 \sin(\Theta_4) \Theta_1 \right) + c_4 \dot{\Theta}_4 = 0
\end{aligned} \tag{4-9}$$

In order to verify that the Type I singular point exists for the non-isotropic system the, time derivative terms are set to zero in Equations (4-6)-(4-9). This results in the following set of algebraic equations.

$$\begin{aligned}
& -\omega^2 (Y_{1E} M_S + S_A \cos(Y_{3E}) + S_B \cos(Y_{4E})) + \\
& + \omega (c_2 (\cos(\omega t) Y_{1E} - \sin(\omega t) Y_{2E}) \sin(\omega t)) - \\
& - \omega (c_1 (\cos(\omega t) Y_{2E} + \sin(\omega t) Y_{1E}) \cos(\omega t)) + \\
& + k_1 (\cos(\omega t) Y_{1E} - \sin(\omega t) Y_{2E}) \cos(\omega t) + \\
& + k_2 (\sin(\omega t) Y_{1E} + \cos(\omega t) Y_{2E}) \sin(\omega t) = 0
\end{aligned} \tag{4-10}$$

$$\begin{aligned}
& -\omega^2 (Y_{1E} M_S + S_A \sin(Y_{3E}) + S_B \sin(Y_{4E})) + \\
& + \omega (c_1 (\sin(\omega t) Y_{1E} + \cos(\omega t) Y_{2E}) \sin(\omega t)) + \\
& + \omega (c_2 (\cos(\omega t) Y_{1E} + \sin(\omega t) Y_{2E}) \cos(\omega t)) + \\
& + k_1 (\cos(\omega t) Y_{2E} - \sin(\omega t) Y_{1E}) \cos(\omega t) + \\
& + k_2 (\sin(\omega t) Y_{2E} + \cos(\omega t) Y_{1E}) \sin(\omega t) = 0
\end{aligned} \tag{4-11}$$

$$S_A (Y_{1E} \sin(Y_{3E}) - Y_{2E} \cos(Y_{3E})) \omega^2 = 0 \tag{4-12}$$

$$S_B (Y_{1E} \sin(Y_{4E}) - Y_{2E} \cos(Y_{4E})) \omega^2 = 0 \tag{4-13}$$

It is easy to prove that the Type I singular point, found earlier for the isotropic system, is also a singular point for the non-isotropic system, especially when the pendulums have the same first moment of inertia $S_A = S_B$. Further investigation showed Type II and Type III singular points also satisfy Equations (4-10) - (4-13) for an arbitrary chosen non-identical pendulum combination.

In order to assess the stability characteristics of the Type I singular point, the differential equations of motions were linearized around this point. The resulting equations, in a matrix vector form, are:

$$[M]\ddot{\bar{Y}} + [D(t) + G]\dot{\bar{Y}} + [K(t) + N]\bar{Y} = 0 \quad (4-14)$$

The inertia matrix is:

$$[M] = \begin{bmatrix} M_S & 0 & -S_A \sin(Y_{3E}) & -S_B \sin(Y_{4E}) \\ 0 & M_S & S_A \cos(Y_{3E}) & S_B \cos(Y_{4E}) \\ -S_A \sin(Y_{3E}) & S_A \cos(Y_{3E}) & S_A R_{BA} & 0 \\ -S_B \sin(Y_{3E}) & S_B \cos(Y_{4E}) & 0 & S_B R_{BB} \end{bmatrix} \quad (4-15)$$

$$\text{Where : } M_S = M_D + M_{BA} + M_{BB} + M_P$$

The time periodic damping and the gyroscopic matrix is:

$$[D(t) + G] = \begin{bmatrix} \chi_2 & -2M_S\omega + (c_2 - c_1)\sigma & -2\omega S_A \cos(Y_{3E}) & -2\omega S_B \cos(Y_{4E}) \\ 2M_S\omega + (c_2 - c_1)\sigma & \chi_1 & -2\omega S_A \sin(Y_{3E}) & -2\omega S_B \sin(Y_{4E}) \\ 2\omega S_A \cos(Y_{3E}) & -2\omega S_A \sin(Y_{3E}) & c_3 & 0 \\ 2\omega S_B \cos(Y_{4E}) & -2\omega S_B \sin(Y_{4E}) & 0 & c_4 \end{bmatrix} \quad (4-16)$$

$$\text{Where : } \sigma = \sin(\omega t) \cos(\omega t)$$

$$\chi_1 = c_1 \cos(\omega t)^2 + c_2 \sin(\omega t)^2$$

$$\chi_2 = c_1 \sin(\omega t)^2 + c_2 \cos(\omega t)^2$$

The time periodic elastic and the non-conservative force matrix is:

$$\begin{aligned}
 & [K(t) + N] = \\
 & \begin{bmatrix}
 -M\omega^2 + \kappa_1 + (c_2 - c_1)\sigma & -\omega\chi_1 - (k_1 - k_2)\sigma & \omega^2 S_A \sin(Y_{3E}) & \omega^2 S_B \sin(Y_{4E}) \\
 \omega\chi_2 - (k_1 - k_2)\sigma & -M\omega^2 + \kappa_2 + (c_1 - c_2)\sigma & -\omega^2 S_A \cos(Y_{3E}) & -\omega^2 S_B \cos(Y_{4E}) \\
 \omega^2 S_A \sin(Y_{3E}) & -\omega^2 S_A \cos(Y_{4E}) & S_A KN_{33} & 0 \\
 \omega^2 S_B \sin(Y_{4E}) & -\omega^2 S_B \cos(Y_{4E}) & 0 & S_B KN_{44}
 \end{bmatrix} \\
 & \hspace{20em} (4-17)
 \end{aligned}$$

Where: $\sigma = \sin(\omega t)\cos(\omega t)$

$$\kappa_1 = k_1 \cos(\omega t)^2 + k_2 \sin(\omega t)^2$$

$$\kappa_2 = k_1 \sin(\omega t)^2 + k_2 \cos(\omega t)^2$$

$$\chi_1 = c_1 \cos(\omega t)^2 + c_2 \sin(\omega t)^2$$

$$\chi_2 = c_1 \sin(\omega t)^2 + c_2 \cos(\omega t)^2$$

$$KN_{33} = Y_{2E} \sin(Y_{3E}) + Y_{1E} \cos(Y_{3E})$$

$$KN_{44} = Y_{2E} \sin(Y_{4E}) + Y_{1E} \cos(Y_{4E})$$

The Cauchy transformation of Equation (4-14) results in a system of first order differential equations with an 8x8 coefficient matrix $[A(t)]$.

$$\dot{\bar{X}} = [A(t)] \bar{X} \quad (4-18)$$

Where:

$$\bar{X} = \begin{bmatrix} \bar{Y} \\ \dot{\bar{Y}} \end{bmatrix} \quad (4-19)$$

The coefficient matrix of the linearized differential equations with time periodic coefficients is:

$$[A(t)] = \begin{bmatrix} [0] & [I] \\ -[M]^{-1}[K(t)+N] & -[M]^{-1}[D(t)+G] \end{bmatrix} \quad (4-20)$$

4.1.1 Stability of homogeneous linear system with time periodic coefficients

This section describes the mathematical background that was applied for the stability analysis. The general time periodic linear system is defined by equation (4-18) where the coefficient matrix $[A(t)]$ is periodic with period $T > 0$, that is $[A(t+T)] = [A(t)]$. Of interest is the stability of the equilibrium point $\bar{X} \equiv \bar{0}$. To solve the problem, we apply the Floquet theorem [28][29].

The fundamental matrix of system of the linearized (4-18) is $[\Phi(t)]$, if the

$$\frac{d[\Phi(t)]}{dt} = [A(t)][\Phi(t)] \quad (4-21)$$

matrix differential equation is satisfied. The following statements can be proved:

- All solutions of equation (4-18) can be written in the form $[\Phi(t)]\bar{c}$, where \bar{c} is a constant vector.
- There exists a fundamental matrix $[\Phi_0(t)]$, that all solutions of (4-18) come up in the form $[\Phi_0(t)]\bar{X}_0$, where $\bar{X}_0 = \bar{X}(0)$ is the initial condition, that is $[\Phi_0(t)] = [I]$, where $[I]$ is the identity matrix.
- All fundamental matrix can be written in the form $[\Phi(t)][\tilde{C}]$, where $[\tilde{C}]$ is a constant matrix.
- For any fundamental matrix $[\Phi(t)]$, $[\Phi(t+T)]$ is also a fundamental matrix.
- There exists constant matrix $[\tilde{C}]$ for which $[\Phi(t+T)] = [\Phi(t)][\tilde{C}]$, where $[\tilde{C}]$ is called the principal matrix of (4-18), $[\tilde{C}] = [\Phi(t)]^{-1}[\Phi(t+T)]$.
- The principal matrix belonging to the fundamental matrix $[\Phi_0(t)]$ assumes the form $[C] = [\Phi_0(t)]^{-1}[\Phi_0(t+T)] = [\Phi_0(0)]^{-1}[\Phi_0(0+T)] = [\Phi_0(0)]$.
- All principal matrices are similar to each other, consequently the eigenvalues of the principal matrix - called the characteristic multipliers (notation: $\lambda_1, \lambda_2, \dots, \lambda_n$) - are invariant, and determined by the system.

- System (4-18) is asymptotically stable if and only if $|\lambda_i| < 1, i = 1, 2, \dots, n$.
- System (4-18) is stable in the Liapunov sense if and only if $|\lambda_i| \leq 1, i = 1, 2, \dots, n$, and if $|\lambda_i| = 1$, then λ_i is simple in the minimal polynomial of the system.

In general the principal matrix can not be determined in an analytic way, but there are several methods to approximate it [16].

4.1.2 Floquet analysis: piecewise approximation

If the coefficient matrix $[A(t)]$ is piecewise constant, then - by the coupling of solutions - the complete solution at time $t = T$ is obtained in the form:

$$\bar{X}(T) = \exp(t_n [A_n]) \exp(t_{n-1} [A_{n-1}]) \dots \exp(t_1 [A_1]) \bar{X}_0 \quad (4-22)$$

$$[A(t)] = \begin{cases} [A_1] & \text{if } 0 \leq t \leq t_1 \\ [A_2] & \text{if } t_1 < t \leq t_1 + t_2 \\ \vdots & \vdots \\ [A_n] & \text{if } t_1 + t_2 + \dots + t_{n-1} < t \leq t_1 + t_2 + \dots + t_n = T \end{cases} \quad (4-23)$$

where $[A_1], [A_2], \dots, [A_n]$ are constant matrices forming the piece-wise constant $[A(t)]$.

So the principal matrix takes the form:

$$[C] = \exp(t_n [A_n]) \exp(t_{n-1} [A_{n-1}]) \dots \exp(t_1 [A_1]) \quad (4-24)$$

If the coefficient matrix $[A(t)]$ is not piecewise constant, then we can replace its elements by piecewise constant values in the following way:

$$[\tilde{A}(t)] = \begin{cases} [A_1] = \left[A \left(\frac{T}{2n} \right) \right] & \text{if } 0 \leq t < \frac{T}{n} \\ \vdots & \vdots \\ [A_k] = \left[A \left(\frac{T}{2n} (2k-1) \right) \right] & \text{if } \frac{T}{n} (k-1) \leq t < \frac{T}{n} k \\ \vdots & \vdots \\ [A_n] = \left[A \left(\frac{T}{2n} (2n-1) \right) \right] & \text{if } \frac{T}{n} (n-1) \leq t < T \end{cases} \quad (4-25)$$

Matrix $[\tilde{A}(t)]$ is also periodic with period T . Applying (4-24) to $[A_1], \dots, [A_k], \dots, [A_n]$ matrices and $t_1 = t_2 = \dots = t_n = T/n$ time intervals, we obtain an approximation of the principal matrix. By examining the eigenvalues, one can approximately determine the stability of system (4-18). The bigger n is, the more closer the approximation is to the actual solution.

The Source code 4-1 represents the MatLab user written function for the analytical investigation of the piecewise approximation to determine stability. This function returns 1 if the investigated system is stable.

```

function OP = StableOperationPWA(N);
global k1 k2 c1 c2 c3 c4 f
T = 1/f;
tStep = T/N;

C = expm(tStep * GetAt_at_t(tStep));
for n = 2:N
    tn = n*tStep;
    C1 = expm(tStep * GetAt_at_t(tn));
    C = C1*C;
end

z = eig(C);
MR = max(abs(z));
if (MR - 1) < 1e-5
    OP = 1;
else
    OP = 0;
end
return

```

Source code 4-1 MatLab code of piecewise approximation method

4.1.3 Floquet analysis with numerical integration: single pass scheme

From a balancing point of view the Type I singular point is the most important. The four DOF ordinary differential equation system was linearized around a calculated Type I singular point and, after the Cauchy transformation, the 8 DOF linear differential equation system, represented by $[A(t)]$, was written to a MatLab file for later processing. During the analytical investigation, this system of differential equations was numerically integrated from zero to the end of the principal period T eight times with different unit initial conditions \bar{X}_{0i} .

\bar{X}_{0i} is a 1x8 column vector with only one nonzero element in the i^{th} row. Source code 4-2 shows the MatLab function ode45 was applied to integrate the differential equation system to obtain the approximate numerical result \bar{X}_A at T time. The resulted

eight column vector was used to generate the constant nonsingular Floquet Principal Matrix $[C]$. According to the Floquet theory, the solution of $\bar{X}(t)$ is bounded for all time if the eigenvalues of the Floquet Principal Matrix $[C]$ have a magnitude less than 1.

```
function OP = StableOperationSPS;
global k1 k2 c1 c2 c3 c4 f
options = odeset('AbsTol',1e-8,'RelTol',1e-8);
w = 2*pi*f;
[f k2 c1 c2]
for j = 1:8
    xo = zeros(1,8);
    xo(j) = 1;
    [t,xa] = ode45('LinDES0T',[0,2*pi/w],xo,options);
    [m,n] = size(xa);
    C(j,1:8) = y(m,1:8);
end
z = eig(C);
MR = max(abs(z));
if (MR - 1) < 1e-8
    OP = 1;
else
    OP = 0;
end
return
```

Source code 4-2 MatLab code of single pass scheme

4.1.4 The result of Floquet analysis

During the generation of the Floquet stability map, two parameters of the rotor system were varied. The first one is a constructional parameter, the spring stiffness in the Θ_2 direction k_2 . The second is an operational parameter, the speed of the rotor ω . For every combination of these two parameters the time periodic coefficient matrix was calculated, the Floquet analysis completed, and the associated stability property was determined. Figure 4.1 shows the non-dimensionalized coarse Floquet stability map. The horizontal axis is the relative angular velocity $\Omega = \omega/\omega_{n1}$ and the vertical axis is the relative spring stiffness defined by: $K = k_2/k_1$. On this stability map the symbol x indicates instability and the symbol dot indicates stability. There are two stable areas separated by an unstable zone. According to the Floquet analysis in the unstable area, the Type I singular point is not stable because at least one of the coordinates of system (Θ_i) is not bounded.

The major purpose for generating the coarse Floquet stability map is to identify the main stability characteristics in the parameter range of interest determined by the possible operational speed and spring stiffness of suspension.

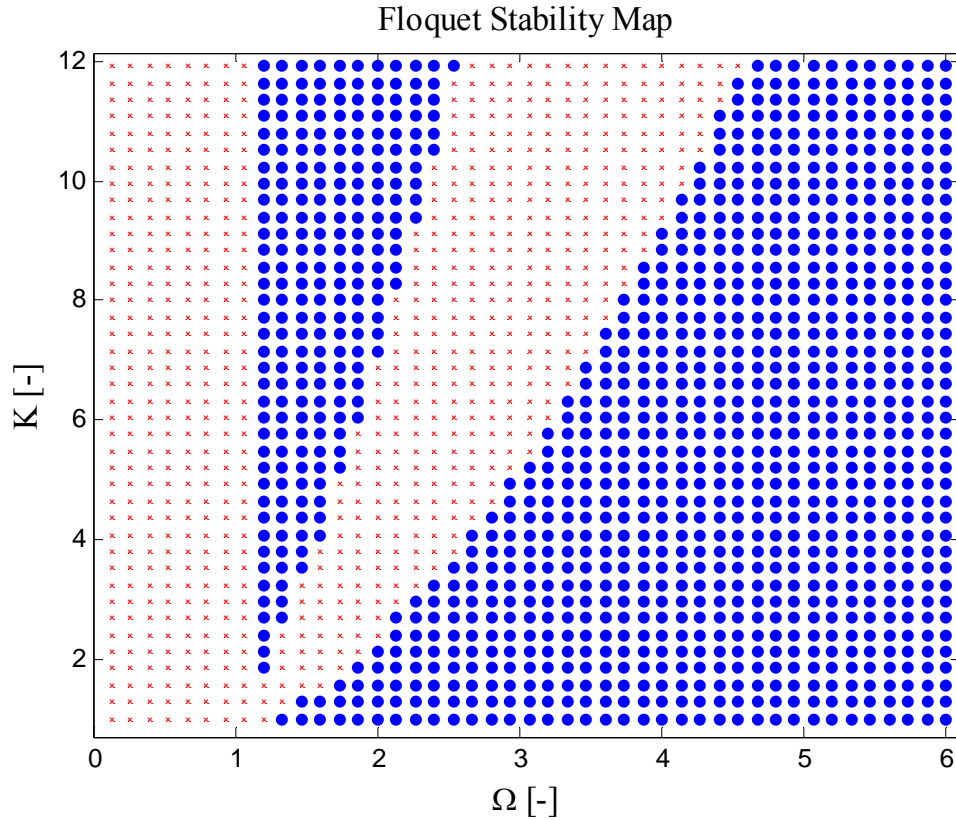


Figure 4.1 Coarse Floquet stability map of Type I singular point

A more sophisticated MatLab code was developed to specifically to target the border of the stable areas. Figure 4.2 shows the fine border of the stable areas with the two resonance lines. The vertical dotted line shows that the first natural frequency is kept constant when the second natural frequency, showed by a dashed line, was varied. By increasing the stiffness of the second spring, the two natural frequencies separate from each other and the stable section between them becomes wider. When the rotor is operating above the second natural frequency, the analysis resulted stability for the Type I singular point.

Figure 4.2 shows specific points as indicated by x and dots. These points are the targets of numerical and experimental validation and they are selected near the borders where the stability properties switch. All of these points were investigated by experiments, A part of this investigation the results of the experimental measurements at five points, identified: A, B, C, D and E, are shown in Figure 4.10 - Figure 4.14 combined with the result of numerical simulations for more direct comparison.

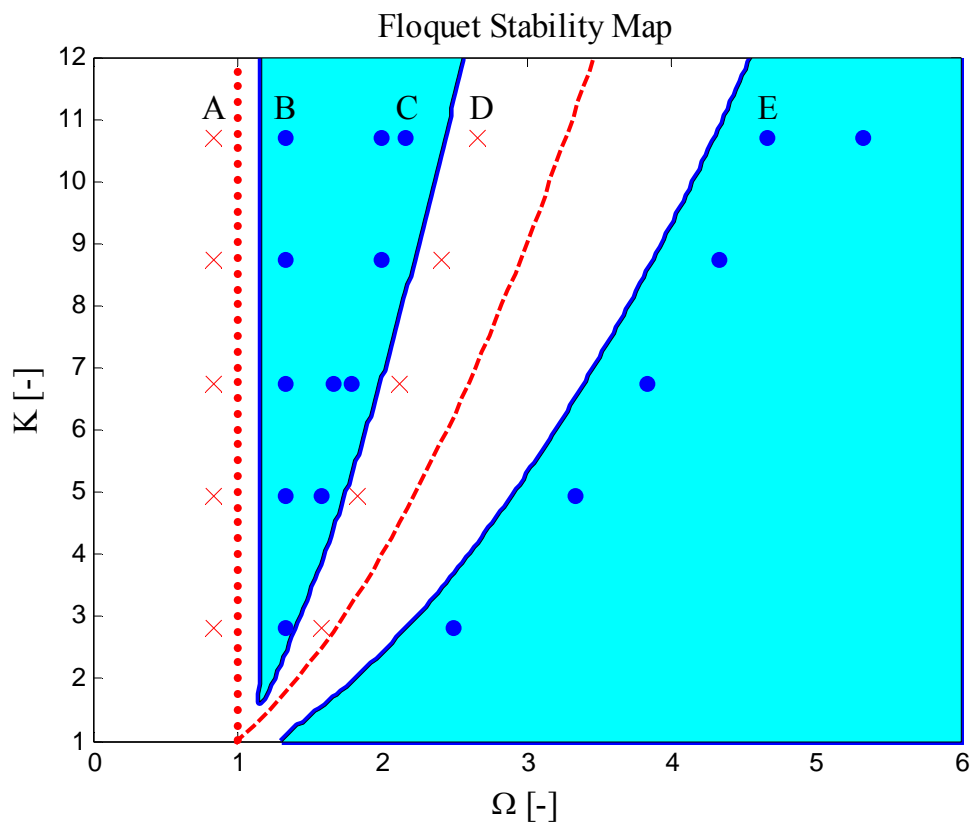


Figure 4.2 Fine Floquet stability map of Type I singular point with the points used for numerical and experimental validation

Both the piecewise approximation and the single pass scheme analytical methods showed similar results, although the piecewise approximation required much less CPU time.

Floquet characteristic multipliers for the Type I singular point

The Floquet characteristic multipliers were used to determine the stability characteristics of specific points on the stability maps, Figure 4.1 and Figure 4.2. If all the characteristic multipliers of the Floquet Principal Matrix $[C]$ are inside the unit circle of the complex plane, the system is considered to be stable. Going along the ABCDE line in Figure 4.2 the stability of the Type I singular point changes. These stability changes can be followed directly on Figure 4.3 as a function of relative running speed, Ω . This figure shows one pair of Floquet characteristic multipliers. These are complex conjugates and they have the biggest magnitude. To generate this special plot, all the constructional parameters were kept constant with only the running speed was varied. These parameters were the same that were used along the ABCDE horizontal line in Figure 4.2.

As the running speed was increased from zero, the characteristic multipliers indicated instability for point A, through the first resonance (where $\Omega = 1$), and stepped inside the unit cylinder. Inside the unit cylinder they indicated the stability of the Type I singular point at locations B and C and then stepped outside the unit cylinder. Before the characteristic multiplier (longest in magnitude) reached the second resonance (around $\Omega = 3.86$) they indicated the unstable property of point D by staying outside the unit cylinder. As the running speed was further increased, the characteristic multipliers stepped inside the unit cylinder again and indicated the Type I singular point is stable at point E. The same course can be followed on three different views of Figure 4.4.

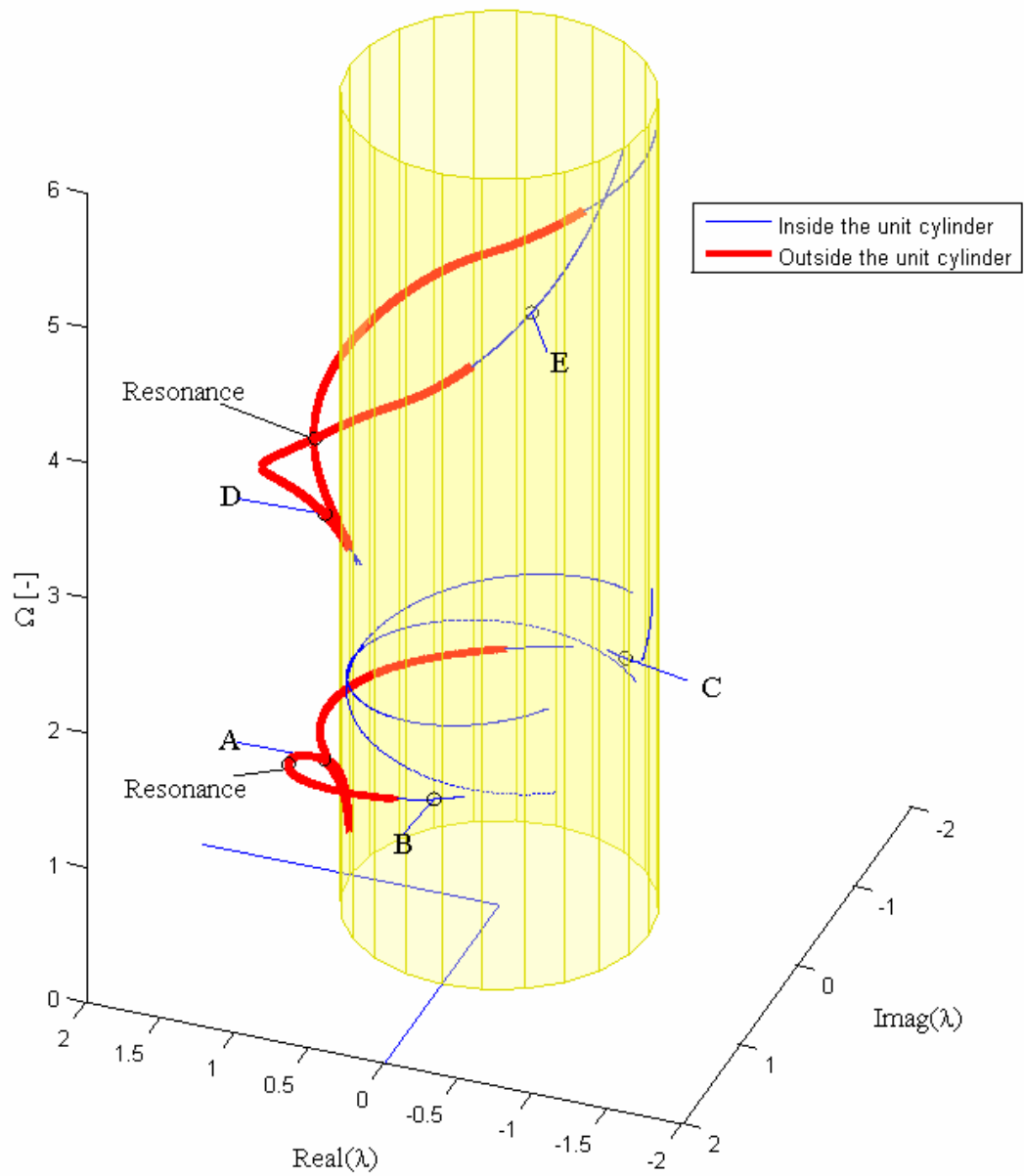


Figure 4.3 The unit cylinder and the biggest Floquet characteristic multiplier as a function of relative running speed.

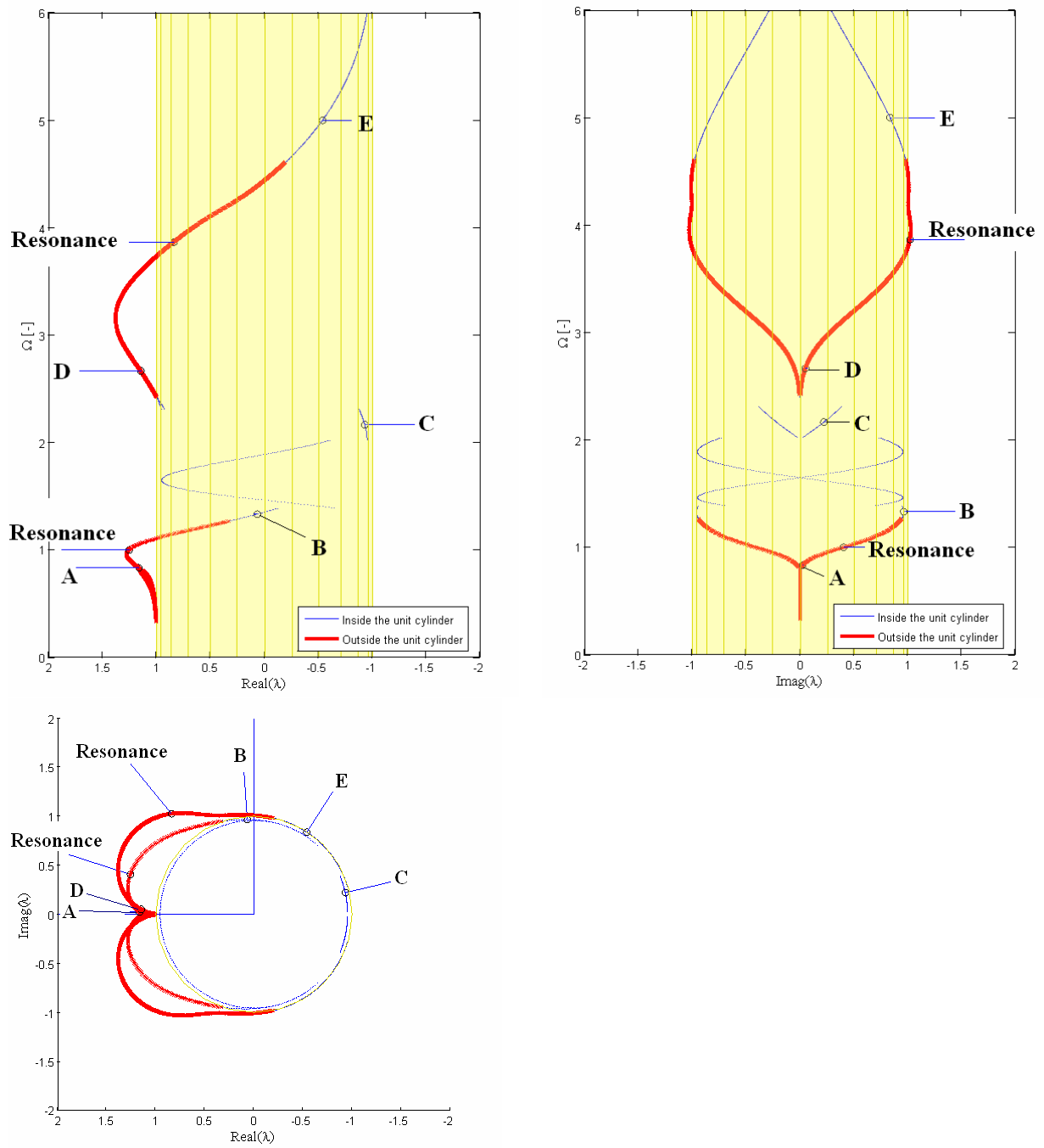


Figure 4.4 Three different views of unit cylinder and the Floquet characteristic multipliers of Type I singular point

4.1.5 Stability changes for different damping coefficients

In order to explore the stability characteristic of the experimental facility, the system parameters were identified by several repeated measurements. These parameters were used to generate the Floquet stability map of the Type I singular point. This stability map was plotted in the plane of the relative running speed Ω and relative spring stiffness K . For this stability map, the damping coefficients of rotor suspension and the pendulums were kept constant. In order to gain better insight into the effect of damping coefficients on the Floquet stability map of the Type I singular point several maps were generated with a different damping coefficients. Figure 4.5 shows a collection of stability maps for different relative damping coefficients for the rotor suspension ζ_{12} . On this plot, five Floquet stability maps can be seen combined with a first and the second resonance curves. During the generation of these plots, the damping coefficients of the pendulums were constant ($c_{34} = 0.001$ [Nms/rad]). Investigation of the size of stable areas, bordered by the different damping curves, shows that there is a certain relative damping coefficient for the rotor suspension where the Type I singular point shows the highest general stability for parameter variation.

In the second phase of the investigation of stability changes for damping, the damping coefficients of the pendulums were varied and the damping of rotor suspension was hold at a constant value. Figure 4.6 shows a series of Floquet stability maps for different damping coefficients of the pendulums, in a similar fashion to that in which it was shown earlier. Examination of the generated stability maps shows that increasing the damping coefficient of pendulums tends to increase the size of the stable area.

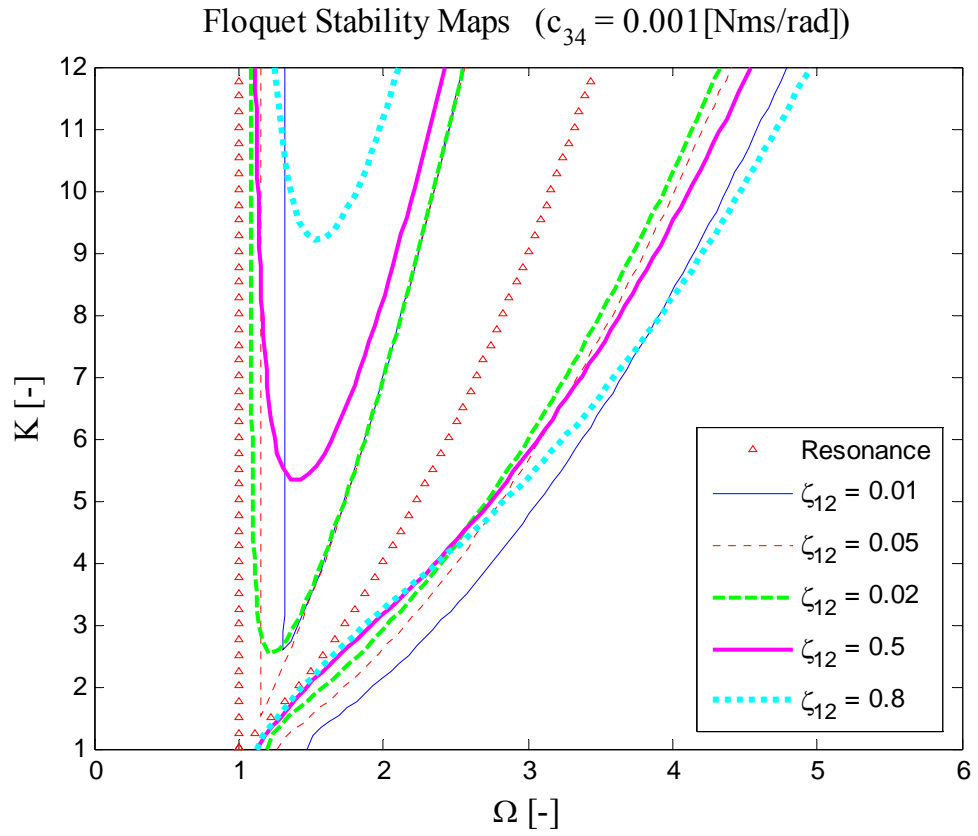


Figure 4.5 Floquet stability map of Type I singular point for different relative damping coefficients of rotor suspension

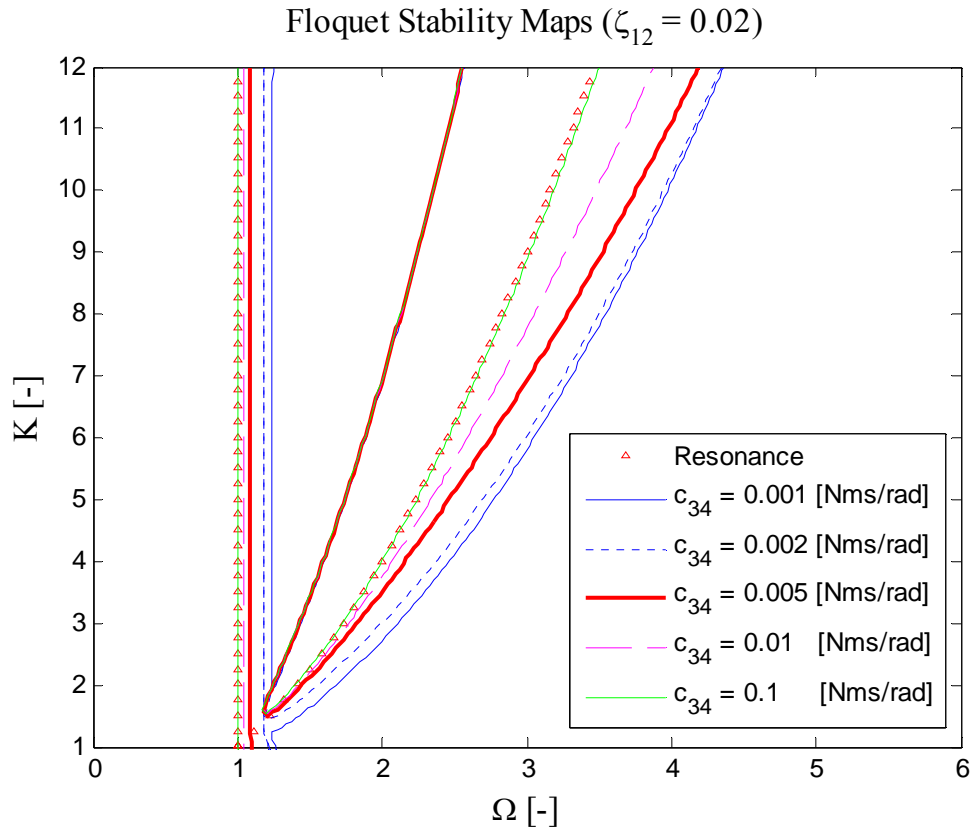


Figure 4.6 Floquet stability map of Type I singular point for different damping coefficients of pendulums

4.2 Experimental facility with non-isotropic suspension

In order to validate the results of the Floquet analysis, the experimental facility was modified and a series of experimental measurements was taken. The following section describes the facility.

4.2.1 Description of experimental facility

Figure 4.7 shows the side view of the experimental apparatus. The rotor assembly (4) is spinning in the horizontal plane attached to the base plate (5). The base plate is mounted on the shaft of the DC motor (11) which is supported by a column (21) attached to the ground with a flexible joint (22). This arrangement allows the rotor assembly to move in near horizontal plane.

The vertical column is supported from the Θ_1 direction by a simple spring (28). From the Θ_2 direction, the column is supported by an adjustable spring system. The two main parts of this system are two rod springs (25) connected in parallel by a threaded rod (27). The rod springs are attached to the side columns by a moveable clamping device (24). By changing the position of these clamping devices the working length of the rod spring can be set. By moving the clamping devices closer to the top of the side columns (23), the working length of the rod spring will be made shorter and the resultant spring stiffness will be higher. In this way, the desired spring stiffness can be set in the Θ_2 direction.

This experimental facility is equipped with three adjustable damping systems. The movement of the rotor can be regulated by an adjustable damper. A disk shape collar (18) is attached to the vertical column (21). Between the aluminum collar and the horizontal

frame plate (20), there is an adjustable air gap. This aluminum collar accommodates a maximum of 36 rare earth magnets (19). The DC motor (11) and aluminum collar (18) with the magnets move together. So the magnets generate eddy currents inside the horizontal frame plate, producing a velocity proportional damping force. This damping force can be adjusted by varying the number of magnets and the size of the air gap between the aluminum collar (18) and the horizontal frame plate (20). The damping coefficient of each pendulum can be adjusted in a similar fashion to that which was described earlier for the test facility with symmetric a suspension.

In order to validate the stability properties of the rotor system, the position of the pendulums must be monitored during rotation. In order to accomplish this, the rotor system is equipped with a wireless data acquisition system. Optical encoder disks (14) are attached to each pendulums and their motion is monitored by optical sensors (15). The wireless electronics and their power source are placed in a plastic box (16) mounted on the top of the pendulum assembly.

The pendulums are locked in position until the rotor reach the desired operational speed and the start-up transients die out. The two lock-release mechanisms (13) are mounted on the bottom plate of the pendulum assembly. The pendulums can be locked when the rotor is stopped and released during rotation.

The pendulum assembly, which was used to study the APB with a symmetric suspension, was designed to be symmetric and balanced after proper manufacturing. In this way, the mass imbalance was controlled only by the brass weights (7). The optical readout system and the release mechanism that was added to the system made it difficult to keep the CG of the rotor system at the center of rotation when the brass weights are

located at their base location. Accordingly, two “base balancer” units (17) were clamped to the bottom plate of pendulum assembly. They were used to balance the rotor assembly when the brass weights are at their base point. After proper balancing, the level of mass imbalance was adjusted by only one of the brass weighs.

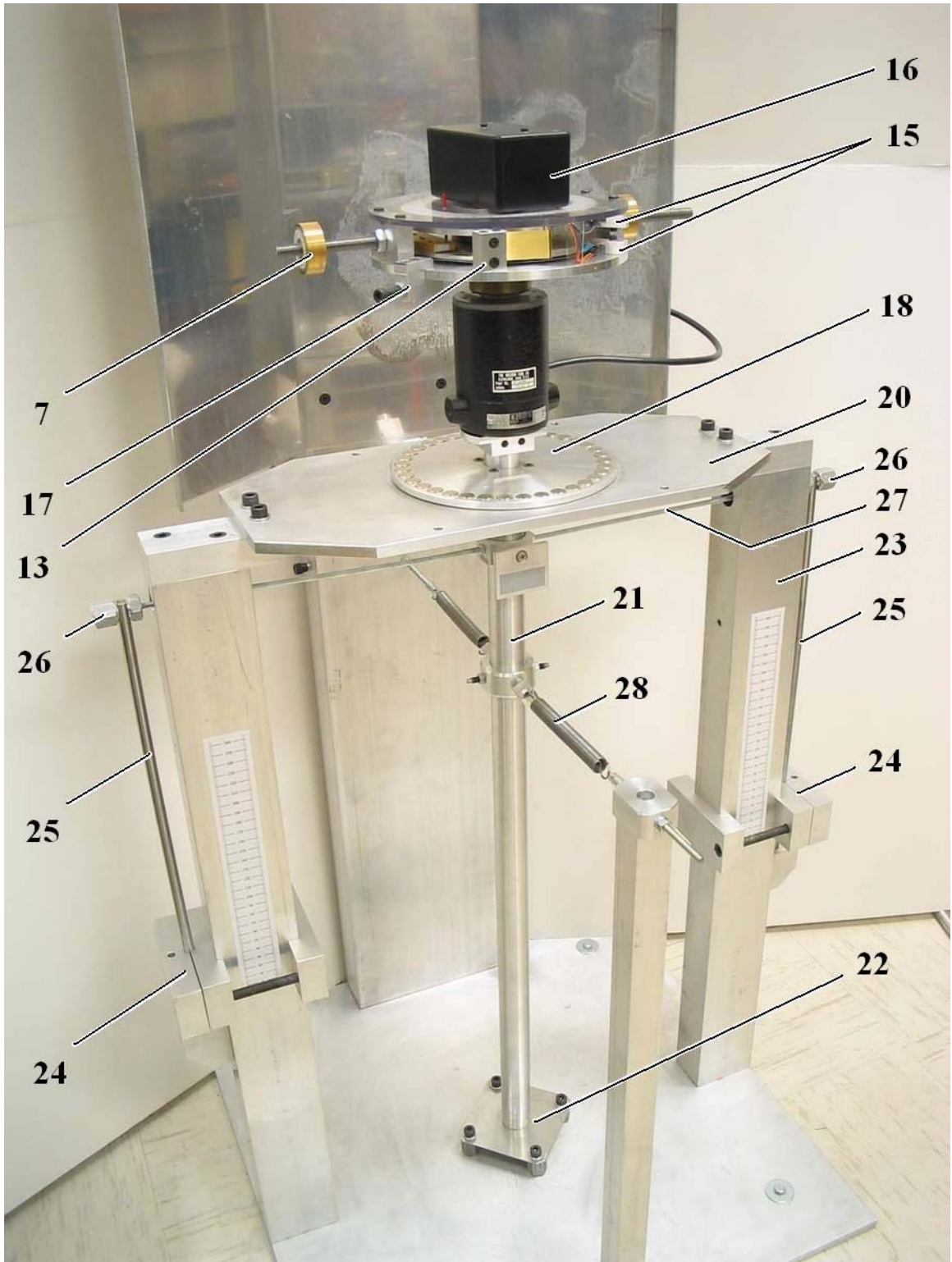


Figure 4.7 Side view of pendulum balancer experimental facility with non-isotropic suspension

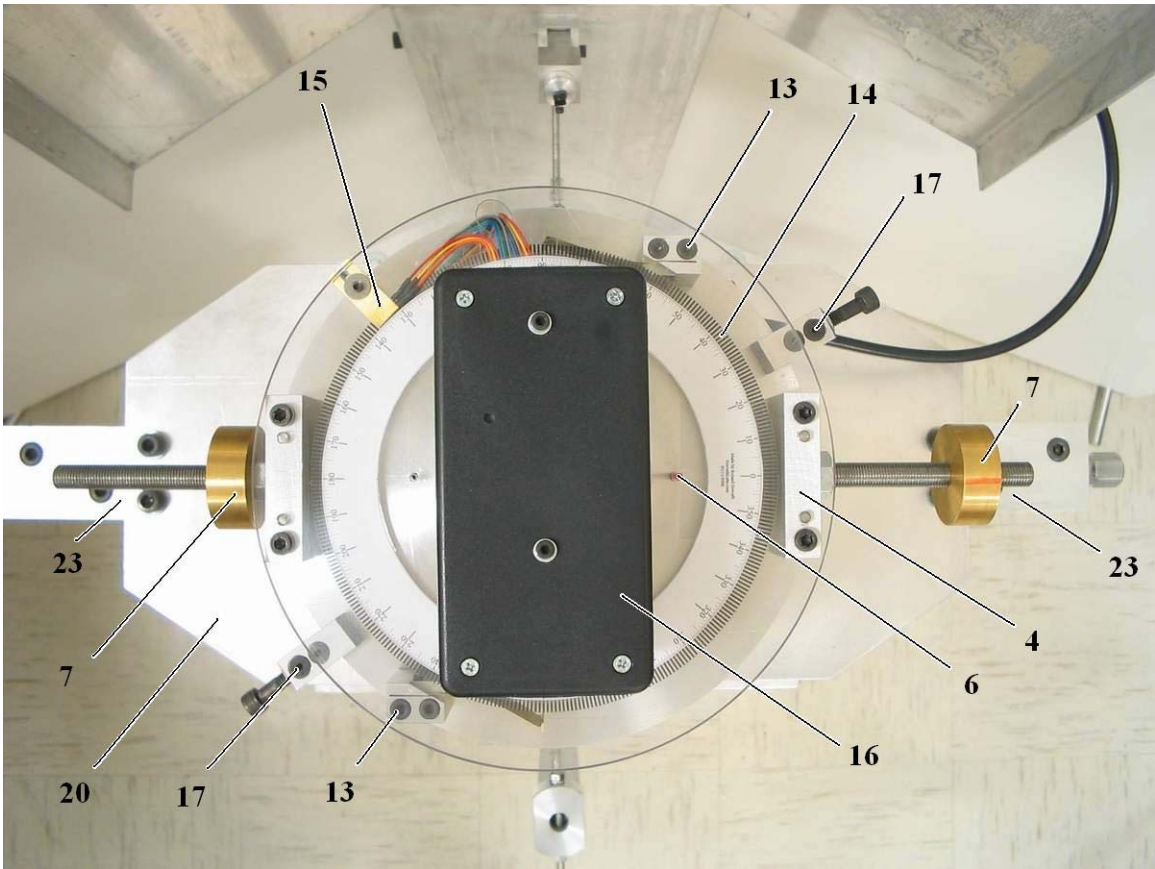


Figure 4.8 Top view of rotor assembly

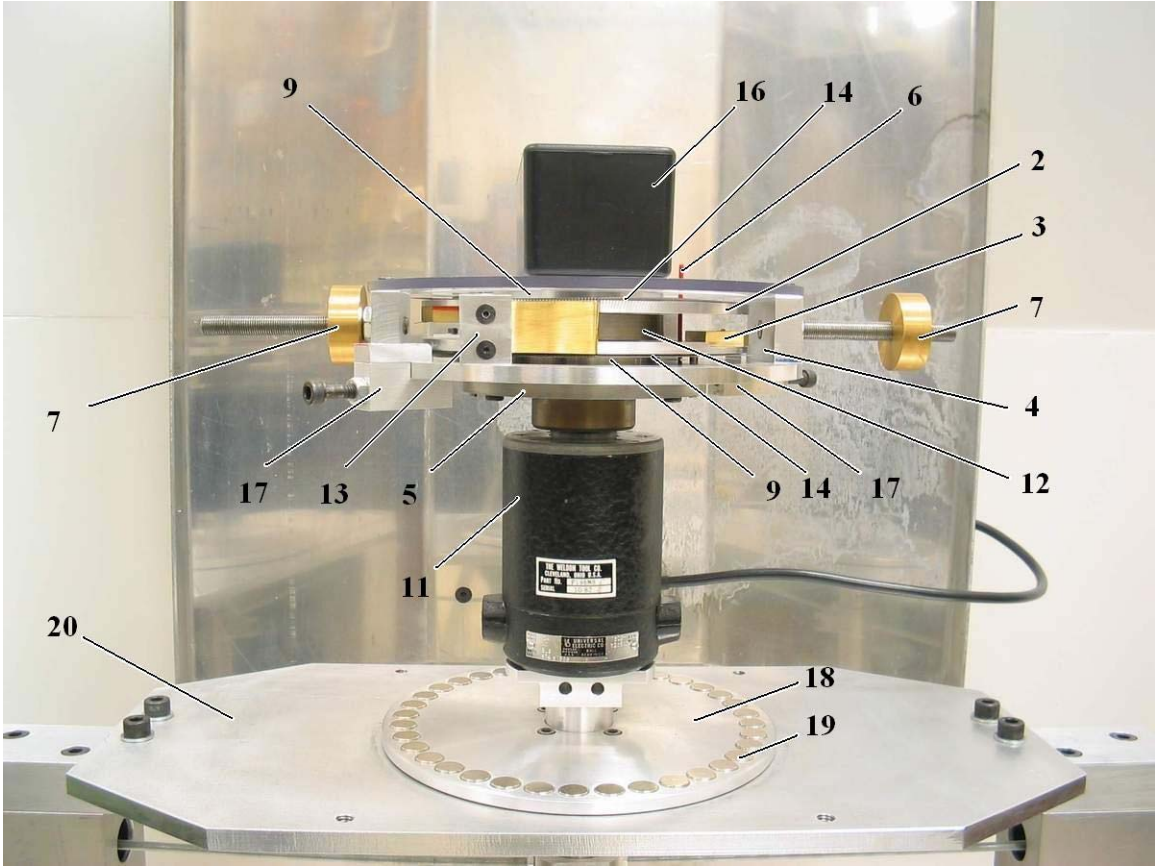


Figure 4.9 Side view of rotor assembly

4.2.2 Description of experimental procedure

In order to validate the results of Floquet analysis and the numerical simulation, a non symmetric suspension had to be provided. The second spring stiffness k_2 in the Θ_2 direction was adjusted by changing the height of a clamping device without modifying the spring stiffness of the suspension in Θ_1 direction. The mass imbalance was constant for every experimental measurement. After the spring stiffness's are set, the pendulums were locked at their base position 0° and 180° by the lock-release mechanism. After start up and the desired rotational speed has been reached, a sufficient amount of time was allowed so that the transients die out. When a steady state vibration level was achieved, the pendulums were released and the following four coordinates were measured and recorded:

- Linear displacements in the Θ_1 and Θ_2 directions provided by laser displacement systems.
- Angular displacements in the Θ_3 , Θ_4 directions provided by an on-board wireless data acquisition system.

4.3 Numerical and experimental investigation

In order to validate the result of the Floquet analysis, a series of numerical simulations and experimental measurements were performed. They are discussed together in this chapter in order to better facilitate their comparison. Figure 4.10 - Figure 4.14 show the results of the numerical simulation and the experimental measurements for the five specific points: A, B, C, D and E shown in Figure 4.2 and Figure 4.3.

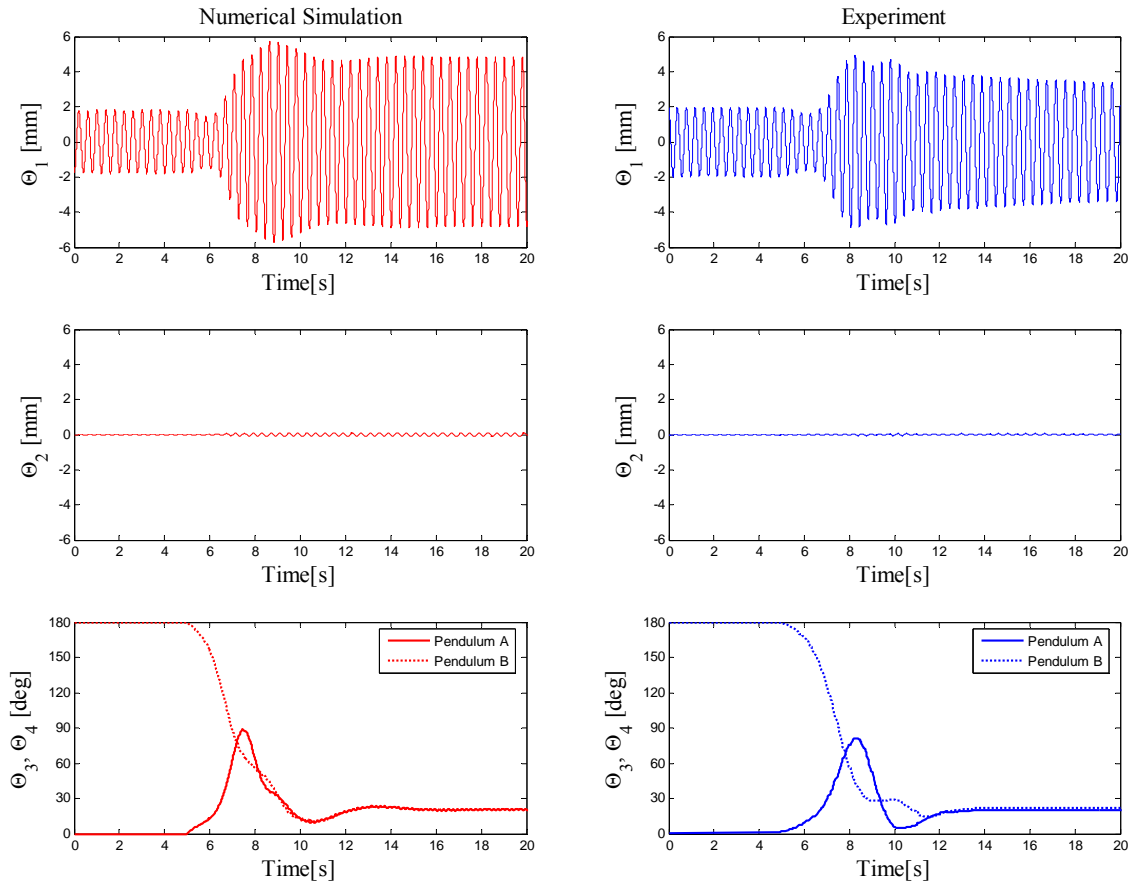


Figure 4.10 Numerical and experimental validation of point A

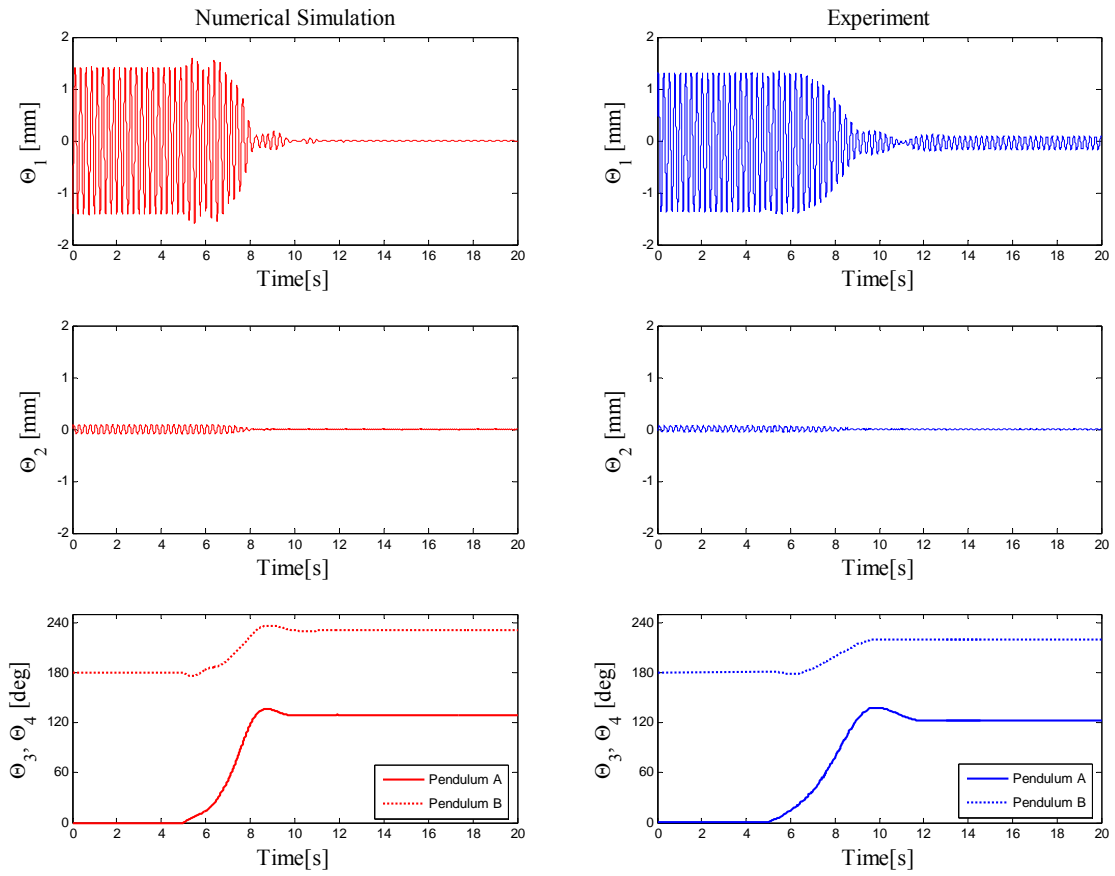


Figure 4.11 Numerical and experimental validation of point B

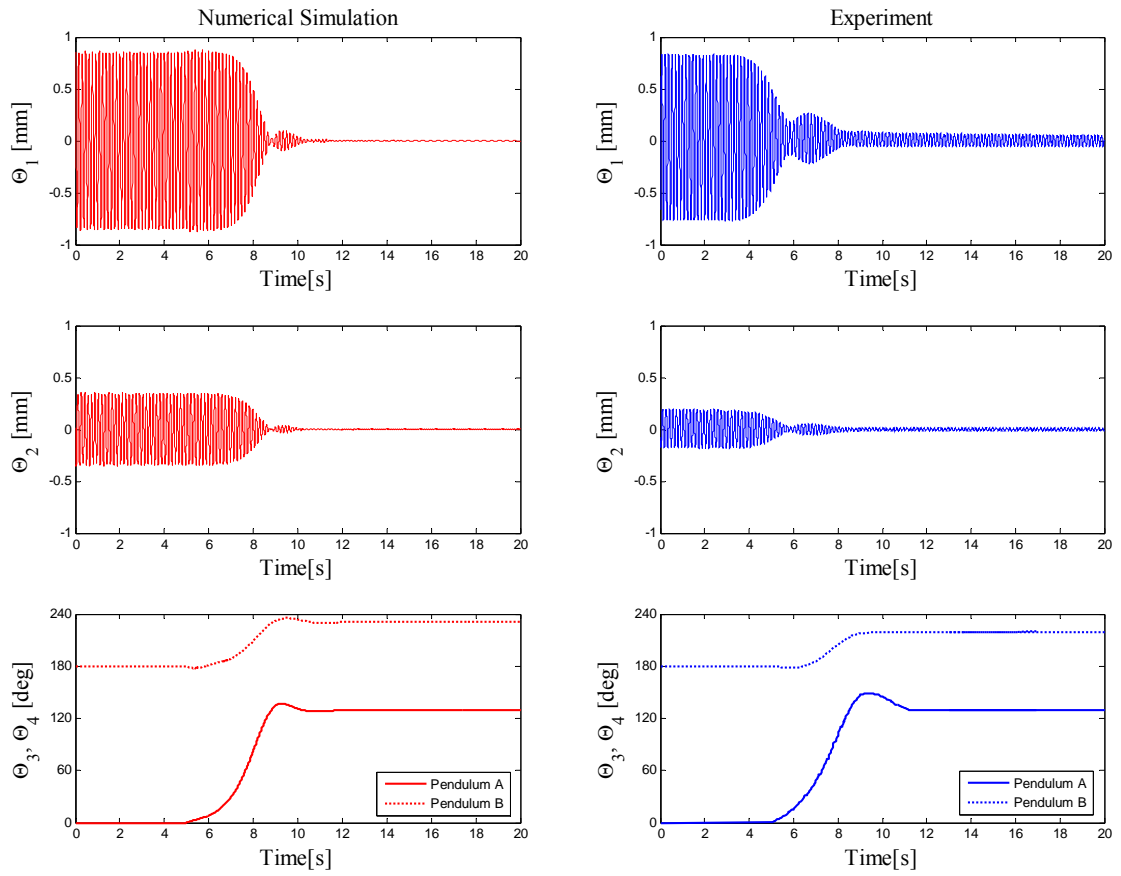


Figure 4.12 Numerical and experimental validation of point C

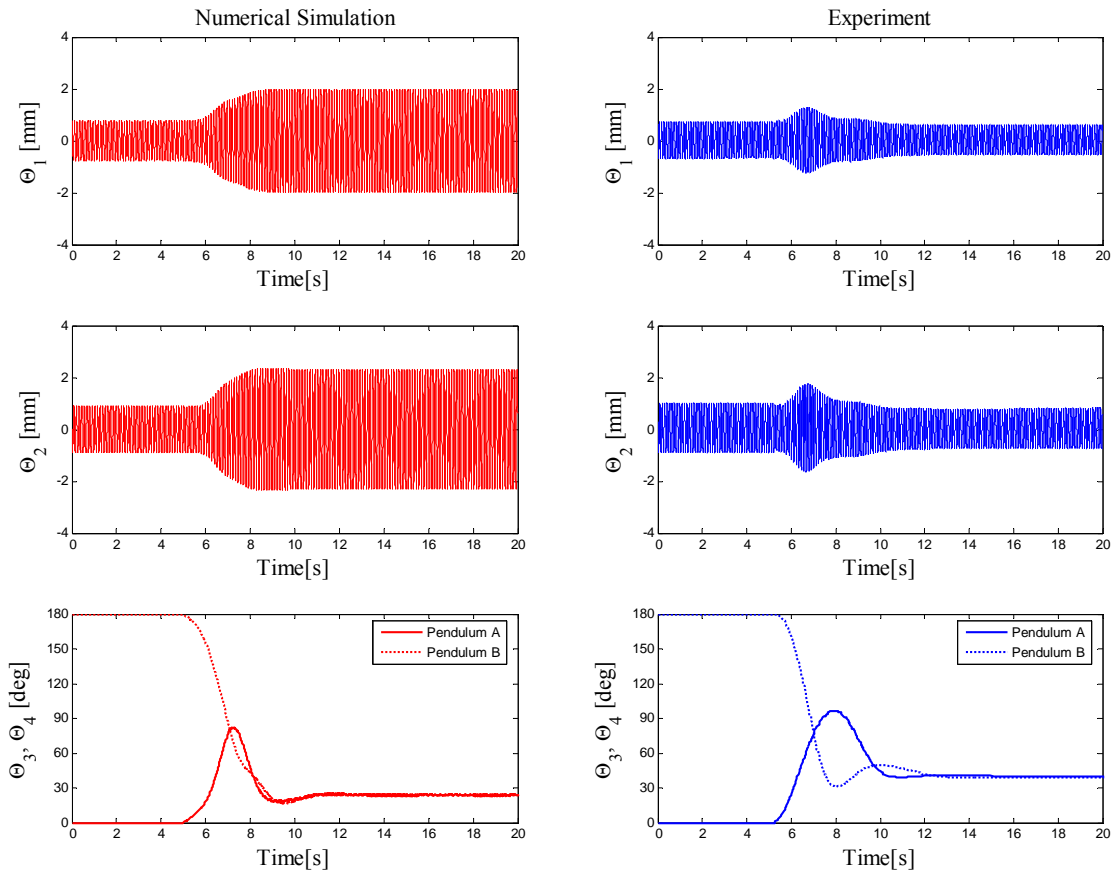


Figure 4.13 Numerical and experimental validation of point D

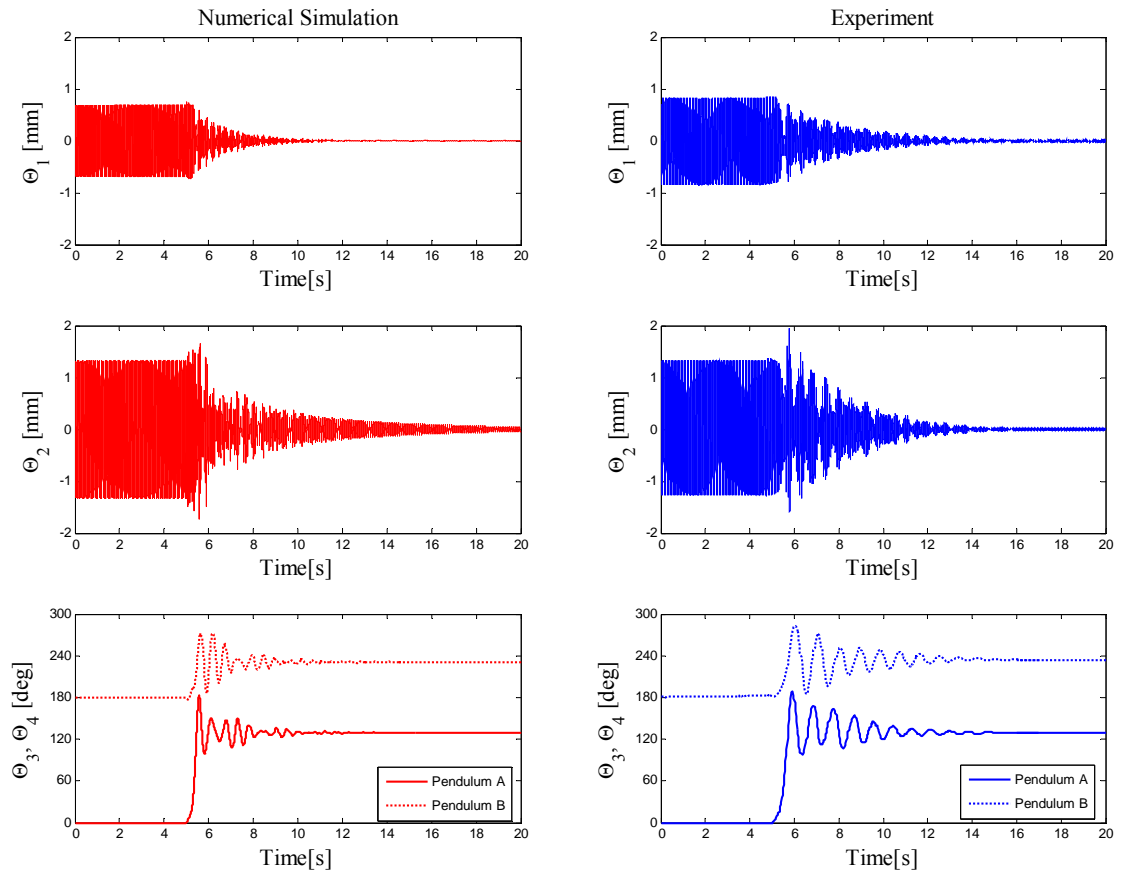


Figure 4.14 Numerical and experimental validation of point E

4.4 Summary of validation

Detailed simulation and experimental validations have proven the existence and location of stable and unstable areas in the Floquet stability map of the Type I singular point. The results of numerical simulations and experimental measurements are nearly identical. This validates the mathematical model that was used for the numerical simulations and the properly identified system parameters. Additionally, the numerical simulations and the experiments have provided information about the stability properties of the Type III singular point. At points A and D the pendulums stayed together, which means that when the Type I singular point loses the stability the Type III singular point becomes stable.

5 CONCLUSIONS AND FUTURE WORK

The dynamic behavior of a pendulum-based passive balancing system has been investigated. A detailed analytical and simulation study has been performed along with extensive experimental testing and validation. Its basic operating principles and stability characteristics have been described. The investigation can be divided in two main parts. In the first part of the research, non-identical the passive pendulum balancer was studied with isotropic suspension and generally sized pendulum systems. Three relative balancing regions - relatively undersized, properly oversized and improperly oversized - have been identified and described in terms of the relative parametric configurations of the pendulums and the rotor imbalance. Three types of singular points were also identified and their associated stability characteristics were investigated in detail, both analytically and experimentally. It was found that near resonance, for relatively high damping of rotor suspension, the Type II and Type III singular points lose stability.

In addition, the influence of shaft misalignment and rolling resistance have been examined in some detail. It was shown that shaft misalignment can have a major effect on the balancing capability of this type of system. Therefore, proper alignment is critical for successful operation. Furthermore, it was demonstrated by repeated experiments that a pendulum balancing system tends to exhibit a much higher consistency of performance than a ball balancer for similar operating conditions. This result was explained by analysis and comparison of rolling resistance and the force distributions for each passive self-balancing system.

As a second part of the investigation, the effect of a non-isotropic suspension on the dynamic behavior of a passive pendulum balancer was investigated. Two different types of Floquet analysis's resulted in coincide stability map of Type I singular point with two separate stable areas. These areas, especially their borders, have been validated by a series of numerical simulations and experimental measurements. Additionally, it was found in the unstable areas where the Type I singular point loses stability, the Type III singular point becomes stable. The pendulums stay together and the center of the rotor has a steady state orbital motion in the space fixed coordinate system.

In order to support and accelerate the application of passive pendulum based rotor balancing systems and to utilize the beneficial features, additional research should be conducted. Specifically:

- Effect of gravity. The application of passive pendulum balancers to horizontally placed rotor systems should be investigated.
- Investigation of the optimal damping level for the pendulums should be conducted.
- Exploration of those areas where the singular points are lost because of near resonance operation and high damping.
- System response for time varying parameters. Identifying the optimum of system parameters and pendulum reaction time for a certain perturbation, induced by sudden change of mass imbalance.
- Exploration of the stability properties of Type III singular point for non-isotropic rotor suspension.

BIBLIOGRAPHY

- [1] Fesca, A.: "Improvement in Centrifugal Machines for Draining Sugar" United States Patent No. 125,036 March 26, 1872

- [2] Ledyard, G.W.: "Automatic Balancer for Centrifugal Machines" United States Patent No. 1,183,745 May 16, 1916

- [3] Leblanc, M.: "Automatic Balancer for Rotating Bodies" United States Patent No 1,209,730 Dec. 26, 1916

- [4] Thearle, E. L.: "A New type of dynamic-balancing machine," Transactions of ASME (Applied Mechanics) 1932, APM-54-12, pp. 131-141.

- [5] Clark, K.: "Domestic Appliance" United States Patent No. 2,405,404 Oct. 29, 1940

- [6] Thearle, E. L.: "Automatic Dynamic Balancers (Part 1-Lebanc balancer)," Machine Design, 1950, Vol. 22, pp.119-124.

- [7] Thearle, E. L.: "Automatic Dynamic Balancers (Part 2- Ring, pendulum, ball balancers)," Machine Design, 1950, Vol. 22, pp. 103-106.

- [8] Sharp, R. S.: "Analysis of a Self-Balancing System for Rigid Rotors," Journal of Mechanical Engineering Science, Vol. 17, No. 4, 1975 Aug, pp. 186-189.

- [9] Kubo, S., Jinouchi, Y., Araki, Y., Inoue, J.: "Automatic Balancer (Pendulum Balancer)," Bulletin of the JSME, 1986, Vol. 29, No. 249, pp. 924-928.

- [10] Bövik, P., Högfors, C.: "Autobalancing of Rotors," Journal of Sound and Vibration, 1986, Vol. 111, No. 3, December 22, pp. 429-440.

- [11] Wettergren, H. L.: "Using Guided Balls to Auto-Balance Rotors," *Journal of Engineering for Gas Turbines and Power*, Vol. 124, No. 4, October 2002, pp. 971-975.
- [12] Huang, W. Y., Chao, C. P., Kang, J. R. , Sung C. K.: "The application of ball-type balancers for radial vibration reduction of high speed optic disk drives," *Journal of Sound and Vibration*, 2002 250(3), pp. 415-430.
- [13] Van De WouW, N., Van Den Heuvel, M. N., Nijmeijer, H., and Van Rooij, J. A.: "Performance of an Automatic Ball Balancer with Dry Friction," *International Journal of Bifurcation and Chaos*, Vol. 15, No. 1 (2005), pp.65-82.
- [14] Green, K. M. I., Friswell, A. R., Champneys, and N. A. J. Lieven, "The Stability of Automatic Ball Balancers", *Proceedings of ISCORMA-3 (2005)*
- [15] Wettergren, H. L.: "Auto-balance anisotropic mounted rotors", *Proceedings of the ASME Design Engineering Technical Conference*, v 6 A, 2001, p 669-674
- [16] Sinha, S.C., Wu, D.-H.: "Efficient computational scheme for the analysis of periodic systems" *Journal of Sound and Vibration*, v 151, n 1, Nov 22, 1991, p 91-117
- [17] Chao, C.-P.; Chiu, C.-W.; Sung, C.-K.; Leu, H.-C.: "Effects of rolling friction of the balancing balls on the automatic ball balancer for optical disk drives", *Proceedings of the ASME/STLE International Joint Tribology Conference, IJTC 2004*, 2004, p 795-806
- [18] Rajalingham, C.; Bhat, R.B.: "Complete balancing of a disk mounted on a vertical cantilever shaft using a two ball automatic balancer" *Journal of Sound and Vibration*, v 290, n 1-2, Feb 21, 2006, p 169-191
- [19] Chung, J.: "Effect of gravity and angular velocity on an automatic ball balancer", *Proceedings of the Institution of Mechanical Engineers, Part C: Journal of Mechanical Engineering Science*, v 219, n 1, January, 2005, p 43-51

- [20] Yang, Q.; Ong, E.-H.; Sun, J.; Guo, G.; Lim, S.-P.: “Study on the influence of friction in an automatic ball balancing system”. *Journal of Sound and Vibration*, v 285, n 1-2, Jul 6, 2005, p 73-99
- [21] Kim, W.; Chung, J.: “Performance of automatic ball balancers on optical disc drives”, *Proceedings of the Institution of Mechanical Engineers, Part C: Journal of Mechanical Engineering Science*, v 216, n 11, 2002, p 1071-1080
- [22] Chao, C.P.; Huang, Y.-D.; Sung, C.-K.: “Non-planar dynamic modeling for the optical disk drive spindles equipped with an automatic balancer”, *Mechanism and Machine Theory*, v 38, n 11, November, 2003, p 1289-1305
- [23] Floquet, M. G., 1883, “Équations Différentielles Linéaires a Coefficients Périodiques” *Ann. Sci. Ec. Normale Super.*, 12, p 47–89.
- [24] Hill, G. W., 1886, “On the Part of the Motion of the Lunar Perigee Which is a Function of the Mean Motions of the Sun and Moon” *Acta Math.*, 8, p 1–36.
- [25] Rayleigh (Strutt), J. W., 1887, “On the Maintenance of Vibrations by Forces of Double Frequency, and on the Propagation of Waves Through a Medium Endowed With a Periodic Structure” *Philos. Mag.*, 24, p 145–159.
- [26] Hsu, C.S.: “On approximating a general linear periodic system” *Journal of Mathematical Analysis and Application* 1974, 45, p 234-251
- [27] Friedmann, P.; Hammond, C. E.; Woo, Tze-Hsin: “Efficient numerical treatment of periodic systems with application to stability problems” *International Journal for Numerical Methods in Engineering*, v 11, n 7, 1977, p 1117-1136
- [28] Farkas, M. (1994): *Periodic Motion*, Springer, New York.
- [29] Hirsch, M. W. – Smale, S. (1974): *Differential Equations, Dynamical Systems and Linear Algebra*, Academic Press, Berkeley.

- [30] Ali Hasan Nayfeh, Dean T. Mook (1995): Nonlinear Oscillations, John Wiley & Sons Inc

- [31] John, M. Vance (1988): Rotordynamics of Turbomachinery, John Wiley & Sons Inc

- [32] Yamamoto, T., Ishida Y.: Linear and Nonlinear Rotordynamics, John Wiley & Sons Inc

- [33] Meirovitch, L. (2001): Fundamentals of Vibrations, McGraw-Hill

- [34] Meirovitch, L. (1996): Principles and Techniques of Vibrations, Prentice Hall

- [35] Wovk, V. (1991): Machinery Vibration: Measurement and Analysis, McGraw-Hill

- [36] Katsuhiko, O. (2003): System Dynamics, Prentice Hall

- [37] Gleick, J. (1988): Chaos: Making a New Science, Penguin USA

- [38] Beranek, L. (1992): Noise and Vibration Control Engineering: Principles and Applications, John Wiley & Sons Inc

- [39] Dimarogonas, A. (1992): Vibration for Engineers, Prentice Hall

- [40] Ginsberg J. (2001): Advanced Engineering Dynamics, Addison-Wesley

- [41] Dahleh, M. D., Thomson, W. T. (1997): Theory of Vibrations with Applications, Prentice Hall

APPENDIX A PARAMETERS OF EXPERIMENTAL FACILITY

Rotor Assembly

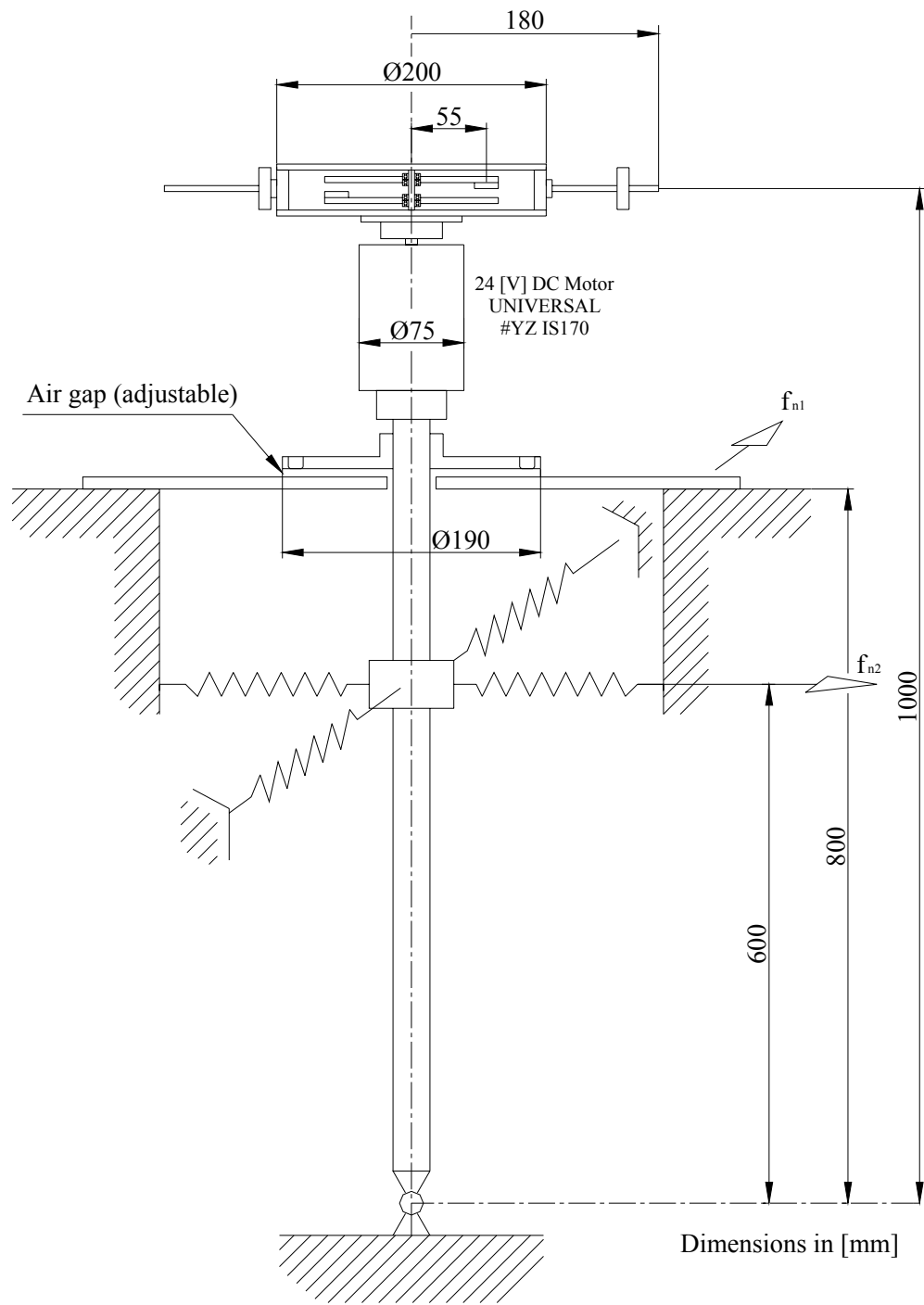
Length of pendulums R_{BA} and R_{BB} :	0.054 [mm]
Mass of pendulums M_{BA} and M_{BB} :	0.075 [kg] (Identical)
Mass of pendulum M_{BB} :	0.019, 0.037, 0.055 [kg] (Non-Identical)
Mass of imbalance M_P :	0.120 [kg]
Mass of entire rotor assembly M_D :	7 [kg]
Damping coefficient of pendulums c_{34} :	0.01-50 [Nsm/rad]
Shift of pendulums suspension R_C :	0-3[mm]

Rotor Suspension

Natural frequency f_{n1} :	3 [Hz]
Natural frequency f_{n2} :	3-11.6 [Hz]
Relative damping coefficient ζ_{12} :	0.001-0.2 [-]

Operational Parameters

Final running speed:	150-1200 [RPM]
----------------------	----------------



Schematic of experimental facility

APPENDIX B MATLAB SOURCE CODES

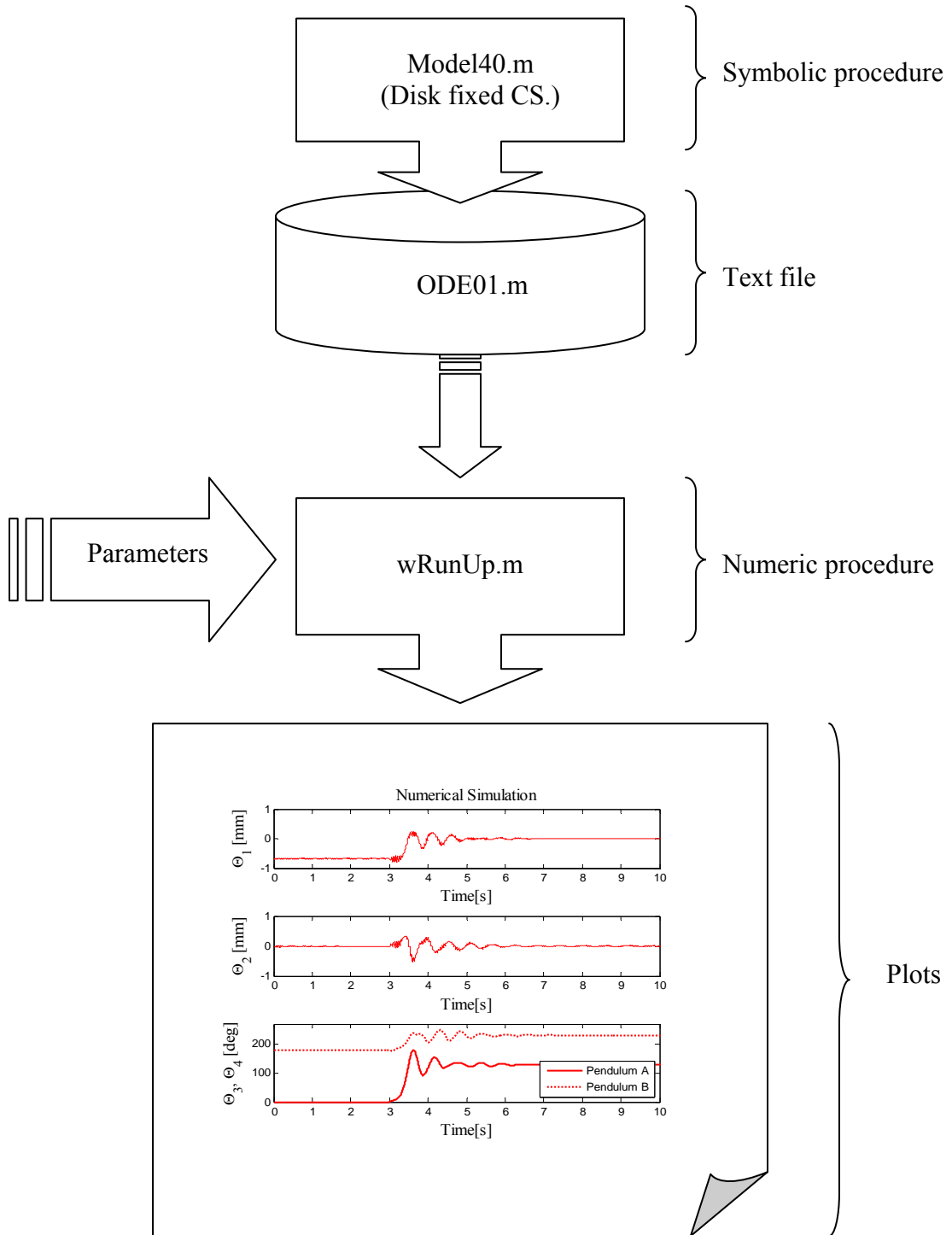


Figure 5.1 Program structure of development and process of ODE system

5.1 MatLab source code: Model40.m

```
more off
clear all
close all
clc
echo on

syms Md          % Mass of Disk
syms MBa         % Balancing mass A
syms MBb         % Balancing Mass B
syms Mp          % Perturbation Mass

syms Rd          % Radius of Disc
syms RBa         % Radius of length of Balancing Pendulum A
syms RBb         % Radius of length of Balancing Pendulum A

syms g           % Gravitational Acc.

syms P3          % Maximum Radial perturbation variable
syms P3t         % Radial perturbation variable as a function of time

syms k1          % spring stiffness of Q1
syms k2          % spring stiffness of Q2
syms k3          % spring stiffness of Q3
syms k4          % spring stiffness of Q4
syms c1          % Viscous Damping of Q1
syms c2          % Viscous Damping of Q2
syms c3          % Viscous Damping of Q3
syms c4          % Viscous Damping of Q4

Y = sym ('Y(t)');
Q1 = sym('Q1(t)');
Q2 = sym('Q2(t)');
Q3 = sym('Q3(t)');
Q4 = sym('Q4(t)');

dtY = diff (Y,'t');
dtQ1 = diff (Q1,'t');
dtQ2 = diff (Q2,'t');
dtQ3 = diff (Q3,'t');
dtQ4 = diff (Q4,'t');

syms t
syms w
syms ddtQ1
syms ddtQ2
syms ddtQ3
syms ddtQ4

I = [1; 0; 0]
I0 = I;
Ip = I;
Ipp = I;
```

```

Ippp  = I;
Ipppp = I;

J = [0; 1; 0]
J0  = J;
Jp  = J;
Jpp = J;
Jppp = J;
Jpppp = J;

K = [0; 0; 1]
K0  = K;
Kp  = K;
Kpp = K;
Kppp = K;
Kpppp = K;

T0_I = [ cos(Y)  sin(Y)  0;
        -sin(Y)  cos(Y)  0;
         0        0      1];

TI_0  = [cos(Y)  -sin(Y)  0;
         sin(Y)  cos(Y)  0;
         0        0      1];

TI_II = [ cos(Q3)  sin(Q3)  0;
         -sin(Q3)  cos(Q3)  0;
         0         0        1];

TII_I = [cos(Q3)  -sin(Q3)  0;
         sin(Q3)  cos(Q3)  0;
         0         0        1];

TI_III = [ cos(Q4)  sin(Q4)  0;
          -sin(Q4)  cos(Q4)  0;
           0         0        1];

TIII_I = [cos(Q4)  -sin(Q4)  0;
          sin(Q4)  cos(Q4)  0;
           0         0        1];

% Inertia Matrix of disk
ID1 = [1/4*Md*Rd^2  0  0
       0  1/4*Md*Rd^2  0
       0  0  1/2*Md*Rd^2]

% ##### in ROTATING CS. #####
% DISK:
wD1 = dtY*Kp
RD1 = Q1*Ip + Q2*Jp
RD0 = TI_0*RD1

VD1 = dtQ1*Ip + dtQ2*Jp + cross(wD1,RD1)
VD0 = TI_0*VD1

```

```

% Perturbation Mass Mp
RMp1 = (Q1+P3t)*Ip + Q2*Jp
RMp0 = TI_0*RMp1

VMp1 = dtQ1*Ip + dtQ2*Jp + cross(wD1, RMp1)
VMp0 = TI_0*VMp1

% Balancing masses
Ip0 = TI_0*Ip
Jp0 = TI_0*Jp
Ipp0 = TI_0 * TIII_I * Ipp
Ippp0 = TI_0 * TIII_I * Ippp
RMBa0 = Q1*Ip0 + Q2*Jp0 + RBa*Ipp0;
RMBb0 = Q1*Ip0 + Q2*Jp0 + RBb*Ippp0;

VMBa0 = DPosVecDT(RMBa0)
VMBb0 = DPosVecDT(RMBb0)

% Kinetic energies
TDr = 1/2*wD1.'*(ID1*wD1)
TDt = 1/2*Md*(VD0.'*VD0)
TMBa = 1/2*MBa*(VMBa0.'*VMBa0)
TMBb = 1/2*MBb*(VMBb0.'*VMBb0)
TMP = 1/2*Mp*(VMp0.'*VMp0)

T = TDr+TDt + TMBa+TMBb + TMP

V = 1/2*k1*RD0(1,1)^2 + 1/2*k2*RD0(2,1)^2
%Potential Energy

D = 1/2*c1*VD0(1,1)^2 + 1/2*c2*VD0(2,1)^2 + 1/2*c3*dtQ3^2 +
1/2*c4*dtQ4^2 %Dissipation Energy

T = convextoshort (T)
V = convextoshort (V)
D = convextoshort (D)
T = simple(T)
V = simple(V)
D = simple(D)

#####
%## Lagrangian Process for 4DOF system ##
#####

Calculating the Matrix Form
dTdtDQ1 = dDF_dtDX(T, 'dtQ1');
DT_DQ1 = DF_DX(T, 'Q1')
DV_DQ1 = DF_DX(V, 'Q1')
DD_DdQ1 = DF_DX(D, 'dtQ1')
E1 = dDT_dtDQ1 - DT_DQ1 + DV_DQ1 + DD_DdQ1
if E1 ~= 0
    E1 = simple(E1)
end

```

```

EoM1 = subs (E1,'ddtQ1','0',0)
M11 = E1-EoM1
M11 = subs (M11,'ddtQ1','1',0);
if M11 ~= 0
    M11 = simple (M11);
end

EoM1 = subs (E1,'ddtQ2','0',0)
M12 = E1-EoM1
M12 = subs (M12,'ddtQ2','1',0);
if M12 ~= 0
    M12 = simple (M12);
end

EoM1 = subs (E1,'ddtQ3','0',0)
M13 = E1-EoM1
M13 = subs (M13,'ddtQ3','1',0);
if M13 ~= 0
    M13 = simple (M13);
end

EoM1 = subs (E1,'ddtQ4','0',0)
M14 = E1-EoM1
M14 = subs (M13,'ddtQ4','1',0);
if M14 ~= 0
    M14 = simple (M14);
end

F1 = subs (E1,'ddtQ1','0',0);
F1 = subs (F1,'ddtQ2','0',0);
F1 = subs (F1,'ddtQ3','0',0);
F1 = subs (F1,'ddtQ4','0',0);
F1 = simple (F1)

%-----
dDT_dtDQ2 = dDF_dtDX(T,'dtQ2')
DT_DQ2    = DF_DX(T,'Q2');
DV_DQ2    = DF_DX(V,'Q2')
DD_DdQ2   = DF_DX(D,'dtQ2')
E2 = dDT_dtDQ2 - DT_DQ2 + DV_DQ2 + DD_DdQ2
if E2 ~= 0
    E2 = simple(E2)
end

EoM2 = subs (E2,'ddtQ1','0',0)
M21 = E2-EoM2
M21 = subs (M21,'ddtQ1','1',0);
if M21 ~= 0
    M21 = simple (M21);
end

EoM2 = subs (E2,'ddtQ2','0',0)
M22 = E2-EoM2
M22 = subs (M22,'ddtQ2','1',0);
if M22 ~= 0

```



```

    M22 = simple (M22);
end

EoM2 = subs (E2,'ddtQ3','0',0)
M23 = E2-EoM2
M23 = subs (M23,'ddtQ3','1',0);
if M23 ~= 0
    M23 = simple (M23);
end

EoM2 = subs (E2,'ddtQ4','0',0)
M24 = E2-EoM2
M24 = subs (M24,'ddtQ4','1',0);
if M24 ~= 0
    M24 = simple (M24);
end

F2 = subs (E2,'ddtQ1','0',0);
F2 = subs (F2,'ddtQ2','0',0);
F2 = subs (F2,'ddtQ3','0',0);
F2 = subs (F2,'ddtQ4','0',0);
F2 = simple (F2)

%-----
dDT_dtDQ3 = dDF_dtDX(T,'dtQ3')
DT_DQ3     = DF_DX(T,'Q3');
DV_DQ3     = DF_DX(V,'Q3')
DD_DdQ3    = DF_DX(D,'dtQ3')
E3 = dDT_dtDQ3 - DT_DQ3 + DV_DQ3 + DD_DdQ3
if E3 ~= 0
    E3 = simple(E3)
end

EoM3 = subs (E3,'ddtQ1','0',0)
M31 = E3-EoM3
M31 = subs (M31,'ddtQ1','1',0);
if M31 ~= 0
    M31 = simple (M31);
end

EoM3 = subs (E3,'ddtQ2','0',0)
M32 = E3-EoM3
M32 = subs (M32,'ddtQ2','1',0);
if M32 ~= 0
    M32 = simple (M32);
end

EoM3 = subs (E3,'ddtQ3','0',0)
M33 = E3-EoM3
M33 = subs (M33,'ddtQ3','1',0);
if M33 ~= 0
    M33 = simple (M33);
end

EoM3 = subs (E3,'ddtQ4','0',0)
M34 = E3-EoM3
M34 = subs (M34,'ddtQ4','1',0);

```

```

if M34 ~= 0
    M34 = simple (M34);
end
F3 = subs (E3,'ddtQ1','0',0);
F3 = subs (F3,'ddtQ2','0',0);
F3 = subs (F3,'ddtQ3','0',0);
F3 = subs (F3,'ddtQ4','0',0);
F3 = simple (F3)

%-----
dDT_dtDQ4 = dDF_dtDX(T,'dtQ4')
DT_DQ4    = DF_DX(T,'Q4');
DV_DQ4    = DF_DX(V,'Q4')
DD_DdQ4   = DF_DX(D,'dtQ4')
E4 = dDT_dtDQ4 - DT_DQ4 + DV_DQ4 + DD_DdQ4
if E4 ~= 0
    E4 = simple(E4)
end

EoM4 = subs (E4,'ddtQ1','0',0)
M41 = E4-EoM4
M41 = subs (M41,'ddtQ1','1',0);
if M41 ~= 0
    M41 = simple (M41);
end

EoM4 = subs (E4,'ddtQ2','0',0)
M42 = E4-EoM4
M42 = subs (M42,'ddtQ2','1',0);
if M42 ~= 0
    M42 = simple (M42);
end

EoM4 = subs (E4,'ddtQ3','0',0)
M43 = E4-EoM4
M43 = subs (M43,'ddtQ3','1',0);
if M43 ~= 0
    M43 = simple (M43);
end

EoM4 = subs (E4,'ddtQ4','0',0)
M44 = E4-EoM4
M44 = subs (M44,'ddtQ4','1',0);
if M44 ~= 0
    M44 = simple (M44);
end

F4 = subs (E4,'ddtQ1','0',0);
F4 = subs (F4,'ddtQ2','0',0);
F4 = subs (F4,'ddtQ3','0',0);
F4 = subs (F4,'ddtQ4','0',0);
F4 = simple (F4)

Orig_E1 = E1
Orig_E2 = E2
Orig_E3 = E3

```

```

Orig_E4 = E4
save Es

M = [M11 M12 M13 M14;
     M21 M22 M23 M24;
     M31 M32 M33 M34;
     M41 M42 M43 M44]

ddtX = [ddtQ1;
        ddtQ2;
        ddtQ3;
        ddtQ4];

A1 = inv(M)
F = [F1;
     F2;
     F3;
     F4]

ddtQ = -inv(M)*F

Orig_F2 = ddtQ(1)
Orig_F4 = ddtQ(2)
Orig_F6 = ddtQ(3)
Orig_F8 = ddtQ(4)

OdeM = fopen ('SF.m','w')
strA = strcat ('Orig_F2 = ',char(Orig_F2),';\n')
fprintf (OdeM,strA)
strA = strcat ('Orig_F4 = ',char(Orig_F4),';\n')
fprintf (OdeM,strA)
strA = strcat ('Orig_F6 = ',char(Orig_F6),';\n')
fprintf (OdeM,strA)
strA = strcat ('Orig_F8 = ',char(Orig_F8),';\n')
fprintf (OdeM,strA)
fclose (OdeM)

##### Writing the ODE file
E1 = Orig_E1
E2 = Orig_E2
E3 = Orig_E3
E4 = Orig_E4

E1 = subs (E1,'dtY', 'w',0);
E1 = subs (E1,'ddtY', 'dtw',0);
E1 = solve (E1,'ddtQ1')
E1 = subs (E1,'Q1', 'q(1)',0);
E1 = subs (E1,'dtQ1', 'q(2)',0);
E1 = subs (E1,'ddtQ1', 'dq(2)',0);
E1 = subs (E1,'Q2', 'q(3)',0);
E1 = subs (E1,'dtQ2', 'q(4)',0);
E1 = subs (E1,'ddtQ2', 'dq(4)',0);
E1 = subs (E1,'Q3', 'q(5)',0);
E1 = subs (E1,'dtQ3', 'q(6)',0);

```

```

E1 = subs (E1,'ddtQ3', 'dq(6)',0);
E1 = subs (E1,'Q4', 'q(7)',0);
E1 = subs (E1,'dtQ4', 'q(8)',0);
E1 = subs (E1,'ddtQ4', 'dq(8)',0);

E2 = subs (E2,'dtY', 'w',0);
E2 = subs (E2,'ddtY', 'dtw',0);
E2 = solve (E2,'ddtQ2')
E2 = subs (E2,'Q1', 'q(1)',0);
E2 = subs (E2,'dtQ1', 'q(2)',0);
E2 = subs (E2,'ddtQ1', 'dq(2)',0);
E2 = subs (E2,'Q2', 'q(3)',0);
E2 = subs (E2,'dtQ2', 'q(4)',0);
E2 = subs (E2,'ddtQ2', 'dq(4)',0);
E2 = subs (E2,'Q3', 'q(5)',0);
E2 = subs (E2,'dtQ3', 'q(6)',0);
E2 = subs (E2,'ddtQ3', 'dq(6)',0);
E2 = subs (E2,'Q4', 'q(7)',0);
E2 = subs (E2,'dtQ4', 'q(8)',0);
E2 = subs (E2,'ddtQ4', 'dq(8)',0);

E3 = subs (E3,'dtY', 'w',0);
E3 = subs (E3,'ddtY', 'dtw',0);
E3 = solve (E3,'ddtQ3')
E3 = subs (E3,'Q1', 'q(1)',0);
E3 = subs (E3,'dtQ1', 'q(2)',0);
E3 = subs (E3,'ddtQ1', 'dq(2)',0);
E3 = subs (E3,'Q2', 'q(3)',0);
E3 = subs (E3,'dtQ2', 'q(4)',0);
E3 = subs (E3,'ddtQ2', 'dq(4)',0);
E3 = subs (E3,'Q3', 'q(5)',0);
E3 = subs (E3,'dtQ3', 'q(6)',0);
E3 = subs (E3,'ddtQ3', 'dq(6)',0);
E3 = subs (E3,'Q4', 'q(7)',0);
E3 = subs (E3,'dtQ4', 'q(8)',0);
E3 = subs (E3,'ddtQ4', 'dq(8)',0);

E4 = subs (E4,'dtY', 'w',0);
E4 = subs (E4,'ddtY', 'dtw',0);
E4 = solve (E4,'ddtQ4')
E4 = subs (E4,'Q1', 'q(1)',0);
E4 = subs (E4,'dtQ1', 'q(2)',0);
E4 = subs (E4,'ddtQ1', 'dq(2)',0);
E4 = subs (E4,'Q2', 'q(3)',0);
E4 = subs (E4,'dtQ2', 'q(4)',0);
E4 = subs (E4,'ddtQ2', 'dq(4)',0);
E4 = subs (E4,'Q3', 'q(5)',0);
E4 = subs (E4,'dtQ3', 'q(6)',0);
E4 = subs (E4,'ddtQ3', 'dq(6)',0);
E4 = subs (E4,'Q4', 'q(7)',0);
E4 = subs (E4,'dtQ4', 'q(8)',0);
E4 = subs (E4,'ddtQ4', 'dq(8)',0);

OdeM = fopen ('DES01.m','w')
fprintf (OdeM,'function dq=dem23(t,q)\n');
fprintf (OdeM,'dq=zeros(8,1);\n');

```

```

fprintf (OdeM,'global g Md MBa MBb Mp RBa RBb P3 P3t tc k1 k2 k3 k4 c1
c2 c3 c4 wf hr RUF Dn phr ts tRelease\n');

fprintf (OdeM,'%#####\n');
fprintf (OdeM,'w = wf;\n');
fprintf (OdeM,'Y = w*t;\n');
fprintf (OdeM,'dtw = 0;\n');
fprintf (OdeM,'%#####\n');

fprintf (OdeM,'P3t = P3;\n');
fprintf (OdeM,'if round(Dn/500)*500 == Dn\n');
fprintf (OdeM,'[t Y w dtw] \n');
fprintf (OdeM,'end\n');

fprintf (OdeM,'if t <= tRelease\n');
fprintf (OdeM,'    q(5) = 0;\n');
fprintf (OdeM,'    q(7) = pi;\n');
fprintf (OdeM,'end\n');

fprintf (OdeM,'dq(1) = q(2);\n')
strA = strcat ('dq(2) = ',char(E1),';\n')
fprintf (OdeM,strA)

fprintf (OdeM,'dq(3) = q(4);\n')
strA = strcat ('dq(4) = ',char(E2),';\n')
fprintf (OdeM,strA)

fprintf (OdeM,'dq(5) = q(6);\n')
strA = strcat ('dq(6) = ',char(E3),';\n')
fprintf (OdeM,strA)

fprintf (OdeM,'dq(7) = q(8);\n')
strA = strcat ('dq(8) = ',char(E4),';\n')
fprintf (OdeM,strA)

fprintf (OdeM,'if t <= tRelease;\n')
    fprintf (OdeM,'q(5) = 0;\n')
    fprintf (OdeM,'dq(5) = 0;\n')
    fprintf (OdeM,'q(6) = 0;\n')
    fprintf (OdeM,'q(7) = pi;\n')
    fprintf (OdeM,'dq(7) = 0;\n')
    fprintf (OdeM,'q(8) = 0;\n')
fprintf (OdeM,'end\n')

fprintf (OdeM,'RUF(Dn,1) = t;\n')
fprintf (OdeM,'RUF(Dn,2) = Y;\n')
fprintf (OdeM,'RUF(Dn,3) = w;\n')
fprintf (OdeM,'RUF(Dn,4) = dtw;\n')
fprintf (OdeM,'RUF(Dn,5) = P3t;\n')
fprintf (OdeM,'Dn = Dn + 1;\n')
fprintf (OdeM,'return;\n')
fclose (OdeM)

```

5.2 MatLab source code: ODE01.m

```

function dq = dem23(t,q)
dq=zeros(8,1);
global g Md MBa MBb Mp RBa RBb P3 P3t tc k1 k2 k3 k4 c1 c2 c3 c4 wf hr
RUF Dn phr ts tRelease
w = wf;
Y = w*t;
dtw = 0;
P3t = P3;
if round(Dn/500)*500 == Dn
[t Y w dtw]
end
if t <= tRelease
    q(5) = 0;
    q(7) = pi;
end
dq(1) = q(2);
dq(2)
=(MBa*w^2*(q(1))+MBb*w^2*(q(1))+Mp*w^2*(q(1))+Md*w^2*(q(1))+Mp*w^2*P3t+
MBb*dtw*(q(3))+Md*dtw*(q(3))+Mp*dtw*(q(3))+MBa*dtw*(q(3))-
c2*sin(Y)*cos(Y)*w*(q(1))+c1*cos(Y)*sin(Y)*w*(q(1))+MBb*RBb*dtw*sin((q(
7)))+MBa*RBa*dtw*sin((q(5)))+2*Mp*w*(q(4))+2*MBa*w*(q(4))+2*MBb*w*(q(4)
)+2*Md*w*(q(4))-(q(2))*c2*sin(Y)^2-
k2*sin(Y)*cos(Y)*(q(3))+k1*cos(Y)*sin(Y)*(q(3))+c1*cos(Y)*sin(Y)*(q(4))
-
c2*sin(Y)*cos(Y)*(q(4))+MBb*RBb*cos((q(7)))*(q(8))^2+MBa*RBa*cos((q(5))
)*(q(6))^2-(q(2))*c1*cos(Y)^2-k1*cos(Y)^2*(q(1))-
k2*sin(Y)^2*(q(1))+MBb*RBb*sin((q(7)))*(dq(8))+MBa*RBa*sin((q(5)))*(dq(
6))+2*MBb*RBb*w*cos((q(7)))*(q(8))+2*MBa*RBa*w*cos((q(5)))*(q(6))+MBa*w
^2*RBa*cos((q(5)))+MBb*w^2*RBb*cos((q(7)))+c1*cos(Y)^2*w*(q(3))+c2*sin(
Y)^2*w*(q(3)))/(MBb+Md+Mp+MBa);
dq(3) = q(4);
dq(4) =(k1*sin(Y)*cos(Y)*(q(1))-MBa*RBa*cos((q(5)))*(dq(6))-
MBb*RBb*cos((q(7)))*(dq(8))+MBa*w^2*RBa*sin((q(5)))+MBb*w^2*RBb*sin((q(
7)))-c2*cos(Y)^2*w*(q(1))-c1*sin(Y)^2*w*(q(1))-
k2*cos(Y)*sin(Y)*(q(1))+(q(2))*c1*sin(Y)*cos(Y)-
(q(2))*c2*cos(Y)*sin(Y)+MBa*RBa*sin((q(5)))*(q(6))^2+MBb*RBb*sin((q(7))
)*(q(8))^2+2*MBb*RBb*w*sin((q(7)))*(q(8))-c1*sin(Y)^2*(q(4))-
k2*cos(Y)^2*(q(3))-c2*cos(Y)^2*(q(4))-
c1*sin(Y)*cos(Y)*w*(q(3))+c2*cos(Y)*sin(Y)*w*(q(3))+2*MBa*RBa*w*sin((q(
5)))*(q(6))-2*Mp*w*(q(2))-MBb*dtw*(q(1))-Mp*dtw*P3t-Md*dtw*(q(1))-
Mp*dtw*(q(1))-MBa*dtw*(q(1))-MBb*RBb*dtw*cos((q(7)))-
MBa*RBa*dtw*cos((q(5)))-
k1*sin(Y)^2*(q(3))+Md*w^2*(q(3))+Mp*w^2*(q(3))+MBb*w^2*(q(3))+MBa*w^2*(
q(3))-2*MBa*w*(q(2))-2*Md*w*(q(2))-2*MBb*w*(q(2)))/(MBb+Md+Mp+MBa);
dq(5) = q(6);
dq(6) =-
(2*MBa*w*(q(2))*RBa*cos((q(5)))+MBa*RBa*dtw*(q(3))*sin((q(5)))+2*MBa*w*
(q(4))*RBa*sin((q(5)))+MBa*RBa*dtw*(q(1))*cos((q(5)))-
MBa*w^2*(q(3))*RBa*cos((q(5)))+MBa*RBa*(dq(4))*cos((q(5)))+MBa*RBa^2*dt
w-
MBa*RBa*sin((q(5)))*(dq(2))+MBa*w^2*(q(1))*RBa*sin((q(5)))+c3*(q(6)))/M
Ba/RA^2;
dq(7) = q(8);

```

```

dq(8) = (-MBb*dtw*(q(1))*RBb*cos((q(7)))-MBb*(dq(4))*RBb*cos((q(7)))-
MBb*dtw*(q(3))*RBb*sin((q(7)))-2*MBb*w*(q(4))*RBb*sin((q(7)))-
MBb*w^2*(q(1))*RBb*sin((q(7)))-2*MBb*w*(q(2))*RBb*cos((q(7)))-
MBb*RBb^2*dtw+MBb*RBb*sin((q(7)))*(dq(2))+MBb*w^2*(q(3))*RBb*cos((q(7))
)-c4*(q(8)))/MBb/RBb^2;
if t <= tRelease;
    q(5) = 0;
    dq(5) = 0;
    q(6) = 0;
    q(7) = pi;
    dq(7) = 0;
    q(8) = 0;
end
RUF(Dn,1) = t;
RUF(Dn,2) = Y;
RUF(Dn,3) = w;
RUF(Dn,4) = dtw;
RUF(Dn,5) = P3t;
Dn = Dn + 1;
return;

```

5.3 MatLab source code: wRunUp.m

```

close all
clear all
clc
echo on

format short
global P g Md MBa MBb Mp MPa MPb Rd RBa RBb P3 k1 k2 k3 k4 c1 c2 c3 c4
wf wb RUF Dn phr ts hr tRelease

ICQ = [1e-16 1e-16 1e-16 pi+0.001]
ICdtQ = [1e-12 1e-12 1e-12 1e-12]

Md = 7 % [kg]
MBa = 0.075; % [kg]
MBb = 0.075; % [kg]
Mp = 2*120.9/1000; % [kg], Part of Md

Rd = 0.1; % [m]
RBa = 0.054; % [m]
RBb = 0.054; % [m]
n = 40 % # of turns
P3 = n*25.4/48 /1000; % Perturbation [m]

k1 = 500;
k2 = 500;
k3 = 0;
k4 = 0;

c1 = 10;
c2 = 10;
c3 = 0.0005;

```

```

c4 = 0.0005;

wf = 20*pi*2;                                % [Hz] Running speed

t0 = 0.01
tRelease = 12
t1 = tRelease + 10;

AbsTol = 1e-6;
RelTol = 1e-6;
Dn = 1;
option = odeset('AbsTol',AbsTol, 'RelTol', RelTol)
[t, xa] = ode45 ('DES01', [t0 t1], [ICQ(1),ICdtQ(1), ICQ(2),ICdtQ(2),
ICQ(3),ICdtQ(3), ICQ(4),ICdtQ(4)],option);

TimeShift = -tRelease+3;

t0 = t;
xa0 = xa;
i = 1;
echo off;
while t(i) < abs(TimeShift)
    i = i + 1;
end
N = size(t0);
N = N(1,1);
L = N-i;
t = t0(i:i+L)+TimeShift;
xa = xa0(i:i+L,1:8);

subplot (3,1,1);
plot (t,xa(:,1)*1000,'r')
SetPlotText ('Time[s]','\Theta_1 [mm]','Numerical Simulation',14);
axis ([0 10 -1 1]);

subplot (3,1,2);
plot (t,xa(:,3)*1000,'r')
SetPlotText ('Time[s]','\Theta_2 [mm]','',14);
axis ([0 10 -1 1]);

subplot (3,1,3);
plot (t,-xa(:,5)*180/pi,'r','LineWidth',2)
hold on
plot (t,360-xa(:,7)*180/pi,'r:','LineWidth',2)
SetPlotText ('Time[s]','\Theta_3, \Theta_4 [deg]','',14);
legend ('Pendulum A','Pendulum B');
box on
axis ([0 10 0 270]);
clc

```